

ABSTRACT

Title of Dissertation: INVESTIGATION OF THE MOLECULAR MECHANISMS OF VASCULAR ENDOTHELIAL DYSFUNCTION IN HUTCHINSON-GILFORD PROGERIA SYNDROME THROUGH *IN VITRO* 2D AND 3D MODELS

Yantenev Gete, Doctor of Philosophy, 2021

Dissertation Directed by: Dr. Kan Cao
Department of Cell Biology and Molecular Genetics
University of Maryland

Hutchinson-Gilford progeria syndrome (HGPS) is a rare genetic disorder with features of accelerated aging. Predominantly, HGPS is caused by a *de novo* point mutation in the *LMNA* gene (c.1824C > T; p.G608G) resulting in progerin, a toxic lamin A protein variant. Children with HGPS typically die from coronary artery diseases or strokes at an average age of 14.6 years. Endothelial dysfunction is a known driver of cardiovascular pathogenesis; however, it is currently unknown how progerin antagonizes endothelial function in HGPS. In this study, I used human iPSC-derived endothelial cell (iPSC-EC) models that cultured under both static and fluidic culture conditions. HGPS iPSC-ECs

show reduced endothelial nitric oxide synthase (eNOS) expression and activity compared to healthy controls and concomitant decreases in intracellular nitric oxide (NO) level, which result in deficits in capillary-like microvascular network formation. In addition, expression of matrix metalloproteinase 9 (MMP-9) was reduced in HGPS iPSC-ECs while expression of tissue inhibitor metalloproteinases 1 and 2 (TIMP1 and TIMP2) were upregulated relative to healthy controls. Moreover, I used an adenine base editor (ABE7.10max-VRQR) to correct the pathogenic c.1824C > T allele in HGPS iPSC-ECs. Remarkably, ABE7.10max-VRQR correction of the HGPS mutation significantly reduced progerin expression to a basal level, rescued nuclear blebbing, increased intracellular NO level, normalized TIMPs, and restored angiogenic competence in HGPS iPSC-ECs. Furthermore, to elucidate the effects of progerin on endothelial cells and vascular remodeling, in collaboration with Dr. Truskey's lab at Duke university, we developed tissue-engineered blood vessels (TEBVs) using iPSC-ECs and smooth muscle cells (iPSC-SMCs) from normal and HGPS patients. Relative to normal TEBVs, HGPS TEBVs showed reduced function and exhibited markers of cardiovascular disease associated with endothelium, including a reduction in both vasoconstriction and vasodilation with increased inflammation markers, VCAM-1 and E-selectin protein. Hence, the TEBV model has identified a role of the endothelium in HGPS. Together, the results of the study provide molecular insights into endothelial dysfunction in HGPS and suggest that ABE7.10max-VRQR could be a promising therapeutic approach for correcting HGPS-related cardiovascular phenotypes.

INVESTIGATION OF THE MOLECULAR MECHANISMS OF VASCULAR
ENDOTHELIAL DYSFUNCTION IN HUTCHINSON-GILFORD PROGERIA
SYNDROME THROUGH *IN VITRO* 2D AND 3D MODELS

by

Yantenew Gete

Dissertation submitted to the Faculty of the Graduate School of the
University of Maryland, College Park, in partial fulfillment
of the requirements for the degree of
Doctor of Philosophy
2021

Advisory Committee:
Professor Kan Cao, Chair
Professor David Mosser
Professor Margaret Scull
Professor Steven Fisher
Professor John Fisher, Dean's representative

© Copyright by
Yantnew Gete
2021

Dedication

To my dearest family, for their endless support and care

Acknowledgements

Throughout my graduate career, God has been so good and blessed me with several individuals who provided me tremendous help and sincere care. Without them, I was not able to accomplish my doctoral study. Despite the challenge, pursuing a Ph.D. enriched my experience that would be a hallmark to my future career path.

First, I would like to thank my mentor Dr. Kan Cao, who has been an inspiration both in science and life. With her guidance, I have gained not only the knowledge of science, but also how to be a good teacher and a researcher with critical perspectives. I greatly appreciate her patience, energy and enormous efforts. With her mentorship, I evolved as independent scientist who thinks concrete research ideas, comes up with troubleshooting strategies, and communicates science effectively.

I also appreciate my committee members for taking their time to provide advice and directions to my research throughout my Ph.D. study. I would like to acknowledge Dr. John Fisher and his group for advising and providing me 3D printed bioreactors that had been a part of crucial experiments of my study. Thanks to Dr. David Mosser, Dr. Steven Fisher, and Dr. Margaret Skull for the feedback on my research progress, and for teaching me to approach my research problems critically and objectively.

I thank Dr. George Truskey's group for collaboration and insightful discussions on developing Tissue Engineered Blood Vessel model for HGPS, and Dr. David Liu's group for providing ABE7.10max-VRQR plasmid construct. Without them, I wouldn't be able to complete the study.

I appreciate all Cao lab members who have been great colleagues and friends. They all made my workplace an enjoyable, respectful and intellectual atmosphere. Thanks to Dr. Zheng-Mei Xiong for teaching me many basic experimental techniques of stem cell differentiation during my first year in Cao lab. I appreciate Dr. Linin Sun for experimental help and insightful discussions. Thanks to Mason Trappio for making my work so much easier. I also thank fellow graduate and undergraduate students Xiaojing Mao, Huijing Xue, Reynold Yu, Sahar Vakili, Neelesh Mapparapu, and Ami Thaivalappil, for exciting scientific discussions and collaborations.

Finally, very special thanks to my dearest family for their endless support and encouragement throughout my life. I am grateful to be blessed with the family who always motivated me to enjoy every moment of my life, and raised me to become who I am today. Thanks to Heli, the love of my life, who encourages me to do my best and cherish my life. I also appreciate my friends for their motivation and support.

Once again, I would like to thank everyone who helped me to achieve my doctoral study. I am excited to take one step forward and to begin another chapter in my future endeavors, and keep pursuing my intrinsic passion.

Table of contents

Dedication -----	ii
Acknowledgements -----	iii
Table of contents -----	v
List of figures -----	ix
List of tables -----	xii
List of abbreviations -----	xiii
Publication information -----	xvii
Chapter 1: Introduction-----	1
1.1 Hutchinson-Gilford Progeria Syndrome -----	1
1.1.1 Laminopathies -----	1
1.1.2 General description of HGPS: A historical perspective-----	2
1.1.3 Clinical manifestations of HGPS-----	3
1.1.4 Molecular basis of HGPS -----	4
1.2 Functions of the nuclear lamins-----	6
1.2.1 Post-translational modifications of lamin A -----	9
1.2.2 HGPS cellular and molecular phenotypes-----	11
1.3 Cardiovascular disorders in HGPS patients: A model for studying normal aging-associated heart disease-----	13
1.3.1 Role of vascular SMC and ECs in HGPS-associated cardiovascular dysfunction-----	16
1.3.2 Endothelial dysfunction in HGPS-----	16
1.3.3 HGPS treatment strategies-----	19

1.3.4	CRISPR/Cas9-mediated adenine base editors (ABEs) as the most promising HGPS treatment-----	21
1.4	Vascular microphysiological systems to model disease-----	24
1.5	Significance of the dissertation -----	27

Chapter 2: Characterize iPSC-derived normal and HGPS vascular

	endothelial cells -----	29
2.1	Introduction-----	29
2.2	Results -----	30
2.2.1	iPSC-derived EC differentiation strategy -----	30
2.2.2	HGPS iPSC-EC express mature EC surface markers-----	32
2.2.3	HGPS iPSC-ECs exhibit abnormal nuclear morphology-----	34
2.2.4	HGPS iPSC-ECs exhibit functional defects in forming capillary-like microvascular networks-----	35
2.3	Discussion -----	38

Chapter 3: Examine the underlying molecular mechanisms of HGPS

	endothelial dysfunction-----	40
3.1	Introduction-----	40
3.2	Results-----	41
3.2.1	HGPS iPSC-ECs exhibit reduced total eNOS expression and activity-----	41
3.2.2	HGPS iPSC-ECs are not able to upregulate eNOS in response to	

shear stress-----	44
3.2.3 HGPS iPSC-ECs angiogenic incompetence is eNOS dependent-----	47
3.2.4 Upregulation of TIMP1, TIMP2, and reduced expression of MMP-9 in HGPS iPSC-----	50
3.2.5 Adenine base editors (ABEs) efficiently correct the pathogenic HGPS mutation in HGPS iPSC-ECs-----	51
3.2.6 ABEs reduce progerin expression and rescue nuclear abnormalities in HGPS iPSC-ECs-----	53
3.2.7 ABEs restore intracellular NO level in HGPS iPSC-ECs-----	55
3.2.8 ABEs normalize TIMPs and increase angiogenic competence in HGPS iPSC-ECs -----	56
3.3 Discussion-----	57

Chapter 4: Elucidate the molecular mechanisms in 3D *in vitro* vascular

tissue model -----	60
4.1 Introduction-----	60
4.2 Results-----	61
4.2.1 Develop and characterize Tissue Engineered Blood Vessel model for normal and HGPS using iPSC-derived SMCs and ECs----	61
4.2.2 HGPS TEBVs exhibited decreased expressions of contractile proteins, and increased progerin and extracellular matrix proteins--	64
4.2.3 HGPS ECs affect TEBVs function-----	65

4.2.4 HGPS TEBVs exhibit inflammation-----	66
4.3 Discussion-----	67
Chapter 5: Summary and future directions-----	69
5.1 Summary-----	69
5.2 Future directions-----	71
Chapter 6: Material and methods-----	75
6.1 Endothelial and smooth muscle cells differentiation-----	75
6.2 Adenine base editor lentiviral vector cloning-----	76
6.3 Lentiviral production-----	77
6.4 Fabrication of fluidic chambers-----	78
6.5 Immunocytochemistry-----	79
6.6 Western blotting-----	79
6.7 RNA extraction, cDNA synthesis, and RT-qPCR-----	80
6.8 Nitric Oxide assays-----	81
6.9 Tube formation assay-----	81
6.10 TEBV fabrication and functional testing-----	82
6.11 Vessel vasoactivity assay-----	83
6.12 Statistical analysis-----	84
Appendices-----	86
Bibliography-----	88

List of figures

Chapter 1: Introduction

Figure 1-1: Scheme of the classic HGPS mutation in the <i>LMNA</i> gene-----	6
Figure 1-2: The lamin A and progerin processing-----	11
Figure 1-3: Fibrosis of the adventitia and atherosclerosis in HGPS -----	14
Figure 1-4: Cardiac fibrosis, adventitial thickening, and loss of capillary density in endothelial progerin expressing mouse models-----	18
Figure 1-5: ABE-mediated A•T to G•C base editing strategy-----	24

Chapter 2: Characterize iPSC-derived normal and HGPS vascular

endothelial cells

Figure 2-1: Schematic illustration of the ECs differentiation strategy for human iPSCs-----	31
Figure 2-2: Characterization of iPSC-derived ECs-----	33
Figure 2-3: Nuclear abnormality of HGPS iPSC-ECs-----	34
Figure 2-4: Capillary-like microvascular network formation defects in HGPS iPSC-ECs-----	36
Figure 2-5: Microvascular networks at different cell densities and time course----	37
Figure 2-6: Capillary-like microvascular network formation defects in progerin overexpressed HUVECs-----	38

**Chapter 3: Examine the underlying molecular mechanisms of HGPS
endothelial dysfunction**

Figure 3-1: Downregulation of eNOS expression and activity in HGPS
iPSC-ECs ----- 43

Figure 3-2: Downregulation of eNOS expression and activity in
progerin-overexpressed HUVECs ----- 44

Figure 3-3: Inability to upregulate eNOS expression in HGPS iPSC-ECs under
shear stress----- 47

Figure 3-4: HGPS iPSC-ECs exhibit lower NO bioavailability in response to
NO donor, SNAP----- 48

Figure 3-5: HGPS iPSC-ECs' angiogenic incompetence is eNOS dependent----- 50

Figure 3-6: Upregulation of TIMP1, TIMP2, and a reduced expression of
MMP-9 in HGPS iPSC-ECs----- 51

Figure 3-7: Correction of HGPS causing mutation by ABE in HGPS iPSC-ECs---- 53

Figure 3-8: Reduction of progerin expression, and rescue of the HGPS nuclear
blebbing phenotype in ABE-corrected HGPS ECs----- 54

Figure 3-9: ABEs restore intracellular NO level in HGPS iPSC-ECs ----- 56

Figure 3-10: ABEs normalize TIMPs and efficiently and increase angiogenic
competence in HGPS iPSC-ECs----- 57

**Chapter 4: Elucidate the molecular mechanisms in 3D *in vitro* vascular
tissue model**

Figure 4-1: Characterization of human iPSC-derived smooth muscle cells----- 63

Figure 4-2: Schematic diagram to develop iPSC-derived TEBVs from healthy
and HGPS patients -----64

Figure 4-3: Characterization of TEBVs fabricated from iPSC-derived vascular
SMCs and ECs of normal and HGPS donors -----65

Figure 4-4: Effects of HGPS ECs on TEBV function----- 66

Figure 4-5: HGPS TEBVs exhibit inflammation----- 67

Chapter 5: Summary and future directions

Figure 5-1: Co-culturing of human iPSC-SMC and ECs form vessel-like structures
on matrigel-based matrix in 24 hours----- 72

Figure 5-2: Experimental setup of perfusion-based bioreactor----- 74

List of table

Table 1: Primer sequences used for RT-PCR experiment-----	85
---	----

List of abbreviations

53BP1	p53 binding protein 1
ABE	Adenine base editor
AON	Antisense oligonucleotide
AAV9	Adeno-associated virus 9
BAC	Bacterial artificial chromosome
BMP4	Bone morphogenic protein-4
BRCA1	Brest cancer 1
CAAX	C: cysteine, A: aliphatic amino acids X: an amino acid
Cas9	CRISPR associated protein 9
CDH5	Cadherin 5
CDK	Cyclin dependent kinase
CRISPR	Clustered regularly interspaced short palindromic repeats
CVD	Cardiovascular disease
DAF-FM	4-Amino-5-Methylamino-2',7'-Difluorescene Diacetate
EC	Endothelial cell
ECM	Extra cellular matrix
EDHF	Endothelium-derived hyperpolarizing factor
EV	Extracellular vesicle
eNOS	Endothelial nitric oxide synthase
FTase	Farnesyltransferase
FTI	Farnesyltransferase inhibitor

GAPDH	Glyceraldehyde 3-phosphate dehydrogenase
GFP	Green florescent protein
GSK3 β	Glycogen synthase kinase-3 beta
HDL	High density lipoprotein
HDR	Homology Directed repair
HGPS	Hutchinson-Gilford Progeria Syndrome
HR	Homologous recombination
HUVEC	Human umbilical vein endothelial cell
ICAM-1	Intracellular adhesion molecule 1
ICMT	Isoprenyl cysteine carboxy methyltransferase
INS	Inner nuclear membrane
iPSC	Induced pluripotent stem cell
LA	Lamin A
LDL	Low density lipoprotein
L-NAME	N-omega-Nitro-L-arginine methylester hydrochloride
miRNA	Micro RNA
MMP	Matrix metalloproteinase
MPS	Microphysiological systems
MYH11	Myosin heavy chain 11
NAC	N-actyl cysteine
NHEJ	Nonhomologous end joining
NO	Nitric oxide
PAM	Protospacer adjacent motif

PECAM-1	Platelet and endothelial cell adhesion molecule 1
PDGF-BB	Platelet-derived growth factor BB
Pg	Progerin
PGA	Polyglycolic acid
PLGA	Poly lactide-coglycolide
PP1	Protein phosphatase 1
pThr495	Phosphorylation at threonine-495
PWV	Pulse wave velocity
ROCK	rho-associated protein kinase
ROS	Reactive oxygen species
RT-PCR	Real time polymerase chain reaction
SIRT1	Sirtuin 1
SMA	Smooth muscle actin
SMC	Smooth muscle cell
SNAP	S-Nitro-N-acetyl-DL-penicillamine
sgRNA	Single guide ribonucleic acid
SRSF	Serine/arginine rich splicing factor
TEBV	Tissue engineered blood vessel
TIMP	Tissue inhibitor metalloproteinase
VCAM-1	Vascular cell adhesion molecule 1
VE-cadherin	Vascular endothelial cadherin
VEGF	Vascular endothelial growth factor
vWF	von Willebrand factor

WS Werner's syndrome
XLB3 Xenopus lamin B3
ZYMPSTE24 Zinc metallopeptidase STE24

Publication information

The data from this dissertation composed the following publications (Atchison et al., 2020; Gete et al., 2021):

Gete YG, Koblan LW, Mao X, Trappio M, Mahadik B, Fisher JP, Liu DR, Cao K. Mechanisms of angiogenic incompetence in Hutchinson-Gilford progeria via downregulation of endothelial NOS. *Aging Cell*. 2021 Jul;20(7):e13388.

Atchison L, Abutaleb NO, Snyder-Mounts E, **Gete Y**, Ladha A, Ribar T, Cao K, Truskey GA. iPSC-Derived Endothelial Cells Affect Vascular Function in a Tissue-Engineered Blood Vessel Model of Hutchinson-Gilford Progeria Syndrome. *Stem Cell Reports*. 2020 Feb 11;14(2):325-337.

Chapter 1: Introduction

1.1 Hutchinson-Gilford Progeria Syndrome (HGPS)

1.1.1 Laminopathies

Recently, nuclear lamin proteins have gained surge of interest because of discoveries of numerous lamin mutations, which are associated with around 20 genetic diseases, collectively known as the laminopathies (Capell & Collins, 2006; Dittmer & Misteli, 2011). On the basis of the tissue affected, laminopathies roughly divided into four groups, (1) disease of the muscle, (2) lipodystrophy syndromes, (3) peripheral neuropathy, and (4) accelerated aging disorders which affect multiple tissues (de Leeuw, Gruenbaum, & Medalia, 2018; Worman & Bonne, 2007).

The first group of laminopathies affect skeletal and cardiac muscle cells, which range from muscle-wasting muscular dystrophies to cardiac condition defects (Dittmer & Misteli, 2011). These include Emery–Dreifuss muscular dystrophy (EDMD), Limb–Girdle muscular dystrophy type 1B (LGMD1B), *LMNA*-related congenital muscular dystrophy (LCMD), and dilated cardiomyopathy with conduction disease (DCM-CD). The second group are lipodystrophy syndrome, which specifically affect adipose tissues, including Dunnigan-type familial partial lipodystrophy (FPLD) and generalized lipodystrophy. The third group are neuropathy, which affect the motor and sensory neurons of the peripheral nervous system. These include the peripheral neuronal disease Charcot–Marie–Tooth (AD-CMT), and generalized neuropathy. The last group are

systemic laminopathies that affect multiple tissues, and are associated with accelerated aging disorders. These include Hutchinson–Gilford progeria syndrome (HGPS), and atypical Werner’s syndrome (WS) (Capell & Collins, 2006; Dittmer & Misteli, 2011; Worman & Bonne, 2007). Most of the disease-causing mutations are missense mutations and they are distributed all along the *LMNA* gene (Dittmer & Misteli, 2011), suggesting a closely associated role of *LMNA* with human aging.

In contrast to *LMNA*, only two diseases are reported to be associated with mutations in the *LMNB1* and *LMNB2* genes, which is probably due to the ubiquitous expression and the importance B-type lamin for viability of mammalian cells (Harborth, Elbashir, Bechert, Tuschl, & Weber, 2001). These include autosomal-dominant leukodystrophy caused by a duplication of *LMNB1* that resulting in higher *LMNB1* expression in brain tissues and acquired partial lipodystrophy caused by several rare *LMNB2* missense mutations (Hegele et al., 2006; Padiath et al., 2006). Despite several studies, the pathological mechanisms of laminopathies, and how the different mutations on the single *LMNA* gene affect its function and lead to a wide range of tissue specific diseases remain unclear.

1.1.2 General description of HGPS : A historical perspective

HGPS is a rare human genetic disease with features of premature aging and occurs in 1 in every 4-8 million live births, affecting both sexes and all races equally (Capell & Collins, 2006; Merideth et al., 2008). As of October 2021, there are 133 known children diagnosed with HGPS around the world (Progeria Research Foundation). Progeria is derived from Greek and means “prematurely old.” The classic HGPS was first

described at the end of the nineteenth-century by Dr. Jonathan Hutchinson and Dr. Hastings Gilford, respectively (Gilford, 1897; Hutchinson, 1886). From 1886 to 2003, HGPS patients were diagnosed by their physical appearance, the so-called “old mannish” look that includes a disproportionally big head, loss of body fat and hair, joint contractures, prominent eyes, thin lips, pointed nose, wrinkled and thin skin, and extreme thinness (Benedicto, Dorado, & Andres, 2021; DeBusk, 1972; Hennekam, 2006). Despite different ethnic backgrounds, children have remarkably similar appearances.

In 2003, the heterozygous *de novo* mutation responsible for HGPS was found within exon 11 of the *LMNA* gene (c.1824C>T, p.G608G) (Eriksson et al., 2003). This mutation activates a cryptic splice donor site that results in mRNA mis-splicing and that ultimately removes 150 nucleotides (50 amino acids), leading to the expression of a lamin A mutant variant called progerin (De Sandre-Giovannoli et al., 2003; Eriksson et al., 2003). Progerin is expressed in most differentiated cells and induces multiple cellular and physiological abnormalities, including defects in nuclear morphology, chromatin disorganization, elevated DNA damage, impaired stem cell maintenance and differentiation, metabolic alterations, autophagy deregulation, and systemic inflammation (Gordon, Rothman, Lopez-Otin, & Misteli, 2014). HGPS patients manifest extreme phenotypes and mainly die in their teens due to cardiovascular diseases (Merideth et al., 2008).

1.1.3 Clinical manifestations of HGPS

HGPS patients appear normal at birth but start to develop premature aging symptoms between 1 and 2 years of age (Merideth et al., 2008). Children with HGPS exhibit major premature aging features that include failure to thrive, alopecia, skin

abnormalities, loss of subcutaneous fat, muscle weakness, osteoporosis, progressive joint contractures, and severe atherosclerosis and cardiac dysfunction, causing premature death at the average age of 14.6 years mainly due to myocardial infarction or stroke (M. R. Hamczyk, del Campo, & Andres, 2018; Merideth et al., 2008; Ullrich & Gordon, 2015). Skin defects are identified by wrinkling, sclerotic skin, and dimpling, while the weak bone architecture is often noted by the problems associated with distal joint and phalanges (Merideth et al., 2008).

In 2008, M. A Merideth *et al.* reported clinical characterization of 15 HGPS patients. The majority of the patients had elevated platelet counts, prolonged prothrombin time, and elevated serum phosphorus. The patients also manifested age-dependent impaired vascular functions that include elevated blood pressure, increased arterial augmentation rate, and adventitial thickening (Merideth et al., 2008). In 2010, M. Olive *et al.* reported structural and immunological comparison of HGPS patients who died of myocardial infarction and non-HGPS individuals. Atherosclerosis in HGPS patients and in normally aged individuals had similar features, including severe stenosis, extensive arterial calcification, inflammation, and evidence of rupture (Olive et al., 2010).

1.1.4 Molecular basis of HGPS

HGPS is a rare, autosomal dominant disorder characterized by phenotypes reminiscent of premature aging (Burtner & Kennedy, 2010). The majority of HGPS cases are caused by a single *de novo* point mutation in the *LMNA* gene (c.1824C > T; p.G608G) located at chromosome 1q21.2 – q21.3 (Eriksson et al., 2003). HGPS mutation is *de novo* mutation, meaning it is a newly arisen sporadic mutation but not inherited

from parents (Eriksson et al., 2003). This mutation activates a cryptic splice donor in exon 11 of the lamin A gene that results in mRNA mis-splicing and that ultimately removes 150 nucleotides (50 amino acids) from the C-terminal portion of the translated protein product. These 50 amino acids include an important proteolytic cleavage site that removes the farnesylated C-terminus from prelamin A to form mature lamin A. Lack of this cleavage site results in the production of a persistently farnesylated, truncated lamin A protein variant called progerin (De Sandre-Giovannoli et al., 2003; Eriksson et al., 2003). Progerin is kept attached to inner nuclear membrane (INM), which prevents from progerin release from lipid anchor, and it affects the nuclear morphology (Goldman et al., 2004). Moreover, progerin affects chromatin organization and alters the gene expressions (Csoka et al., 2004; Gonzalo & Kreienkamp, 2015; McCord et al., 2013).

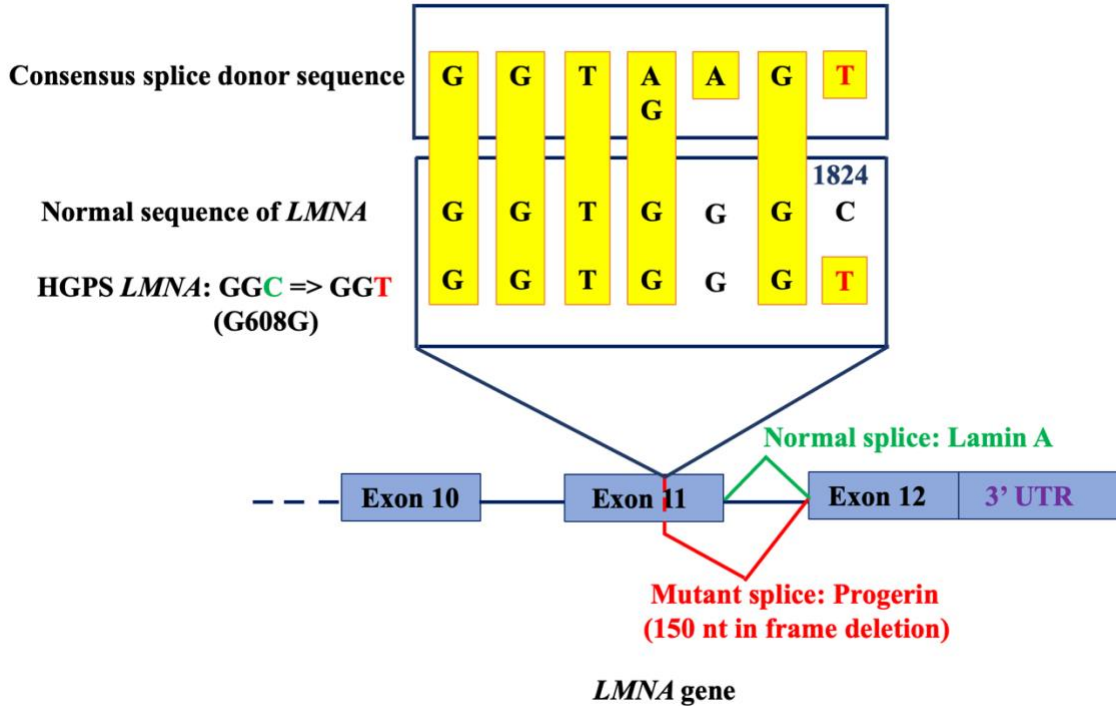


Figure 1-1: Scheme of the classic HGPS mutation in the *LMNA* gene. The 1824 cysteine in the wild type *LMNA* sequence was mutated into thymine in HGPS (indicated by red), making the sequence closer to the consensus splice donor sequence. This mutation activates a cryptic splice donor site that can be recognized by the spliceosome, resulting in a 150 nucleotides in frame deletion and yield a mutant lamin A protein called progerin. The figure adapted and modified with permission from (Eriksson et al., 2003).

1.2 Functions of the nuclear lamins

The nuclear lamins are type V intermediate filament proteins that locate at the interface between chromatin and the inner nuclear membrane (Dittmer & Misteli, 2011). The lamin proteins are divided into A and B types based on structural and protein expression patterns. Mammalian lamin genes encode *LMNA*, *LMNB1* and *LMNB2*, which express at least seven protein isoforms. The *LMNA* gene mainly encodes two A type lamins: lamin A and lamin C (Capell & Collins, 2006). *LMNA* also encodes two minor products: lamin A Δ 10 and lamin C2 (H. Zhang, Kieckhafer, & Cao, 2013). In addition to A type lamins, there are three B type lamin proteins: lamin B1 encoded by *LMNB1*, lamin B2 and lamin B3 encoded by *LMNB2*. While A type lamins are highly regulated throughout mammalian development and exclusively expressed in differentiated somatic cells, B type lamins are present ubiquitously in all cell types (Burke & Stewart, 2013; Capell & Collins, 2006).

As lamins are intermediate filament superfamily proteins, they involve in the maintenance of nuclear shape and mechanical stability (Dechat, Adam, Taimen, Shimi, & Goldman, 2010; Goldman, Gruenbaum, Moir, Shumaker, & Spann, 2002). In support of this, cells either deficient in lamins or expressing mutant lamin protein usually display misshapen nuclei, and impaired viability under mechanical strain (Goldman et al., 2004;

Houben, Ramaekers, Snoeckx, & Broers, 2007). Apart from serving as a scaffold to the nucleus in the cell, nuclear lamina participates in important cellular processes, including chromatin remodeling, DNA replication, DNA damage response, and transcription (Burke & Stewart, 2006; Dittmer & Misteli, 2011; Gruenbaum & Foisner, 2015).

Nuclear lamins in chromatin organization: Lamins are global regulators of chromatin and have at least two chromatin binding regions (Dechat, Adam, & Goldman, 2009; Dittmer & Misteli, 2011). The roles of lamins in the regulation of chromatin were illustrated in studies of cardiomyocytes and mouse embryonic fibroblasts (MEFs) derived from *Lmna* deficient mice, which revealed a partial loss of peripheral heterochromatin, ectopic chromosome condensation and mis-positioning of centromeric heterochromatin (Galiouva, Bartova, Raska, Krejci, & Kozubek, 2008; Nikolova et al., 2004). Moreover, global heterochromatin changes induced by lamin perturbation are often observed by altered levels of chromatin-associated epigenetic histone marks, including decreased levels of the heterochromatin markers histone H3 lysine 9 trimethylation (H3K9me₃), H3K27me₃, and increased levels of H4K20me₃ (Dechat et al., 2010; Dittmer & Misteli, 2011; Hakelien, Delbarre, Gaustad, Buendia, & Collas, 2008; McCord et al., 2013).

Nuclear lamins in DNA replication: Lamins have also been implicated in DNA replication. At the onset of mitosis, nuclear lamina is phosphorylated by cyclin B/CDK1, which leads to its disassembly and allows mitotic spindles to interact with kinetochores (Hagting, Jackman, Simpson, & Pines, 1999; Stuurman, Heins, & Aebi, 1998). During this process, B type lamins are associated with disassembled nuclear envelopes while A type lamins are soluble and distributed evenly in the entire cell till the end of mitosis

(Cao, Capell, Erdos, Djabali, & Collins, 2007; Dechat et al., 2008). The evidence of lamin in DNA replication comes from studies that demonstrated in assembly systems, lamin deficient *Xenopus* extracts produce nuclei that cannot replicate their DNA (Meier, Campbell, Ford, Stick, & Hutchison, 1991). Moreover, the expression of dominant-negative lamin B mutants has been shown to inhibit DNA replication (Spann, Moir, Goldman, Stick, & Goldman, 1997).

Nuclear lamins in DNA damage and repair: A number of recent studies have shown the important role of lamins in DNA damage repair. Most DNA damage and repair studies focused on the expression of progerin, the toxic mutant lamin A variant that causes HGPS. Cells expressing progerin have a defect in recruiting the repair factor p53-binding protein (53BP1) to the sites of DNA damage that is evidenced by the increased levels of the double-stranded break marker gamma H2AX, and are more sensitive to DNA damage agents (B. Liu et al., 2005). Moreover, progerin expression also affects expressions of the crucial DNA damage regulators ATR and ATM, and the double-stranded break repair factors Rad50 and Rad51 (Manju, Muralikrishna, & Parnaik, 2006; H. Zhang et al., 2016). Although the mechanisms of lamins in DNA damage and repair have yet to be elucidated, the current studies suggest the important role of lamins in DNA damage and repair.

Nuclear lamins in transcription: Several studies have reported the roles of lamins in transcriptional regulation. Perturbation of lamin organization by dominant negative A-type lamin mutants inhibits RNA polymerase II transcription and disrupts the localization of the initiation factor TATA-binding protein (Kumaran, Muralikrishna, & Parnaik, 2002;

Spann, Goldman, Wang, Huang, & Goldman, 2002). Lamin A/C also associates with numerous transcriptional regulators, either directly or indirectly, including Rb, Gcl, Mok2, cFos and Srebp1 (Zastrow, Vlcek, & Wilson, 2004). Hence, lamins bind many transcriptional regulators and can affect gene expression either by sequestration of the factors or by influencing the assembly of core transcriptional complexes (Gonzalez, Navarro-Puche, Casar, Crespo, & Andres, 2008).

1.2.1 Post-translational modifications of lamin A

LMNA gene mainly encodes for the inner nuclear membrane proteins lamin A and C, two major structural components of the eukaryote cell nucleus (Goldman et al., 2002). Lamin A is synthesized via a prelamin A intermediate, and undergoes multistep post-translational processing. First, cysteine is farnesylated by farnesyltransferase on its C-terminal CaaX motif, then the remaining three amino acids are cleaved by the zinc metalloprotease ZMPSTE24. The C-terminal cysteine is then carboxymethylated by the isoprenylcysteine carboxyl methyltransferase (ICMT). Finally, the last 15 amino acids are cleaved again by ZMPSTE24 to produce the unfarnesylated, mature lamin A. The HGPS causing mutation activates a cryptic splice site in exon 11 of the *LMNA* gene resulting in the deletion of 50 amino acids near the C terminus, abolishing the second ZMPSTE24 cleavage site and producing a truncated and permanently farnesylated prelamin A called progerin that incorporates abnormally into the nuclear lamina and causes multiple toxic effects to the cells (Dechat et al., 2008; Eriksson et al., 2003; Goldman et al., 2004; Young, Yang, Davies, Jung, & Fong, 2013) (Figure 1-2).

Progerin antagonizes normal lamin A function in a dominant-negative manner, leading to nuclear abnormalities (Booth-Gauthier et al., 2013; Goldman et al., 2004;

Xiong et al., 2016), genomic instability (Gonzalo & Kreienkamp, 2015; H. Zhang et al., 2016; H. Zhang, Xiong, & Cao, 2014), alters redox homeostasis (N. Kubben et al., 2016; Xiong et al., 2017), changes chromatin structure, and histone methylation (Shumaker et al., 2006).

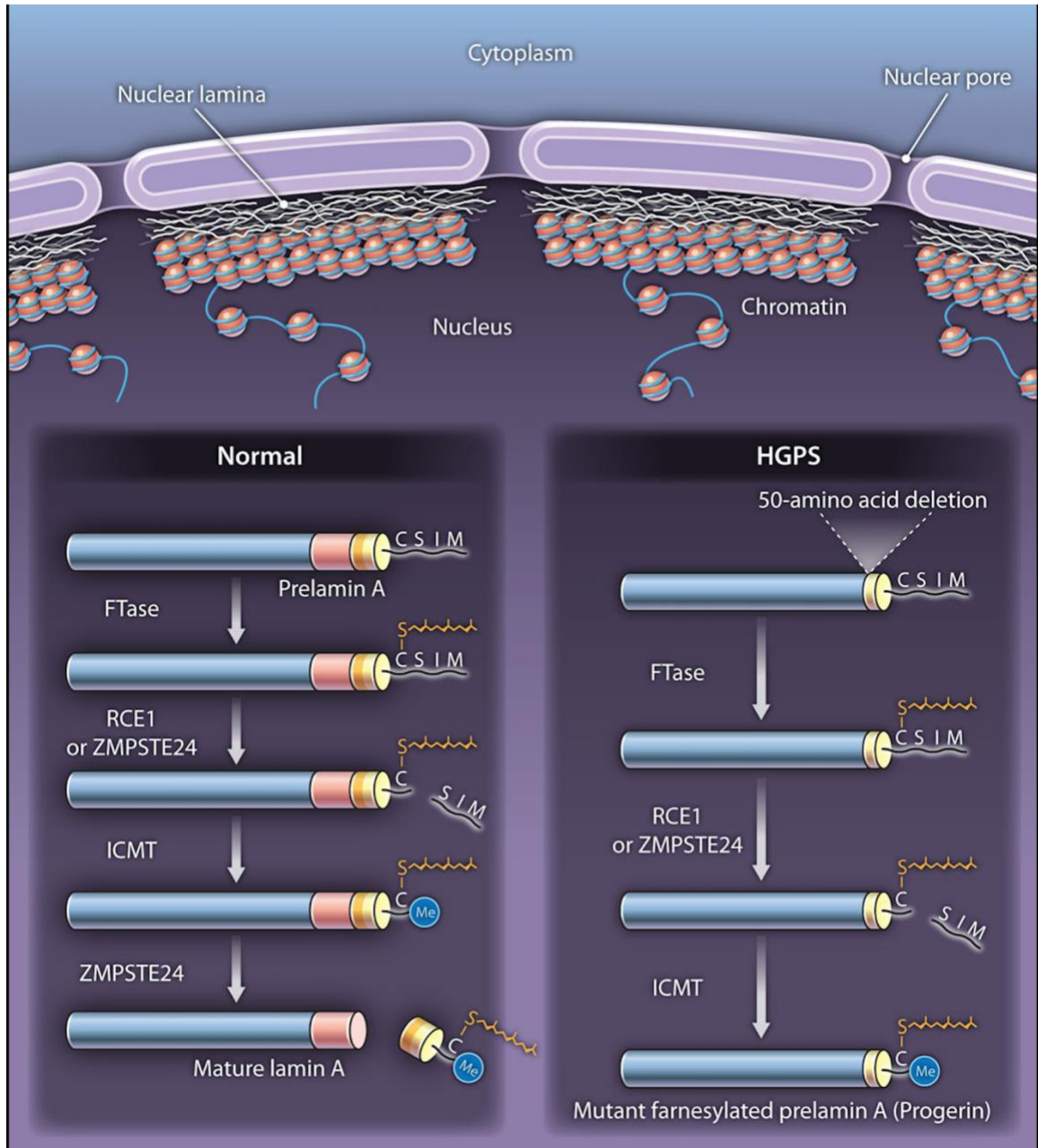


Figure 1-2: The lamin A and progerin processing. Prelamin A undergoes four posttranslational processing steps. First, the cysteine of the carboxyl-terminal *CaaX* motif (–CSIM) is farnesylated by FTase. Second, the last three amino acids (–SIM) are clipped off by either RCE1 or ZMPSTE24. Third, the newly exposed carboxyl-terminal farnesyl cysteine is methylated by protein-S-isoprenyl cysteine O-methyltransferase (ICMT). Fourth, the carboxyl-terminal 15 amino acids of the protein (the orange and yellow segments), including the farnesyl cysteine methyl ester, are clipped off by ZMPSTE24, producing mature lamin A (the blue and red segments). HGPS is caused by a point mutation in codon 608 of prelamin A that changes mRNA splicing, resulting in a 50–amino acid deletion in prelamin A (the red and orange segments). This deletion eliminates the ZMPSTE24 cleavage site, preventing the biogenesis of lamin A and resulting in the accumulation of a farnesylated, internally truncated prelamin A called progerin. The figure adapted with permission from (Young et al., 2013).

1.2.2 HGPS cellular and molecular phenotypes

Although the mechanistic details leading to HGPS pathology are not fully elucidated, key cellular responses have been identified. HGPS characterized by abnormal nuclear morphology, altered chromatin structure and epigenetic modifications, defective DNA damage repair and genome instability, altered redox homeostasis, and mitochondrial dysfunctions (Cao et al., 2007; Dechat et al., 2010; Dittmer & Misteli, 2011; Goldman et al., 2004; Xiong et al., 2016; Xiong et al., 2017; H. Zhang et al., 2016). The permanently farnesylated feature of progerin disrupts the spatial distribution of nuclear pore complex and alters nuclear shape (Goldman et al., 2004). Thus, nuclear blebbing phenotype is the hallmark of HGPS nucleus.

Progerin also affects global chromatin structure and epigenetic markers. These evidenced by altered levels of chromatin-associated epigenetic histone marks, including decreased levels of the heterochromatin markers histone H3 lysine 9 trimethylation

(H3K9me3), H3K27me3, and increased levels of H4K20me3 (Dechat et al., 2010; Dittmer & Misteli, 2011; Hakelien et al., 2008).

In addition, HGPS cells are characterized by defective DNA damage and genome instability. This was illustrated in study expressing progerin reveal a defect in recruiting the repair factor p53-binding protein (53BP1) to the sites of DNA damage that was evidenced by the increased levels of the double-stranded break marker gamma H2AX, and were more sensitive to DNA damage agents (B. Liu et al., 2005; H. Zhang et al., 2016). Moreover, progerin expression also affects expressions of the crucial DNA damage regulators ATR and ATM, and the double-stranded break repair factors Rad50 and Rad51 (Manju et al., 2006; H. Zhang et al., 2016).

Progerin also activates the pro-inflammatory nuclear factor kappa B (NF- κ B) pathway; it decreases the activity of the deacetylase Sirtuin1 (SIRT1) (Baohua Liu et al., 2012) which regulates the antioxidant activity and energy balance. In addition, progerin impairs antioxidant capability as observed by reduced NRF2 levels (Magda R. Hamczyk et al., 2019; Nard Kubben et al., 2016). Consequently, reactive oxygen species (ROS) levels increase which causes double stranded DNA breaks, inhibiting proliferation and producing cell senescence (Shane A. Richards, Joanne Muter, Pamela Ritchie, Giovanna Lattanzi, & Christopher J. Hutchison, 2011; H. Zhang et al., 2016).

Mitochondrial deficiency is also a typical feature of HGPS cells. First evidence of mitochondrial dysfunction in HGPS was demonstrated in the study that revealed down-regulation of mitochondrial phosphorylation proteins in HGPS patients compared to healthy subjects (Rivera-Torres et al., 2013). Similarly, mitochondrial ATP synthesis was reduced in HGPS fibroblast (Pagano et al., 2014). Studies from our lab also revealed that

HGPS fibroblasts display swollen and fragmented mitochondria (Xiong et al., 2016; Xiong et al., 2017). Moreover, the HGPS cells exhibited disrupted mitochondrial membrane potentials and increased ROS (Xiong et al., 2016).

1.3 Cardiovascular disorder in HGPS patients: A model for studying normal aging-associated heart disease

The main cause of death in most HGPS patients is cardiovascular failure, so it is crucial to decipher the underlying mechanisms to design therapies (P. B. Baker, Baba, & Boesel, 1981; Gordon et al., 2014). The data accumulated over two decades indicate that the key cardiovascular phenotypes in HGPS patients are accelerated atherosclerosis, vascular stiffening, prominent medial and adventitial fibrosis, calcification, vascular SMC loss, left ventricle diastolic dysfunction, and cardiac valve disease, which collectively lead to premature death from myocardial infarction or stroke (Benedicto et al., 2021; Gordon et al., 2014; M. R. Hamczyk & Andres, 2018; Merideth et al., 2008). Interestingly, there are many similarities between cardiovascular pathology of HGPS patients and normal old individuals (Olive et al., 2010).

Like normal physiological aging, noninvasive imaging and autopsy in HGPS patients indicate atherosclerosis and cardiovascular calcification (Merideth et al., 2008). In a compiled report of four HGPS cases, F. L. DeBusk reported that most HGPS patients die of heart failure or myocardial infarction due to primarily coronary atherosclerosis, and varying degrees of generalized atherosclerosis affecting the large arteries (DeBusk, 1972). Another common feature in physiological aging and HGPS is vascular calcification that affects the aorta and mitral valves, and is a cause for CVD-associated

morbidity in both populations. In a review of 12 HGPS patient autopsies, P. B. Baker *et al.* also reported that atherosclerosis related coronary artery occlusion and calcification of the aortic mitral valves were common (P. B. Baker *et al.*, 1981).

In addition, HGPS is also characterized by vessel stiffening, which is noninvasively calculated from the pulse wave velocity (PWV). PWV is a highly reliable, blood pressure-independent predictor of cardiac events (Gerhard-Herman *et al.*, 2012; M. R. Hamczyk *et al.*, 2018). Analysis of a 21-patient cohort by M. Gerhard-Herman *et al.* revealed that all the HGPS patients exhibited vascular stiffening, evidenced by high carotid-femoral PWV values comparable to those adults older than 60 years that were corroborated by other studies (Gerhard-Herman *et al.*, 2012; Prakash *et al.*, 2018). Hence, HGPS was classified as a disease of vascular stiffening similar to CVD in normal aging. Subsequently, PWV and arterial wall echodensity became major cardiovascular readouts of therapeutic efficacy in HGPS clinical trials (Benedicto *et al.*, 2021).

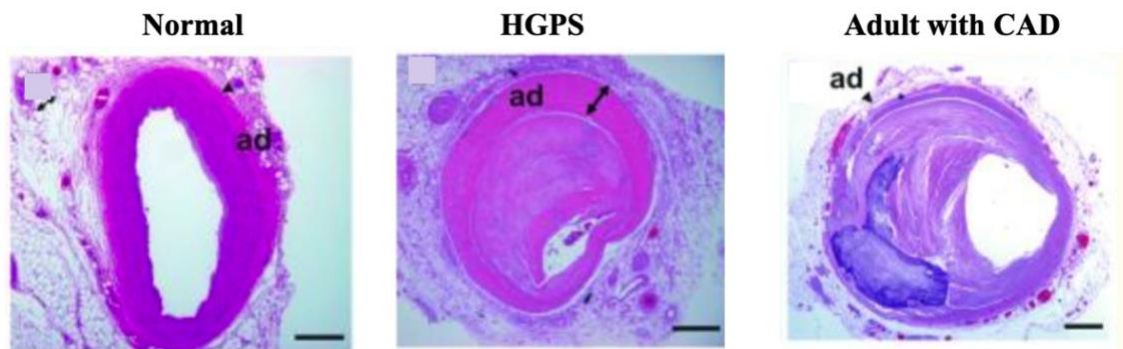


Figure 1-3: Fibrosis of the adventitia and atherosclerosis in HGPS. H&E staining of selected tissues from a 16-year-old normal, 16-year-old HGPS patient, mid-right coronary characterized by an enlarged and highly fibrotic adventitia (arrow), and a 93-year-old with advanced atherosclerosis. Arrowhead points to the adventitia. ad indicates adventitia (Scale bars: 50 μm). The figure adapted with permission from (Olive *et al.*, 2010).

The other similarity between HGPS and normal physiological aging is the expression of progerin in both populations (Burtner & Kennedy, 2010; Lopez-Otin, Blasco, Partridge, Serrano, & Kroemer, 2013). Despite being 50 fold lower than the HGPS patients, progerin is detected in normal individuals, even before teenage years (Gordon et al., 2014). This is because the classic HGPS mutation is a pre-mRNA splicing mutation, which activates a sporadic intronic splice site, present in normal individuals (Cao, Blair, et al., 2011; Cao et al., 2007; McClintock et al., 2007; Rodriguez, Coppede, Sagelius, & Eriksson, 2009; Scaffidi & Misteli, 2006). Since progerin functions in a dominant negative manner, a small accumulation could elicit sufficient toxic effects to the cells. There is accumulated evidence about the role of progerin in many aspects of generalized aging and cardiovascular health. Particularly, the atherosclerotic plaques in HGPS are similar to those found in aging individuals (Olive et al., 2010). Moreover, vascular stiffening in HGPS is much like that seen in normal aging and manifested in both populations by increased PWV (Gerhard-Herman et al., 2012).

Although many cardiovascular alterations in HGPS patients similar to physiological aging, HGPS patients lack many of the classical cardiovascular risk factors. For example, like healthy children, HGPS patients have similar levels of mean plasma cholesterol, low-density lipoprotein (LDL)-bound and high-density lipoprotein (HDL)-bound cholesterol, triglyceride, and median C-reactive protein (Gerhard-Herman et al., 2012; Gordon et al., 2016; Merideth et al., 2008). Thus, the study of the mechanisms of cardiovascular disease (CVD) in HGPS also provides a unique opportunity to identify the mechanisms of CVD in non-HGPS individuals in the absence of confounding risk factors

or aging-associated chronic diseases that can influence cardiovascular health (Gordon et al., 2014; M. R. Hamczyk et al., 2018).

1.3.1 Role of vascular SMCs and ECs in HGPS-associated cardiovascular dysfunction

Vascular SMCs and ECs are major structural and functional elements of the vessel wall and play an indispensable role in regulating vascular homeostasis and tone (Vanhoutte, Shimokawa, Feletou, & Tang, 2017). Pathological analysis of the arteries of HGPS patients indicates noticeable progerin expression in vascular SMCs and ECs. Vascular SMC loss in HGPS patient arteries is a major cause of the development of atherosclerosis (Benedicto et al., 2021; J. Zhang et al., 2011). Besides, endothelial dysfunction is a key determinant of initiation and progression of atherosclerosis. This is mainly because of the increased endothelial permeability facilitates subendothelial lipid deposition and leukocyte infiltration to into the intima that drives atherosclerosis plaque formation (Libby & Hansson, 2015). Since the individual functions of vascular SMC and EC are dependent on proper communication between these cell types, slight perturbations to this signaling circuit may generate a feedback loop with a detrimental effect on vessel structure and function (Benedicto et al., 2021).

1.3.2 Endothelial dysfunction in HGPS

The vascular endothelium plays a pivotal role in maintaining vascular homeostasis and tone by releasing various factors that regulate vascular smooth muscle cell function, inflammation, immune regulation, platelet aggregation, and thrombosis

(Gimbrone & Garcia-Cardena, 2016; Vanhoutte et al., 2017). One mechanism by which these processes are regulated by the endothelium is by activating endothelial nitric oxide synthase (eNOS), the enzyme responsible for nitric oxide (NO) production (Ignarro et al., 2001; Y. M. Yang, Huang, Kaley, & Sun, 2009). Endothelial dysfunction disrupts vascular homeostasis and tone, leading to cardiovascular disease (Gimbrone & Garcia-Cardena, 2016; Vanhoutte, 2009; Widmer & Lerman, 2014).

The role of progerin in endothelial dysfunctions and cardiovascular abnormalities has been explored in animal models. Osmanagic-Myers et al. generated VE-cadherin promoter-driven progerin in transgenic mice and showed early signs of diastolic dysfunction accompanied by cardiac hypertrophy, perivascular and interstitial fibrosis, and premature death (Osmanagic-Myers et al., 2019). Similarly, Sun et al. generated Tie2-driven progerin expression in a transgenic line and demonstrated endothelial dysfunction as a trigger of systemic aging (Sun et al., 2020) (Figure 1-4). In addition, Dorado et al. showed vascular degenerations and cardiovascular complications in a knockin minipig model of HGPS (Dorado et al., 2019). These results provide strong evidence that progerin accumulation induces defects in endothelium and cardiovascular abnormalities.

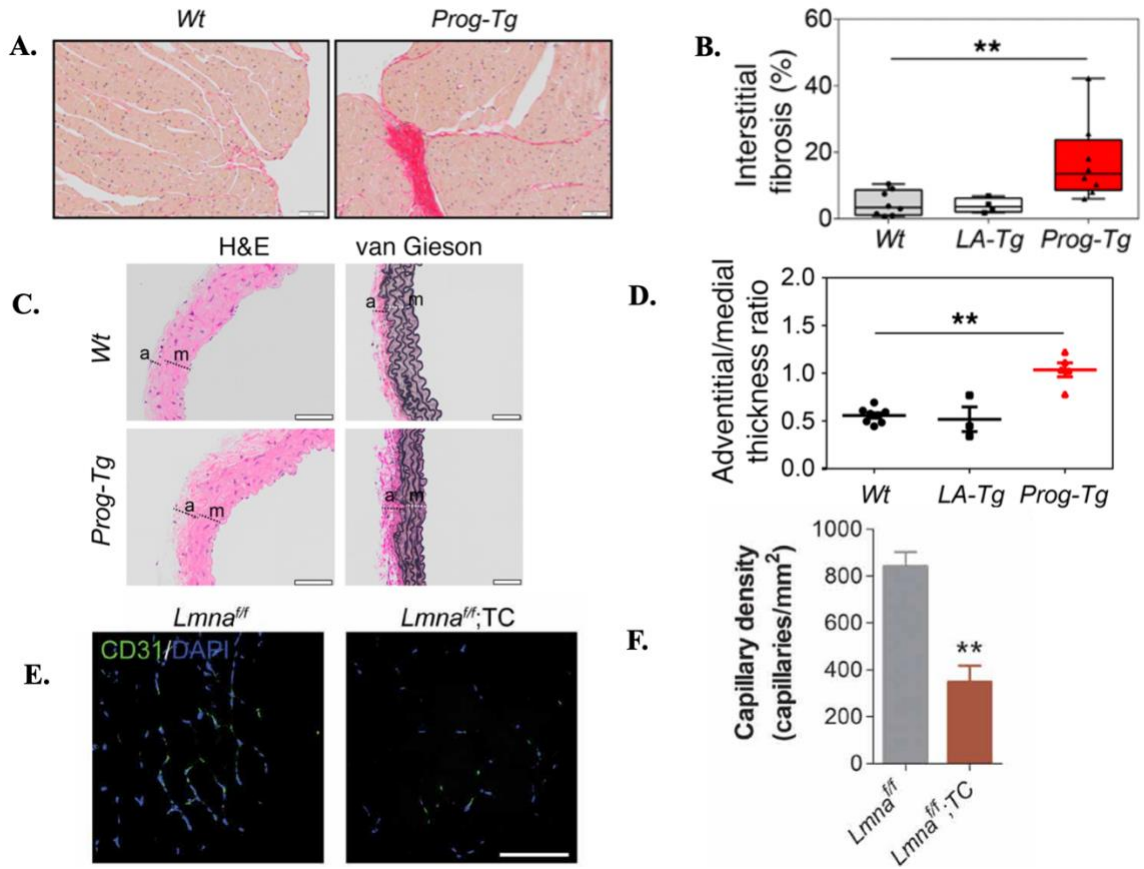


Figure 1-4: Cardiac fibrosis, adventitial thickening, and loss of capillary density in endothelial progerin expressing mouse models. (A) Representative cardiac cross sections stained with picosirius red in *Wt* and *Prog-Tg* mice. Scale bars: 50 μ m. (B) Left ventricular myocardial interstitial fibrosis ($n = 8$ *Wt* and *Prog-Tg*, $n = 4$ *LA-Tg*, age >27 weeks). Kruskal-Wallis 1-way ANOVA, multiple comparisons versus *Wt* control group reveal $*P < 0.05$ or $**P < 0.01$ for *Prog-Tg* and not significant for *LA-Tg* mice (Dunn's method). (C) Representative aorta sections stained with H&E, and van Gieson. (D) Graph shows adventitia (a) to media (m) thickness ratio ($n=8$ *Wt*, $n=3$ *LA-Tg*, $n=5$ *Prog-Tg*; age >30 weeks). One-way ANOVA, multiple comparisons versus *Wt* control group reveal $**P < 0.01$ for *Prog-Tg* and not significant for *LA-Tg* mice (Dunn's method). (E) Immunofluorescence staining, and (F) quantification of CD31⁺ gastrocnemius muscle in *Lmna*^{fl/fl};TC and *Lmna*^{fl/fl} mice. Scale bar, 50 μ m. DAPI, 4',6-diamidino-2-phenylindole. Images A-D adapted from (Osmanagic-Myers et al., 2019), and images E-F from (Sun et al., 2020) with permission.

One important process orchestrated by vascular ECs is angiogenesis, the process of sprouting new blood vessels from the existing vasculature. Angiogenesis is a major adaptive response to physiological stress and is an endogenous repair mechanism following ischemic injury (Lahtenvuo & Rosenzweig, 2012; Potente & Carmeliet, 2017; Senger & Davis, 2011). Interestingly, angiogenic defects determined by reduced myocardial perfusion and decreased vascular density were observed in both knockin minipig and endothelium-specific transgenic mouse models of HGPS (Dorado et al., 2019; Sun et al., 2020). The molecular mechanisms of progerin-induced angiogenic incompetence are currently unknown.

1.3.3 HGPS treatment strategies

Different treatment strategies have been developed for HGPS. The first approach was decreasing the progerin farnesylation using lonafarnib, a type of farnesyltransferase inhibitor (FTI) (Capell et al., 2008). In 2007, single arm clinical trial of lonafarnib showed that the treatment increased body weight, improved vascular stiffness and bone mineral density (Gordon et al., 2012; Gordon et al., 2018). To target the possible alternate prenylation of progerin that couldn't be achieved by lonafarnib alone, pravastatin and zoledronate were proposed. However, a single arm triple therapy trial using lonafarnib, pravastatin, and zoledronate on 37 participants revealed only additional bone mineral density with no major benefit beyond that were seen with lonafarnib alone (Gordon et al., 2016). After the culmination of 13 years of clinical research involving four clinical trials, in 2020 U.S. Food and Drug Administration approved lonafarnib now branded 'Zokinvy' for the treatment of HGPS. The clinical trial results show that Zokinvy treatment extends

the patient life by at least 2.5 years (Gordon et al., 2018). Everolimus, an inhibitor of mammalian target of rapamycin (mTOR), has also been proposed for HGPS therapeutics as it enhances autophagic degradation of progerin, improves abnormal nuclear shape, decreases senescence of HGPS fibroblast, and extends the lifespan of HGPS mouse model (Cao, Graziotto, et al., 2011; Graziotto, Cao, Collins, & Krainc, 2012). Recently, the study corroborated by showing genetic reduction of mTOR extends lifespan in mouse model of HGPS (Cabral et al., 2021). Currently, to acquire synergetic therapeutic effect, a phase I/II monocentric trial (NCT02579044) of everolimus in combination with lonafarnib is in progress.

The other treatment strategy focuses on inhibition of prelamin A aberrant splicing, which includes morpholino antisense oligonucleotides (Erdos et al., 2021; Lee et al., 2016; Puttaraju et al., 2021), antidiabetic metformin (Larsson et al., 2012), and MG132 (Harhoury et al., 2017). Treatment of these drugs revealed that they transcriptionally decrease the RNA binding protein splicing factor SRSF (serine/arginine-rich splicing factor) in HGPS human and mouse fibroblasts (Harhoury et al., 2018). Recently, two studies in RNA therapeutics demonstrated that antisense oligonucleotide drug, SRP-2001, decreased progerin transcript and protein expression in aorta, and increased lifespan of progeria mice over 60% (Erdos et al., 2021). Another study using RNA therapeutic drug, L-B143 also showed a 90-95% progerin transcript decrease in liver, heart and aorta of progeria mice (Puttaraju et al., 2021).

In addition, multiple approaches have been proposed to decrease the noxious downstream effects of progerin. The treatment strategies mainly counteract reactive oxygen species (ROS) generation, mitochondrial dysfunction, and inflammation

(Harhoury et al., 2018). In this regard, HGPS fibroblast treated with ROS scavenger N-acetyl cysteine (NAC) reduced unreparable DNA damage and improved cell growth in culture (S. A. Richards, J. Muter, P. Ritchie, G. Lattanzi, & C. J. Hutchison, 2011). Similarly, *in vitro* treatment of HGPS fibroblast with rho-associated protein kinase (ROCK) inhibitor (Y-27632) decreased ROS level through improving mitochondrial function (H. T. Kang et al., 2017). Xiong *et al.* have also demonstrated that Methylene Blue, a traditional mitochondrial targeting antioxidant, increases proliferation and delays senescence of HGPS fibroblasts (Xiong et al., 2016; Xiong et al., 2017). Sodium salicylate, an inhibitor of NF- κ B activation, also reduces inflammation, and extends longevity of *Lmna*^{G609G/G609G} progeria mouse model (Osorio et al., 2011). Progerin has strong binding affinity for lamin A/C and exerting a negative dominant effect (Gordon et al., 2014). Accordingly, Lee et al. identified new chemicals (JH4) that can block the interaction of progerin and lamin A/C, and the JH4 treatment improved progeroid phenotypes and increased lifespan of *Lmna*^{G609G/G609G} mouse (S. M. Kang et al., 2021; Lee et al., 2016). Therefore, treatment strategies for HGPS associated to progerin accumulation may rely on multi-approaches combination, including decreasing its farnesylation, increasing degradation, and reducing its toxic downstream effects. Despite the modest benefits in the above proposed treatment strategies, none of them solve the problem from the source (Harhoury et al., 2018).

1.3.4 CRISPR/Cas9-mediated adenine base editors (ABEs) as the most promising HGPS treatment

The clustered regularly interspaced short palindromic repeat (CRISPR) gene-editing system has been a promising therapeutic alternative for human diseases (Amoasii et al., 2017; Gao et al., 2018; Sander & Joung, 2014; Y. Yang et al., 2016). The system comprises Cas9 endonuclease protein directed by a single guide RNA (sgRNA) to a target DNA locus and a protospacer adjacent motif (PAM). The endonuclease generates a double strand DNA break which is repaired through either non-homologous end-joining (NHEJ) or homology-directed repair (HDR) in the presence of a donor template (Komor, Badran, & Liu, 2017). Due to the premature senescence phenotype and double-strand DNA damage repair deficiency in HGPS cells (Y. Liu et al., 2008; Musich & Zou, 2009), it has been challenging to correct the HGPS mutation (*LMNA* c.1824C > T; p.G608G) using HDR method of the standard CRISPR/Cas9 approach. Recently, two groups independently proposed a CRISPR/Cas9-based strategy against HGPS through abrogation of the production of lamin A and progerin without affecting lamin C (Beyret et al., 2019; Santiago-Fernandez et al., 2019) as lamin A appears to be dispensable in mice (Fong et al., 2006; Osorio et al., 2011). Although the reported approach enhances the health and extends the lifespan of progeria mice—*Lmna*^{G609G/G609G}, the consequence of disrupting lamin A in human is unknown. In addition, the low efficiency and the unwanted random insertion and deletion (indels) of the standard CRISPR/Cas9 system make the approach daunting for translational application (Cong et al., 2013; Cox, Platt, & Zhang, 2015; Ran et al., 2013). To circumvent these limitations, a novel HGPS therapeutic approach, “base editing”, a modified CRISPR/Cas9 system with a fusion of a catalytically impaired Cas9 and laboratory-evolved adenosine deaminase, has been

developed (N. M. Gaudelli et al., 2017; L. W. Koblan et al., 2021; Komor, Kim, Packer, Zuris, & Liu, 2016).

Recently, base editors have been developed as powerful genome editing reagents for correcting or installing single nucleotide transition point mutations by performing targeted chemical transformation of single DNA bases in the genome without generating double stranded breaks (Rees & Liu, 2018). Adenine base editors (ABEs) are genome editing agents that contain a catalytically impaired CRISPR-Cas nuclease fused to an evolved single-stranded deoxyadenosine DNA deaminase enzyme that can precisely mediate A•T-to-G•C edits in genomic DNA (Nicole M. Gaudelli et al., 2017; Koblan et al., 2018) (Figure 1-5) such as that present in HGPS, while cytosine base editors convert C•G-to-T•A. Recently, in collaboration with Dr. Liu group at Harvard, we have been used ABE-based gene editing method to correct the pathogenic HGPS allele in patient-derived fibroblast cell lines and in a mouse model of the disease which demonstrated that DNA correction restores normal RNA splicing, reduces progerin protein abundance, restored nuclear morphology, corrected aortic histopathology, extended animal lifespan, and improved animal vitality (L.W. Koblan et al., 2021). Thus, unlike the standard CRISPR/Cas9-based approach for HGPS (Beyret et al., 2019; Santiago-Fernandez et al., 2019), the ABE-mediated gene-editing system efficiently corrected the mutation without affecting the lamin A expression, with minimal byproducts and without requiring double-strand breaks or donor DNA templates, providing a very promising mode of intervention for clinical application.

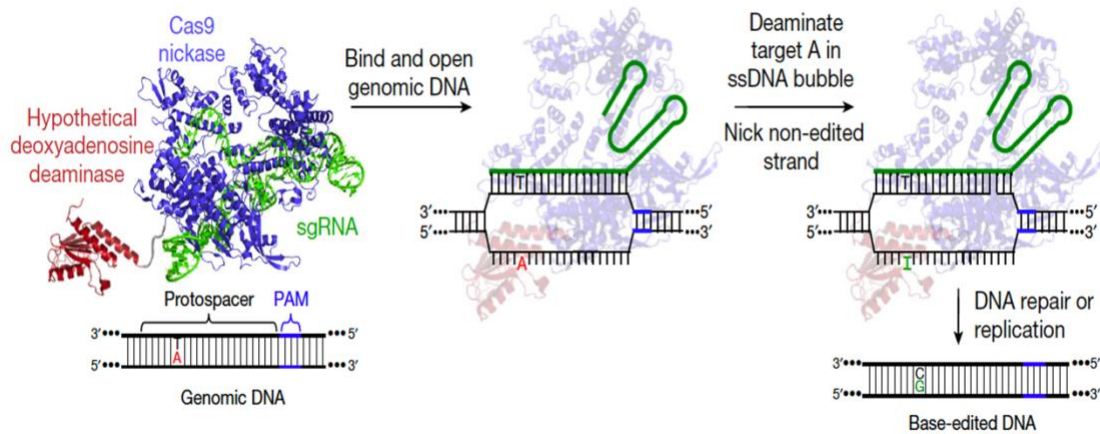


Figure 1-5: ABE-mediated A•T to G•C base editing strategy. ABEs contain a hypothetical deoxyadenosine deaminase, which is not known to exist in nature, and a catalytically impaired Cas9. They bind target DNA in a guide RNA-programmed manner, exposing a small bubble of single-stranded DNA. The hypothetical deoxyadenosine deaminase domain catalyzes conversion of adenine to inosine within this bubble. Following DNA repair or replication, the original A•T base pair is replaced with a G•C base pair at the target site. The figure adapted with permission from (N. M. Gaudelli et al., 2017).

1.4 Vascular microphysiological systems to model disease

Recently, there has been a growing interest in the tissue engineering and medical fields toward using tissue-engineered systems or microphysiological systems to model normal and disease states *in vitro* and develop treatment and diagnostic alternatives (Jones & Zhang, 2016; Truskey, 2018). The major motivation is to better mimic the physiological microenvironment of diseases and human conditions. In this regard, 3D human tissue models fill the gap of the 2D and animal models, and result in higher clinical translation outcomes (Q. Zhang, Zhang, & Truskey, 2020). This is because, unlike 2D culture, 3D human tissue models better recapitulate the morphology and the physiological state of the native tissue (Truskey, 2018). Human microphysiological

systems (MPS) have been developed to improve the accuracy of experimental predictions, minimize experimental time and cost, and reduce patient risk (Q. Zhang et al., 2020). Experiments that use microphysiological systems are highly reproducible and can be used for functional assays as well as genomic, metabolomic, and histological analysis (Truskey, 2016). To study the initiation and progression of vascular disease, tissue engineered blood vessels (TEBVs) have been designed to model many vascular diseases, including atherosclerosis, HGPS, and thrombotic disorders (Atchison, Zhang, Cao, & Truskey, 2017; Fernandez et al., 2016; Robert et al., 2013; Zheng et al., 2012).

Current approaches to fabricate TEBVs are divided into two major categories, scaffold based or self-assembly (Q. Zhang et al., 2020). The scaffold-based method comprises either synthetic polymer or natural extracellular matrix (ECM) for *in-vitro* cell seeding. The essential requirements for synthetic polymers are biocompatibility and biodegradability. Recently, Polyglycolic acid (PGA) and Poly (lactide-co- glycolide) acid (PLGA) are biodegradable polymers widely used in TEBVs (Coenen, Bernaerts, Harings, Jockenhoevel, & Ghazanfari, 2018). Natural biological hydrogels and ECM proteins such as collagen, elastin, fibrin, gelatin, and modified hyaluronic acid have also been used as scaffold materials (Song, Rumma, Ozaki, Edelman, & Chen, 2018). These scaffolds have improved biocompatibility and provide adhesion sites for binding of cell surface integrins or cleavage sites to matrix metalloproteinases (MMPs), which facilitate cell attachment, cell migration and cell proliferation (Truskey, 2016; Q. Zhang et al., 2020). Despite their benefit, the long manufacturing time for the vessels using synthetic polymers as scaffold poses a great challenge for their application as a disease model system (Q. Zhang et al., 2020). Another source of natural scaffold is to decellularize TEBVs by depleting tissue

and cells from allogenic or xenogeneic sources that preserved the natural architecture of the ECM of the vessels (Song et al., 2018).

Self-assembly is another approach to manufacture TEBVs. Self-assembly utilizes the ECM produced by seeded cells as the vessel structural supports (Q. Zhang et al., 2020). With self-assembly method, a confluent layer form by cells that rolled into a tubular structures to mimic the vessel (L'Heureux et al., 2006; L'Heureux, Paquet, Labbe, Germain, & Auger, 1998). The major limitation for TEBVs generated by this method is the long manufacturing time, which makes it difficult to use for disease modeling purposes (Q. Zhang et al., 2020).

Extrusion of a matrigel solution containing endothelial cells and smooth muscle cells enabled self-organized of an arteriole-like structure, termed vesseloids (Andrique et al., 2019). The vesseloids show key vessel properties, including a restrictive endothelial barrier and smooth muscle cell contractility (Q. Zhang et al., 2020). The vessels also respond to inflammatory stimuli causing the endothelial cells to express the leukocyte adhesion molecules VCAM-1 and ICAM-1. The advantage of this novel approach is that vessels can be rapidly produced without a thick layer of ECM, in contrast to most methods to fabricate TEBVs (Truskey, 2016; Q. Zhang et al., 2020).

Thus, vascular microphysiological system provides an effective platform for the investigation of vascular development, vascular disease modeling, and evaluation of drug safety and efficacy (Truskey & Fernandez, 2015). The vascular microphysiological system also creates physiologically relevant microenvironments that closely model the *in vivo* environments (Truskey, 2018; Q. Zhang, Bosch-Rue, Perez, & Truskey, 2021; Q. Zhang et al., 2020).

1.5 Significance of this dissertation

My primary goal of this study is to investigate the underlying molecular mechanisms of vascular endothelial dysfunction in HGPS. Given that the primary cause of death in most HGPS patients is cardiovascular failure and progerin induces endothelial dysfunction, it is crucial to decipher the underlying molecular mechanisms in order to design effective therapeutics. Since HGPS is a very rare disease, and the patients are very frail, it is challenging to obtain patient-derived tissue-specific cell-lines to study HGPS disease mechanisms (Gordon et al., 2014). In addition, primary ECs have donor-to-donor variations, and very difficult to maintain in culture for longer time, because they have limited proliferation rate. Hence, to circumvent this challenge, in chapters 2 and 3, I have generated patient-specific iPSCs and developed an *in vitro* differentiation system to create a stable source of HGPS iPSC-ECs. Using this system, I demonstrated that HGPS leads to eNOS-mediated angiogenic incompetence driven by reduced intracellular NO level and associated protein expression changes of metalloproteinases, TIMPs, and important cell surface proteins responsible for sensing shear stresses. Furthermore, I demonstrated that ABEs correction of the HGPS mutation significantly reduced progerin expression to a basal level, rescued nuclear blebbing, increased intracellular NO level, normalized TIMPs, and restored angiogenic competence in HGPS iPSC-EC. Given that HGPS is a fatal premature aging disease, the improvement of angiogenic competence by this approach provides a promising path of intervention for clinical application. Moreover, minimal random insertion and deletion (indels) of the ABE gene editing approach offers feasible translational application.

Finally, in collaboration with Dr. Truskey's lab at Duke university, we have developed normal and HGPS 3D vascular tissue model that recapitulates the HGPS disease pathology, including progerin expression, loss of SMCs, and inflammation. The TEBV also exhibited EC dependent vasodilation and contraction defects. Thus, given the ultra-rarity of HGPS patients who can be enrolled in trials and the limitations of animal models to translate therapeutics, the TEBV model using iPSC-derived vascular SMC and ECs provide feasible and effective opportunity to study the HGPS disease mechanisms and test the effectiveness of potential therapeutics. Together, this study will provide molecular insights into endothelial dysfunction in HGPS and suggest that ABE7.10max-VRQR could be a promising therapeutic approach for correcting HGPS-related cardiovascular phenotypes.

Chapter 2: Characterize iPSC-derived normal and HGPS vascular endothelial cells

2.1 Introduction

HGPS is an ultra-rare autosomal dominant disorder characterized by phenotypes reminiscent of premature aging (Burtner & Kennedy, 2010). HGPS is caused by accumulation of progerin, a toxic lamin A mutant variant. Progerin induces endothelial dysfunction and cardiovascular alterations, which lead HGPS patients fail to thrive and death (Benedicto et al., 2021; M. R. Hamczyk et al., 2018; Osmanagic-Myers et al., 2019).

To investigate the underlying mechanisms of endothelial dysfunction in HGPS, direct *in vitro* culture of primary ECs from HGPS patients is the ideal system. However, there are several challenges regarding this strategy. First, HGPS is an ultra-rare disease and the patients are very frail, so it is challenging to obtain patient-derived tissue-specific cell lines to directly study the HGPS disease mechanism (Gordon et al., 2014). Secondly, there is donor-to-donor variations, and it is very difficult to maintain primary ECs in culture for longer time, because they have limited proliferation rate (Poh et al., 2005). Considering the challenges, establishing an alternative source to acquire HGPS ECs is essential.

In recent years, with the emergence of iPSCs, there has been an increasing interest among scientists in using iPSC to model specific diseases. iPSCs could be transformed from various adult cells, including fibroblasts or blood cells, and have been widely used

for *in vitro* disease models (Shi, Inoue, Wu, & Yamanaka, 2017). The pluripotency gives iPSCs the potential to differentiate into cells from all three germ layers (ectoderm, mesoderm, and endoderm), including ECs (Bao et al., 2015; Patsch et al., 2015; Takahashi & Yamanaka, 2006). Given iPSCs differentiation potentials and established EC differentiation from healthy donors exhibit mature vascular features, I hypothesized that iPSC-derived ECs from HGPS donors exhibit mature vascular features with the progeroid phenotypes. Therefore, I have generated patient-specific iPSCs to lineage specific differentiation and developed an *in vitro* differentiation system using an established protocol in (Patsch et al., 2015) as a stable source of ECs. Characterization of the differentiated EC revealed that both healthy and HGPS iPSC-EC exhibit mature endothelial vascular properties, such as forming vascular networks and expressing mature endothelial cell surface markers. On the other hand, HGPS iPSC-ECs exhibit progeria specific phenotypes, including progerin expression and abnormal nuclear morphology.

2.2 Results

2.2.1 iPSC-derived EC differentiation strategy

Normal and HGPS endothelial cells (ECs) were differentiated from a pair of well-characterized normal and HGPS iPSC lines (Material Methods) (Atchison et al., 2020; Atchison et al., 2017; Choi et al., 2018; Xiong, LaDana, Wu, & Cao, 2013; H. Zhang et al., 2014). Using iPSCs generated from HGPS and normal donors, I have developed an *in vitro* monolayer differentiation system to acquire HGPS and normal control vascular ECs based on an established protocol in (Patsch et al., 2015) with few modifications (Figure 2-1). The differentiation protocol is segmented in two stages, which recapitulates the

developmental process occurring during embryogenesis (Patsch et al., 2015). First, human iPSCs are cultured for four days in a chemically defined medium supplemented with wnt agonist, glycogen synthase kinase-3beta (GSK3 β) inhibitor (CHIR99021), and bone morphogenetic protein-4 (BMP4) to induce commitment of the cells to the mesodermal lineage. Second, the mesodermal state cells cultured for two days in a different medium containing vascular endothelial growth factor (VEGF) and Forskolin to induce functional endothelial cells. After day six of differentiation, the iPSC-ECs sorted using PE-CD144 conjugated antibody, and the mature iPSC-ECs are maintained with complete endothelial stempro media with VEGF and subcultured when they reach 80 to 90% confluency.

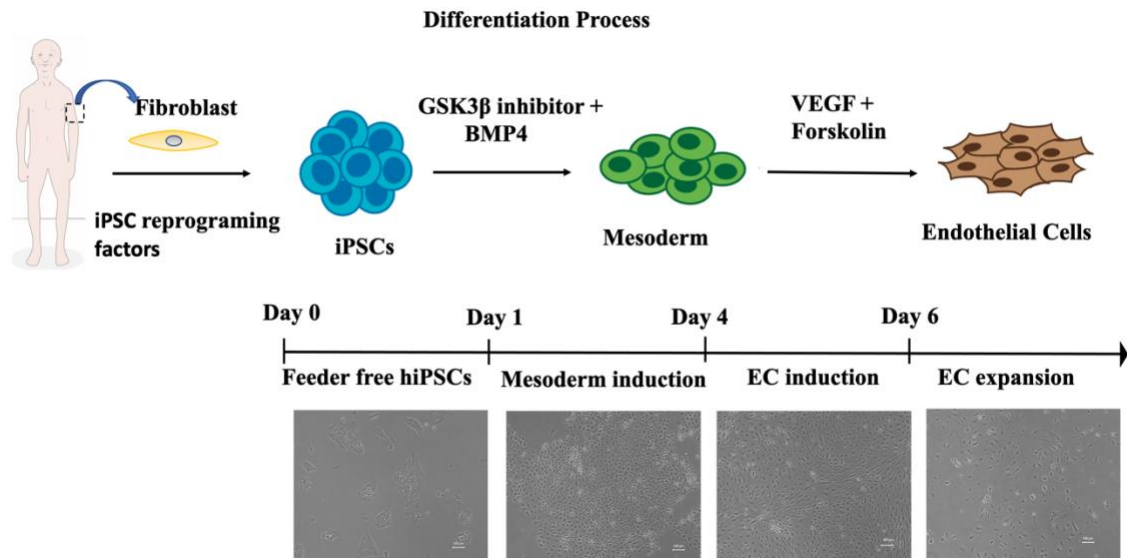


Figure 2-1: Schematic illustration of the endothelial cells differentiation strategy for human iPSCs. First, healthy or HGPS derived human iPSCs are cultured for four days in a chemically defined medium supplemented with GSK3 β inhibitor (CHIR99021) and BMP4 to induce commitment of the cells to the mesodermal state. Second, the cells are cultured for two days in a different medium containing VEGF and Forskolin to induce functional endothelial cells. iPSCs, induced pluripotent stem cells; GSK3 β , glycogen synthase kinase-3beta; BMP4, bone

morphogenetic protein-4; VEGF, vascular endothelial growth factor. The differentiation protocol adapted and modified with permission from (Patsch et al., 2015).

2.2.2 HGPS iPSC-EC express mature endothelial cell surface markers

Normal and HGPS iPSC-ECs were characterized using endothelial specific cell surface markers. Control and HGPS iPSC-ECs both express human vascular endothelial cadherin (hVE-cadherin) and platelet endothelial cell adhesion molecule-1 (PECAM-1, aka CD31), indicating consistent differentiation in both HGPS and normal controls (Figure 2-2). In addition, both progerin transcription and protein expression were abundant in HGPS iPSC-ECs (Figure 2-2c,d). Next, I examined the endothelial characteristics of these cells. In normal endothelium, PECAM-1 transmits mechanical force while VE-cadherin comprises the mechanosensory complex necessary for EC function and shear stress response (Tzima et al., 2005). Therefore, I examined PECAM-1 and VE-cadherin expression in HGPS iPSC-ECs.

In HGPS iPSC-ECs, the transcript abundance of both PECAM-1 (4-fold) and VE-cadherin (CDH5) (3-fold) was significantly reduced relative to normal controls (Figure 2-2b). The reduced transcript abundance of PECAM-1 in HGPS iPSC-ECs led to a 4-fold decrease in PECAM-1 protein abundance relative to healthy controls (Figure 2-2d,e) although VE-cadherin protein abundance was comparable to healthy controls. Reduced PECAM-1 transcript and protein abundance in HGPS iPSC-ECs suggests a defect in sensing and responding to shear stress in these cells.

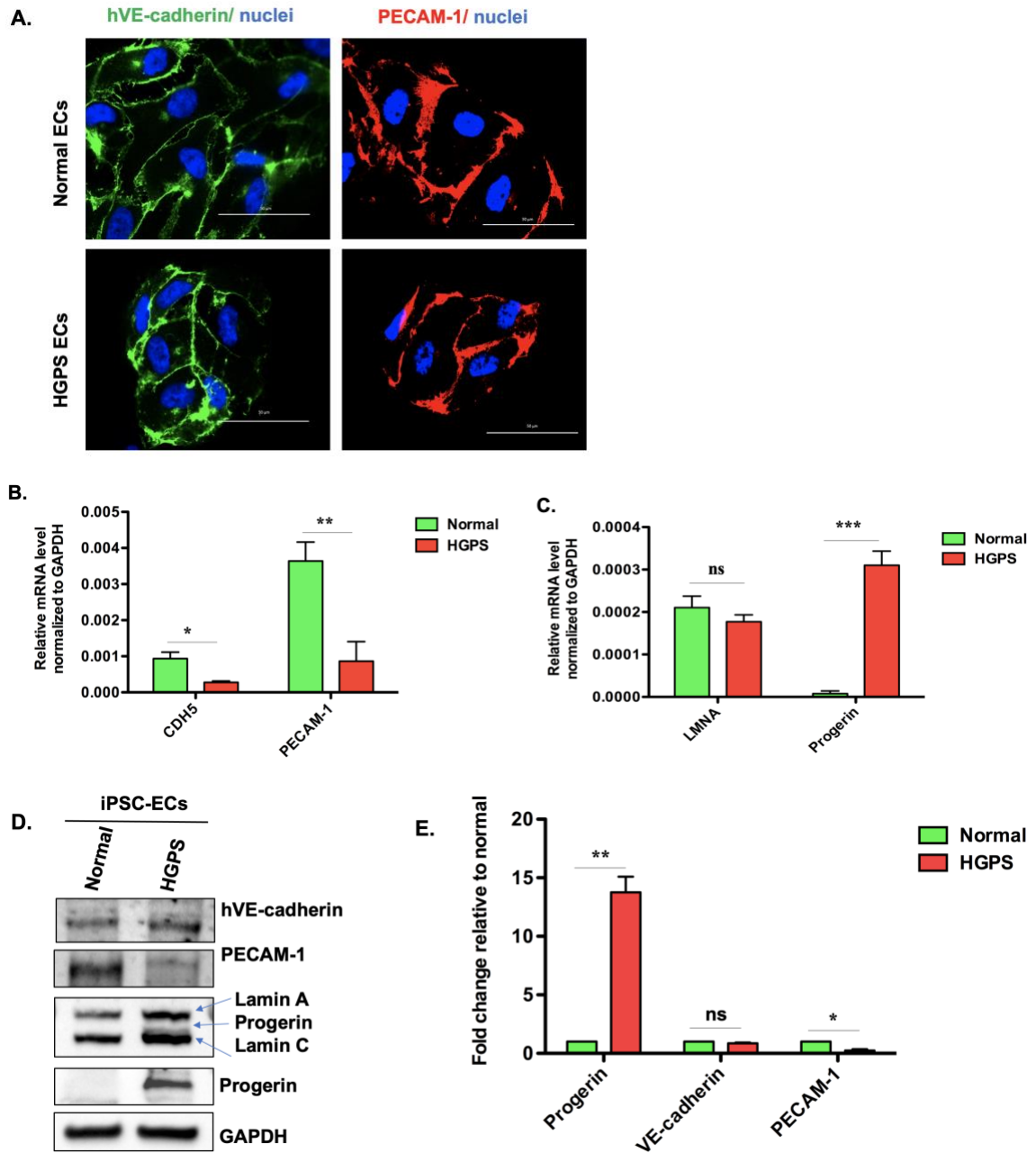


Figure 2-2: Characterization of iPSC-derived ECs. (A) Representative images of immunofluorescence staining of ECs with specific EC surface markers, hVE-cadherin and PECAM-1 (scale bars =50 μ m). (B) RT-qPCR analysis of endothelial-specific marker genes, CDH5 and PECAM-1. Their relative mRNA levels were normalized to GAPDH. (C) RT-qPCR analysis of *LMNA* and progerin in normal and HGPS iPSC-ECs. (D) Western blot analysis with indicated antibodies on the cell lysates of normal and HGPS iPSC- ECs. (E) Quantification of

fold changes of the western band densitometry in HGPS relative to the normal control. Data are presented as mean \pm SEM, * $p < 0.05$; ** $p < 0.01$; *** $p < 0.001$; ns = not significant, $n =$ three independent experiments).

2.2.3 HGPS iPSC-ECs exhibit abnormal nuclear morphology

Abnormal nuclear morphology is the hallmark of HGPS nucleus (Booth-Gauthier et al., 2013; Goldman et al., 2004). To characterize the nuclear morphology, I used immunofluorescent stain of lamin A/C and progerin specific antibody. The result showed progerin protein was abundant in HGPS iPSC-ECs, leading to significant nuclear abnormalities compared to normal controls that were evidenced by more than three-fold of abnormal nuclei in HGPS iPSC-EC ten days post-differentiation (Figures 2-2c,d; 2-3 a,b).

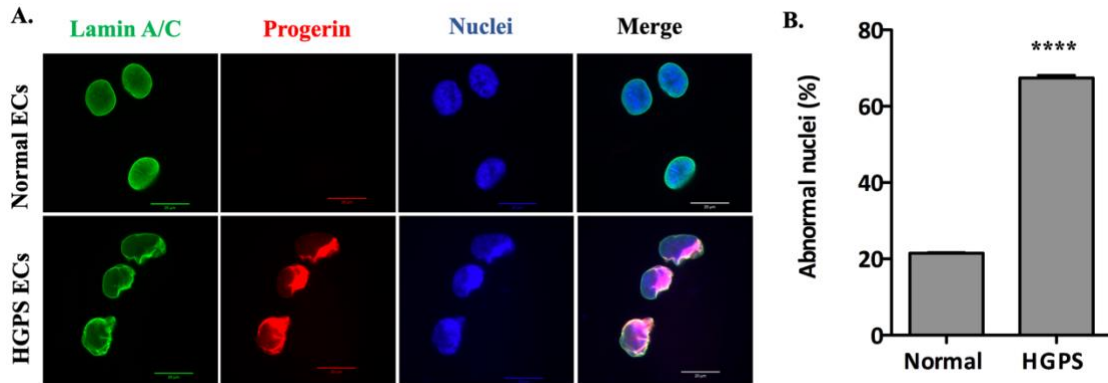
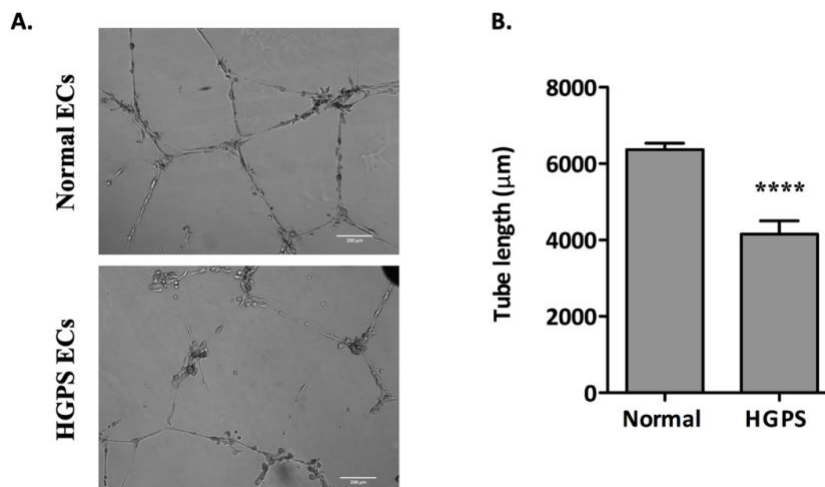


Figure 2-3: Nuclear abnormality of HGPS iPSC-ECs. (A) Representative images of immunofluorescence staining with anti-lamin A/C, anti-progerin antibody, and DAPI on normal and HGPS iPSC-ECs (scale bars = 20 μ m). (B) Quantification of the percentage of abnormal nuclei in normal and HGPS iPSC-ECs. Data are presented as mean \pm SEM, **** $p < 0.0001$; $n =$ three independent experiments; for nuclear morphology, $n > 120$ cells per group).

2.2.4 HGPS iPSC-ECs exhibit functional defects in forming capillary-like microvascular networks

Angiogenesis is a well-established property of ECs (Lahtenvuo & Rosenzweig, 2012; Potente & Carmeliet, 2017; Senger & Davis, 2011). Given the observation of angiogenic defects determined by reduced myocardial perfusion and decreased vascular density in both knockin minipig and endothelium-specific transgenic mouse models of HGPS (Dorado et al., 2019; Sun et al., 2020), I hypothesized that progerin protein accumulation and consequential endothelial cell dysfunction would negatively impact angiogenesis in HGPS iPSC-ECs. Indeed, phase-contrast image analysis revealed that HGPS iPSC-ECs form microvascular networks with significantly shorter capillary-like structures than normal controls. HGPS microvascular tube structures average 4000 μm , significantly shorter than the average 6000 μm for normal controls (Figure 2-4a,b). Despite the difference in angiogenic potentials, VE-cadherin was aligned with the tube structures in both control and HGPS samples; suggesting appropriate tubular architecture was formed in both normal and HGPS iPSC-ECs (Figure 2-4c).



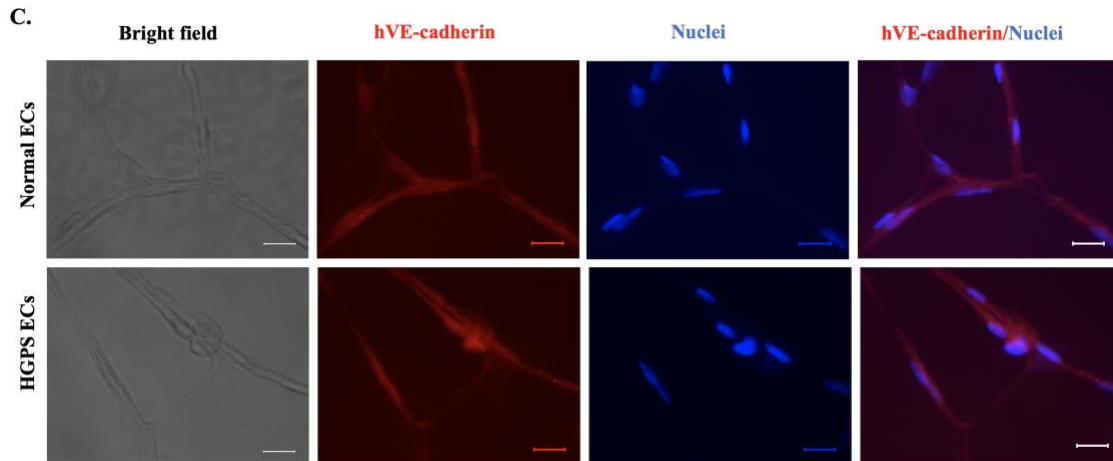


Figure 2-4: Capillary-like microvascular network formation defects in HGPS iPSC-ECs. (A) Matrigel-based tube formation assay to assess the angiogenic activity of normal and HGPS iPSC-ECs (scale bars = 200 μ m). (B) Quantification of tube length per field. (C) Images of VE-cadherin staining on the capillary-like vascular networks formed by normal or HGPS iPSC-ECs at 16 hours. Scale bars = 200 μ m. Data are presented as mean \pm SEM, **** p < 0.0001, n = three independent experiments).

To further characterize the angiogenic defect in HGPS iPSC-ECs, I examined tube structure formation at different cell densities and time points. I observed shorter and fragmented capillary-like tubes in HGPS iPSC-ECs relative to healthy controls at all tested cell densities (10000, 5000, and 2500 cells/well; Figure 2-5a). Time course studies further revealed that at a density of 5000 cells/well, normal and HGPS iPSC-ECs first formed capillary-like microvascular networks at 4 hours post-seeding. Microvascular networks generated by HGPS iPSC-ECs began disintegrating at 8 hours post-seeding and shrank dramatically after 11 hours while the microvascular networks generated by normal cells were stable (Figure 2-5b, supplemental videos 1a,b). These results indicate angiogenic defects in the HGPS iPSC-ECs.

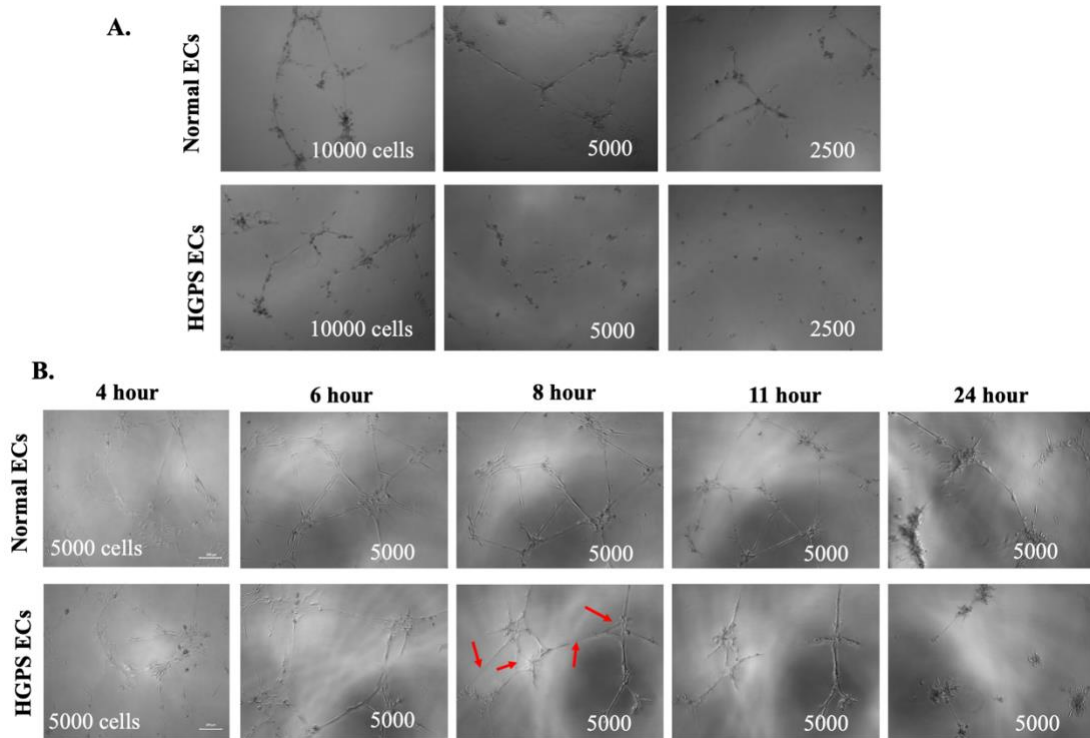


Figure 2-5: Microvascular networks at different cell densities and time course. (A) Phase contrast images of tube structures formed by normal or HGPS iPSC-ECs at indicated cell densities after 18 hours. (B) Phase contrast images of tube structures formed by normal and HGPS iPSC-ECs at the cell density of 5000 per well during a time-course experiment (scale bars = 200 μm).

To confirm that angiogenic incompetence was directly induced by progerin, I used a lamin overexpression assay in human umbilical vein endothelial cells (HUVECs). HUVECs were transduced with lentiviruses expressing a GFP only control, a GFP–lamin A fusion protein, and a GFP-progerin fusion protein (Figure 2-6a). Progerin overexpressing HUVECs exhibited a significant reduction in capillary-like microvascular network formation compared to the GFP–lamin A and GFP expressing controls after 18 hours (Figure 2-6 a,b), confirming that progerin induces angiogenic defects in ECs.

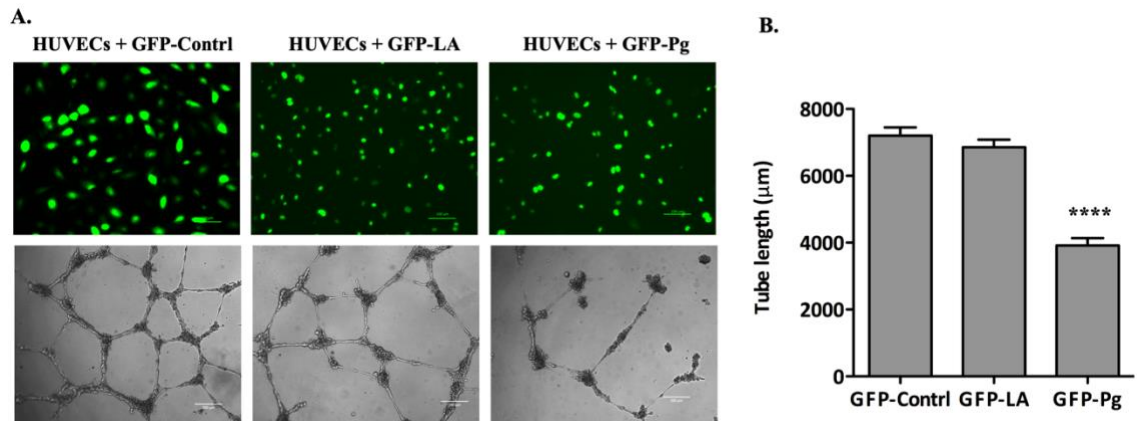


Figure 2-6: Capillary-like microvascular network formation defects in progerin over-expressed HUVECs. (A) Matrigel-based tube formation assay to assess vascular network formation activity of HUVECs transduced with GFP-control, GFP-lamin A, or GFP-progerin lenti-viral vectors after 18 hours (scale bars = 100 μm *top*, 200 μm *bottom*). (B) Quantification of tube length per field. HUVEC, human umbilical vein endothelial cells; GFP, green fluorescent protein; LA, lamin A; Pg, progerin. Data are presented mean \pm SEM, **** $P < 0.0001$; n = nine fields per group).

2.3 Discussion

The underlying cause of death in most HGPS patients is a cardiovascular failure. Since HGPS is a very rare disease, and because the patients are very frail, it is challenging to obtain patient-derived tissue-specific cell lines to study HGPS disease mechanisms (Gordon et al., 2014). I have generated patient-specific iPSCs to circumvent this challenge and developed an *in vitro* differentiation system to create a stable source of HGPS iPSC-ECs (Figure 2-1). The iPSC-ECs express hVE-cadherin and PECAM-1 and form capillary-like microvascular networks, exhibiting the vascular properties typical of mature ECs (Figure 2-2). Interestingly, the reduced transcript abundance of PECAM-1 in HGPS iPSC-ECs led to a 4-fold decrease in PECAM-1 protein abundance relative to healthy controls although VE-cadherin protein abundance was comparable to healthy

controls. Reduced PECAM-1 transcript and protein abundance in HGPS iPSC-ECs suggests a defect in sensing and responding to shear stress in these cells (Tzima et al., 2005). Progerin transcript and protein were also abundant in HGPS iPSC-ECs, leading to significant nuclear abnormalities compared to normal controls.

Moreover, matrigel based tube formation assay revealed that HGPS iPSC-ECs form microvascular networks with significantly shorter and fragmented capillary-like structures than normal controls suggesting that HGPS iPSC-EC have angiogenic defects. Progerin overexpressing HUVECs exhibited a significant reduction in capillary-like microvascular network formation compared to the GFP–lamin A and GFP expressing controls after 18 hours confirming that progerin induces angiogenic defects in ECs.

The results in this chapter are consistent with the recent endothelial specific progerin expressed transgenic mouse model that demonstrated decrease of capillary density (Sun et al., 2020). In addition, Dorado et al. showed vascular degenerations and cardiovascular complications in a knockin minipig model of HGPS (Dorado et al., 2019). These results provide strong evidence that progerin accumulation induces endothelial dysfunction and cardiovascular abnormalities and the molecular mechanisms need to be deciphered.

Chapter 3: Examine the underlying molecular mechanisms of HGPS endothelial dysfunction

3.1 Introduction

The vascular endothelium plays a pivotal role in maintaining vascular homeostasis and tone by releasing various factors that regulate vascular smooth muscle cell function, inflammation, immune regulation, platelet aggregation, and thrombosis (Gimbrone & Garcia-Cardena, 2016; Vanhoutte et al., 2017). One mechanism by which these processes are regulated by the endothelium is by activating endothelial nitric oxide synthase (eNOS), the enzyme responsible for nitric oxide (NO) production (Ignarro et al., 2001; Y. M. Yang et al., 2009). Endothelial dysfunction disrupts vascular homeostasis and tone, leading to cardiovascular disease (Gimbrone & Garcia-Cardena, 2016; Vanhoutte, 2009; Widmer & Lerman, 2014).

The role of progerin in endothelial dysfunctions and cardiovascular abnormalities has been explored *in vivo* and *in vitro*. Osmanagic-Myers et al. generated VE-cadherin promoter-driven progerin in transgenic mice and showed early signs of diastolic dysfunction accompanied by cardiac hypertrophy, perivascular and interstitial fibrosis, and premature death (Osmanagic-Myers et al., 2019). Similarly, Sun et al. generated Tie2-driven progerin expression in a transgenic line and demonstrated endothelial dysfunction as a trigger of systemic aging (Sun et al., 2020). In addition, Dorado et al. showed vascular degenerations and cardiovascular complications in a knockin minipig model of HGPS (Dorado et al., 2019). Furthermore, a broad derangement of HGPS iPSC-

ECs structure and function reported in (Matrone et al., 2019). These results provide strong evidence that progerin accumulation induces defects in endothelium and cardiovascular abnormalities.

One important process orchestrated by vascular endothelial cells is angiogenesis, the process of sprouting new blood vessels from the existing vasculature. Angiogenesis is a major adaptive response to physiological stress and is an endogenous repair mechanism following ischemic injury (Lahtenvuo & Rosenzweig, 2012; Potente & Carmeliet, 2017; Senger & Davis, 2011). The role of eNOS in angiogenesis was examined by eNOS deficient mice that shows reduced angiogenesis and blood flow compared to their wild type controls (Fukumura et al., 2001). Interestingly, angiogenic defects determined by reduced myocardial perfusion and decreased vascular density were observed in both knockin minipig and endothelium-specific transgenic mouse models of HGPS (Dorado et al., 2019; Sun et al., 2020). The molecular mechanisms of progerin-induced angiogenic incompetence are currently unknown. Given the angiogenesis defects in HGPS iPSC-EC, I hypothesized that progerin causes downregulation of eNOS expression and activity, and a concomitant decrease in intracellular NO level, which results in defects in forming microvascular networks in HGPS iPSC-ECs.

3.2 Results

3.2.1 HGPS iPSC-ECs exhibit reduced total eNOS expression and activity

Having determined that progerin expression antagonizes microvascular network formation, I next sought to characterize how progerin expression alters eNOS function, a key regulator of angiogenesis, in ECs (Lu, Wang, & Qian, 2015; Senger & Davis, 2011;

Zhao, Vanhoutte, & Leung, 2015). Besides its expression level, eNOS activity is typically controlled through protein-protein interactions and multisite phosphorylation events, specifically, phosphorylation at threonine-495 by protein kinase C suppresses its activity, both of which determine vascular density and NO production in the endothelium (Fukumura et al., 2001; Kolluru, Siamwala, & Chatterjee, 2010; Kukreja & Xi, 2007; Mount, Kemp, & Power, 2007; Y. M. Yang et al., 2009).

Western blot analysis from lysates of normal and HGPS iPSC-ECs revealed that total eNOS expression was 2-fold lower in HGPS iPSC-ECs relative to normal controls (Figure 3-1a). To assay eNOS function, I measured the abundance of phosphorylated threonine-495 eNOS, an inhibitory marker of eNOS activity (Fleming, 2010; Kolluru, Siamwala, et al., 2010). HGPS iPSC-EC expression of phosphorylated threonine-495 eNOS was nearly 4-fold higher than normal controls (Figure 3-1a,c). These results establish that progerin accumulation reduces total eNOS abundance and activity in HGPS endothelial cells.

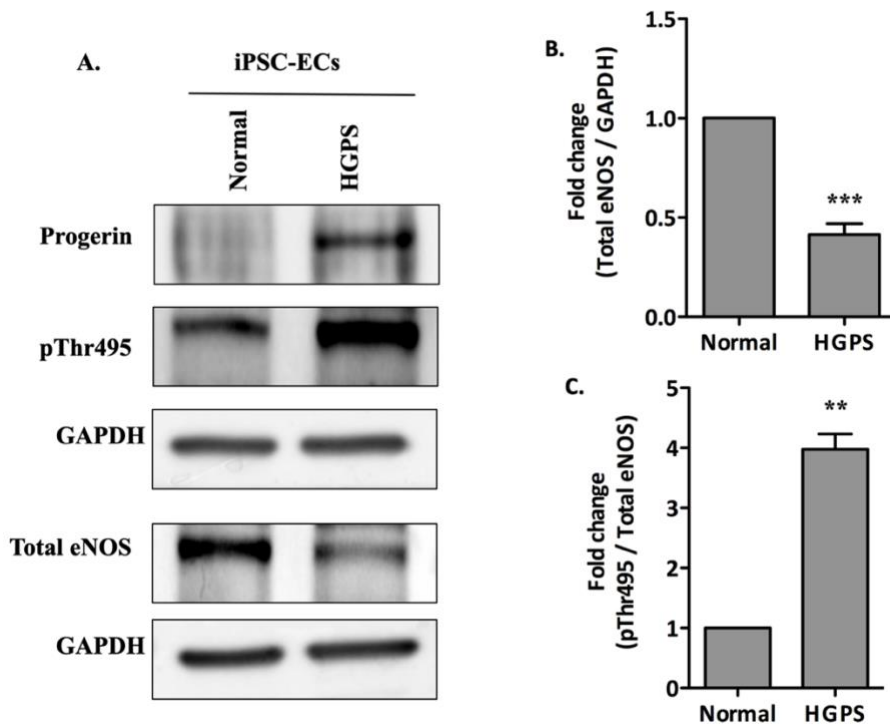


Figure 3-1: Downregulation of eNOS expression and activity in HGPS iPSC-ECs. (A) Western blotting analysis with indicated antibodies on the lysates of normal and HGPS iPSC-ECs. (B-C). Quantification of fold change for western blot band densitometry of total eNOS level normalized to GAPDH, and relative phosphorylated Thr495 level normalized to corresponding total eNOS, respectively. Data are presented as mean \pm SEM, ** $p < 0.01$; *** $p < 0.001$, $n =$ three independent experiments). ECs, endothelial cells; eNOS, endothelial nitric oxide synthase; pThr495, phospho-threonine 495.

Similar results were observed in transiently progerin over-expressed HUVECs. HUVECs were transduced with lentiviruses expressing a GFP only control, a GFP-lamin A fusion protein, and a GFP-progerin fusion protein. Western blot analysis from whole cell lysates showed that total eNOS expression and activity were significantly lower in progerin overexpressed HUVECs than the GFP only control and lamin A fusion protein

(Figure 3-2a,c). These results confirm that progerin reduces total eNOS abundance and activity in HGPS endothelial cells.

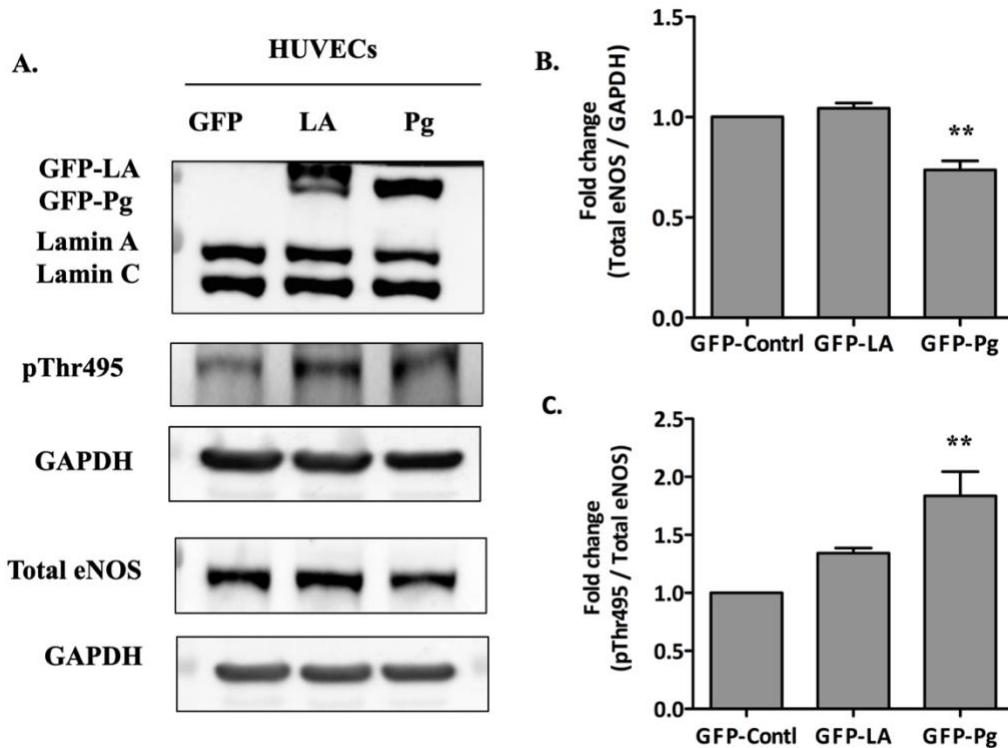


Figure 3-2: Downregulation of eNOS expression and activity in progerin-overexpressed HUVECs. (A) Western blotting analysis with indicated antibodies on the lysates of HUVECs transduced with GFP-control, GFP-lamin A, or GFP-Progerin vectors. (B-C). Quantification of fold change for western blot band densitometry of total eNOS level normalized to GAPDH, and relative phosphorylated Thr495 level normalized to corresponding total eNOS, respectively. HUVEC, human umbilical vein endothelial cells; eNOS, endothelial nitric oxide synthase; pThr495, phospho-threonine 495; GFP, green fluorescent protein; LA, lamin A; Pg, progerin. Data are presented as mean \pm SEM, ** $p < 0.01$, at least three independent replicates were performed in each experiment).

3.2.2 HGPS iPSC-ECs are not able to upregulate eNOS in response to shear stress

Shear stress stimulates eNOS expression and NO production (Boo et al., 2002; Cheng et al., 2005; Kolluru, Sinha, et al., 2010; W. Wang et al., 2010). Given that HGPS iPSC-ECs show a 4-fold reduction of PECAM-1 expression in (Figure 1-2c,d) and

downregulated eNOS expression and activity (Figure 3-1a,c), I hypothesized that the HGPS iPSC-ECs might have defects in sensing shear stress. Therefore, I used a fluidic culture chamber with a flow of 5 mL/min to evaluate the functional properties of normal and HGPS iPSC-ECs in response to shear stress. Fluidic culture chambers were fabricated using the EnvisionTEC Perfactory IV 3D printer, with EShell®300 as the printing material, as reported in (Lembong, Lerman, Kingsbury, Civin, & Fisher, 2018). Prior to cell seeding, flow chambers were coated with fibronectin. Theoretical shear stress profiles inside the flow chambers were calculated using the flow simulation feature of the computational modeling software SOLIDWORKS (Figure 3-3a). Up to 5 mPa was computed in the flow chamber, which is significantly below the reported shear stress value that causes mechanical damage and detachment of the ECs (Y. Zhang et al., 2016).

After seeding for 18 hours, 24 hours of shear stress was applied to iPSC- ECs, which were then probed for eNOS expression. HGPS iPSC-ECs show a significant reduction of total eNOS expression relative to normal controls under both static and fluidic conditions (Figure 3-3b,c). Normal iPSC- ECs that experience applied sheer force (when cultured under fluidic conditions) show a significant induction of eNOS expression relative to cells cultured under static conditions. Remarkably, HGPS iPSC- ECs, show similar levels of eNOS expression under static and fluidic conditions (Figure 3-3b,c), resulting in a significant depletion of intracellular NO levels in HGPS iPSC- ECs compared to normal controls under fluidic culture conditions (Figure 3-3d). Together, these results suggest that while eNOS expression is induced by shear stress in normal control ECs, HGPS iPSC-ECs have defects in responding to the shear stress and therefore fail to upregulate eNOS expression.

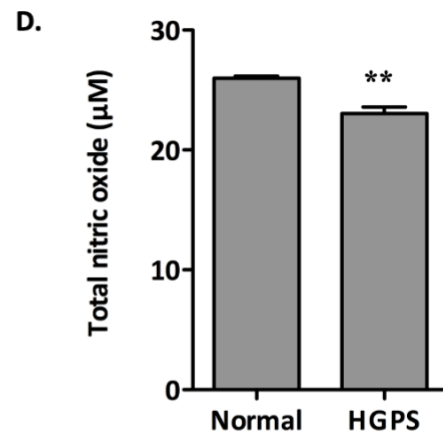
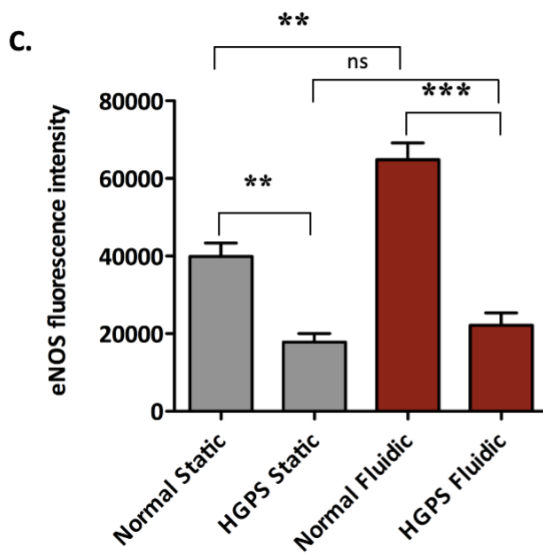
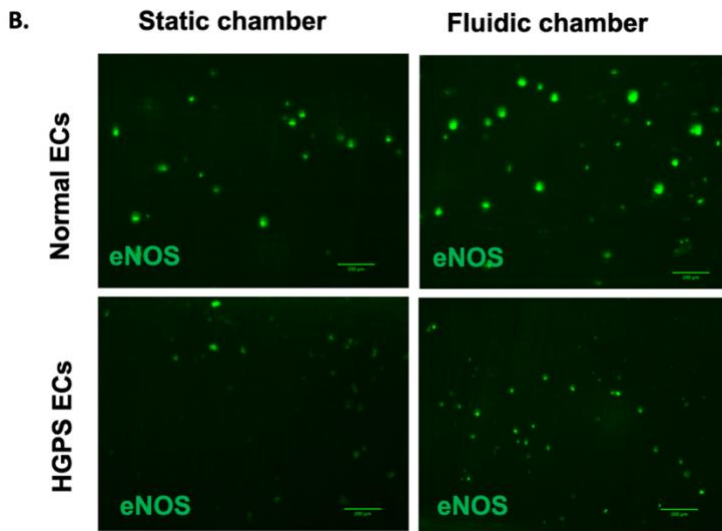
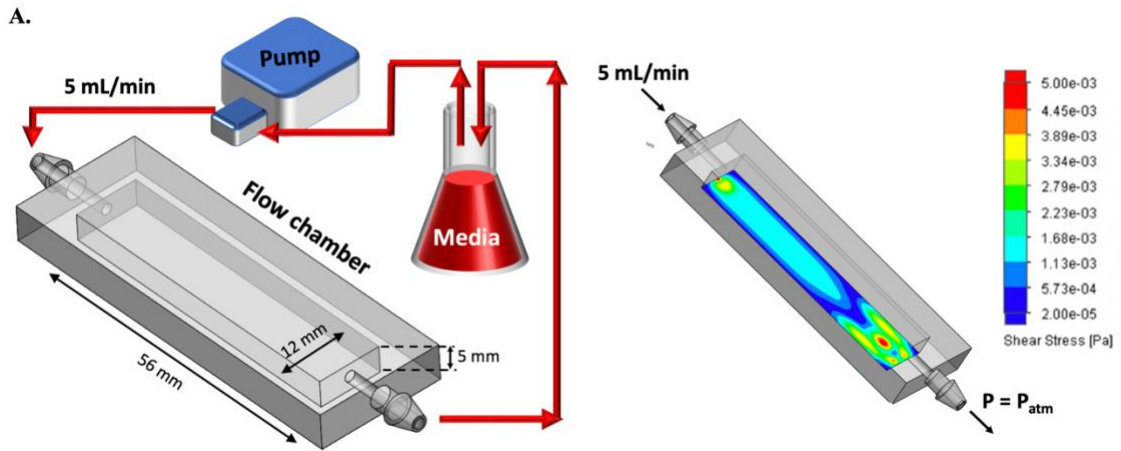


Figure 3-3: Inability to upregulate eNOS expression in HGPS iPSC-ECs under shear stress. (A) Schematic illustration of the experimental setup of the fluidic culture chamber (*left*), and shear stress distribution on inner chamber surfaces from fluid flow simulation (*right*). (B) Immunofluorescence staining of eNOS in normal and HGPS iPSC-ECs under static and fluidic culture conditions (scale bars = 200 μ m). (C). Quantification of the eNOS fluorescence signal intensity. (D) Total intracellular NO level using a colorimetric assay in normal and HGPS ECs in the fluidic chamber. Data are presented as mean \pm SEM, **P < 0.01; ***P < 0.001; n= three independent experiments).

3.2.3 HGPS iPSC-ECs angiogenic incompetence is eNOS dependent

I next sought to determine whether progerin-induced eNOS deficiency is directly responsible for the angiogenic incompetence in HGPS iPSC-ECs. To do so, I treated HGPS iPSC-ECs and normal control ECs with an eNOS inhibitor (0.2 mM N-omega-Nitro-L-arginine methyl ester hydrochloride; L-NAME) and nitric oxide donor S-Nitroso-N-acetyl-DL-penicillamine (SNAP), and measured intracellular NO abundance. Fluorescence image analysis of NO, measured by 4-Amino-5-Methylammino-2',7'-Difluorofluorescence Diacetate (DAF-FM) staining, was performed for both normal and HGPS iPSC-ECs treated with SNAP and L-NAME. Intracellular NO is significantly reduced in HGPS iPSC-ECs compared to normal controls. SNAP treatment significantly increases intracellular NO at 0.25, 0.5 and 1 mM concentration both in normal and HGPS iPSC-ECs. When normal ECs were treated with L-NAME; however, intracellular NO levels were reduced to a similar level as in HGPS ECs (Figure 3-4a,b). These results suggest that intracellular NO levels are reduced in HGPS iPSC-ECs, likely due to impaired eNOS activity in these cells.

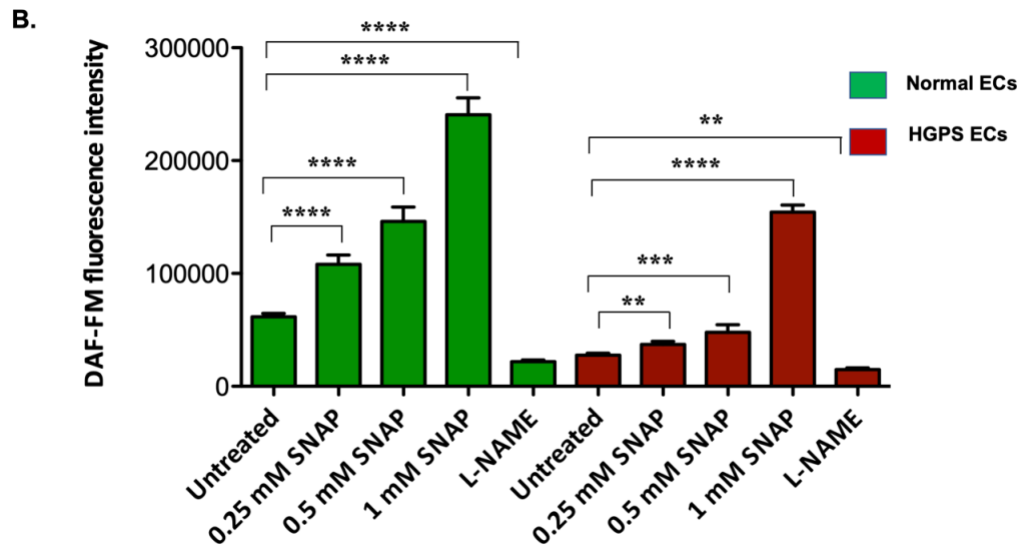
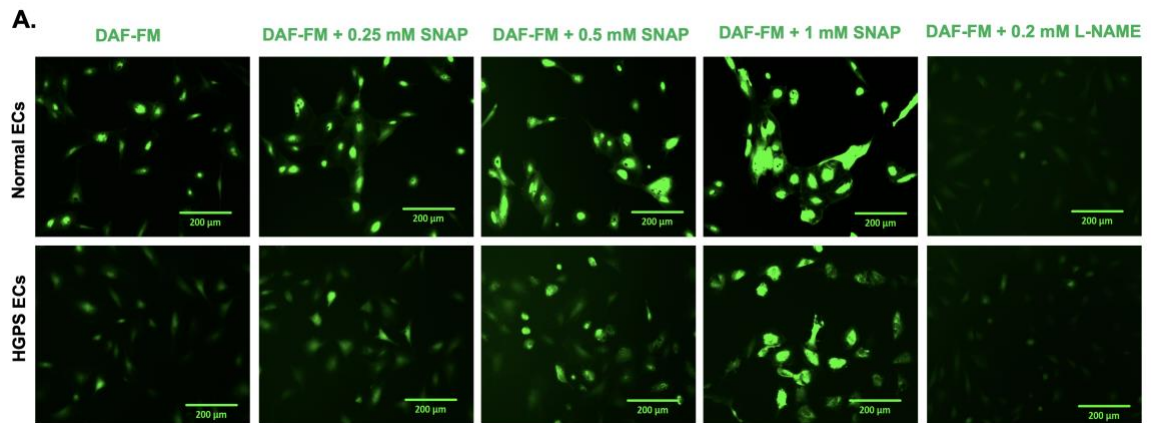


Figure 3-4: HGPS iPSC-ECs exhibit lower NO bioavailability in response to NO donor, SNAP. (A) Fluorescence images of NO, measured by DAF-FM staining, were generated in normal and HGPS ECs either untreated or treated with 0.25, 0.5 and 1 mM nitric oxide donor SNAP, and with 0.2 mM L-NAME, an eNOS inhibitor (scale bars = 200 μ m). (B). Quantification of the DAF-FM fluorescence intensity for intracellular NO level in normal and HGPS iPSC-ECs. DAF-FM, 4-Amino-5-Methylammino-2',7'-Difluorofluorescence Diacetate; SNAP, S-Nitroso-N-acetyl-L-DL-penicillamine; L-NAME, N-omega-Nitro-L-arginine methyl ester hydrochloride.

As described above, eNOS function and associated NO levels in cells affect endothelial angiogenic potential. I therefore examined the angiogenic competence of L-NAME treated normal control ECs. Indeed, similar to HGPS iPSC-ECs, normal iPSC-ECs treated with L-NAME show defective vascular network formation. In contrast, SNAP treatment at 0.25 mM and 0.5 mM concentration significantly increases the microvascular network formation while at 1 mM concentration, it suppresses angiogenic efficiency of both normal and HGPS iPSC-ECs (Figure 3-5a,b). These results establish that eNOS deficiency is a key factor causing the angiogenic incompetence in HGPS iPSC-ECs.

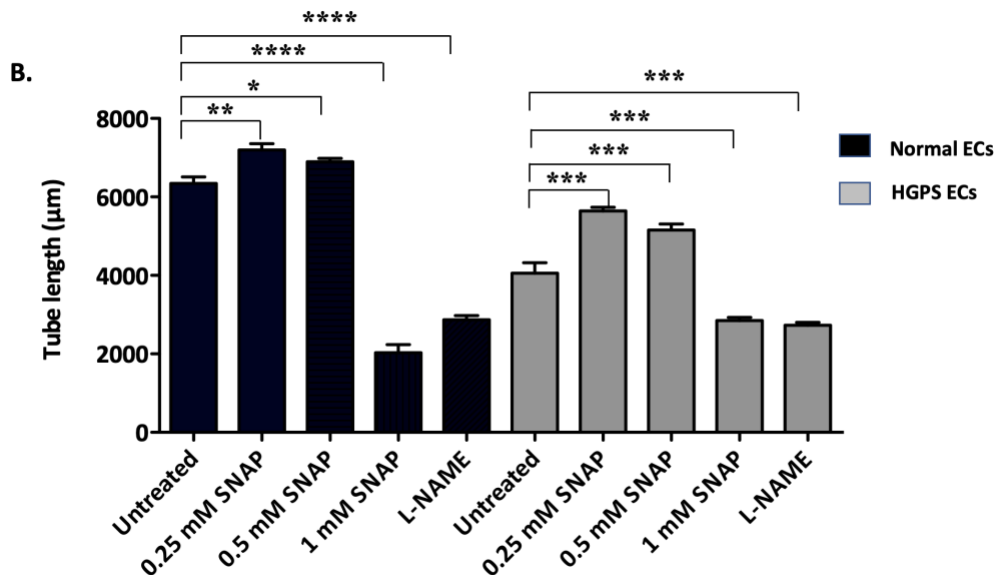
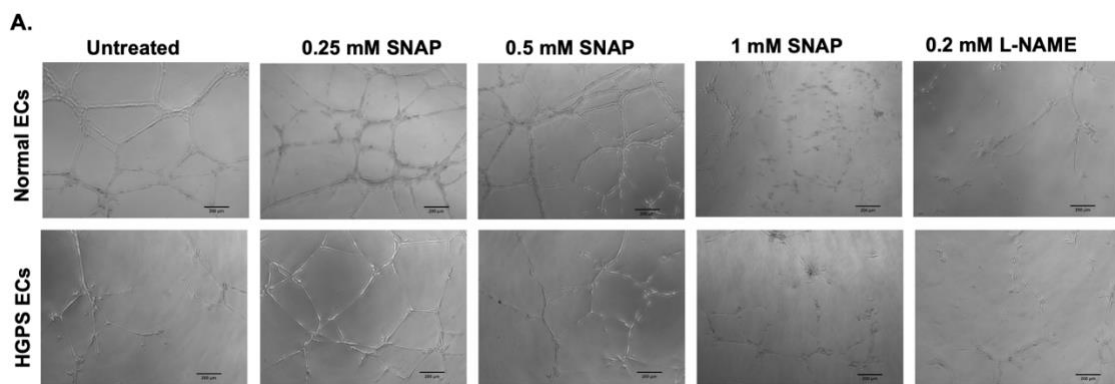


Figure 3-5: HGPS iPSC-ECs angiogenic incompetence is eNOS dependent. (A) Matrigel-based tube formation assay to assess the angiogenic activity of normal and HGPS iPSC-ECs either untreated or treated with 0.25, 0.5 , and 1 mM nitric oxide donor SNAP, and with 0.2 mM L-NAME (scale bars = 200 μ m). (B). Quantification of tube length per field. DAF-FM, 4-Amino-5-Methylammino-2',7'-Difluorofluorescence Diacetate; SNAP, S-Nitroso-N-acetyl-DL-penicillamine; L-NAME, N-omega-Nitro-L-arginine methyl ester hydrochloride. Data are presented as mean \pm SEM, *p < 0.05, **p < 0.01, ***p < 0.001, ****p < 0.0001; n= 9 fields per group.

3.2.4 Upregulation of TIMP1, TIMP2, and a reduced expression of MMP-9 in HGPS iPSC-ECs

The matrix metalloproteinases (MMPs) and their specific inhibitors (tissue inhibitors of metalloproteinases; TIMPs), were recently described to be important regulators of angiogenesis (Brew, Dinakarbandian, & Nagase, 2000; Davis & Senger, 2005; Ebrahim et al., 2011; Nagase, Visse, & Murphy, 2006; Saito et al., 2001). I therefore tested whether the expression profile of well-established MMPs and their specific inhibitors differed in HGPS iPSC-ECs relative to normal controls (MMP-1, MMP-2, MMP-7, MMP-9, MMP-14, and their inhibitors TIMP1 and TIMP2) (A. H. Baker, Edwards, & Murphy, 2002; Lee, Tsang, Diaz, Wei, & Stetler-Stevenson, 2010; Saito et al., 2001; Seo et al., 2003). Immunoblot analysis showed a 6-fold increase of TIMP1 and a 5-fold increase of TIMP2 in HGPS iPSC-ECs relative to normal controls, while MMP-9 (4-fold) was significantly reduced (Figure 3-6a,b). The elevated expression of TIMP1 and TIMP2 in combination with suppressed expression of MMP-9 in HGPS iPSC-ECs likely limits the ability of these cells to degrade their extracellular matrix (ECM). Failure to degrade the ECM may suppress angiogenic VEGF signaling, possibly leading to the observed angiogenic incompetence in HGPS iPSC-ECs.

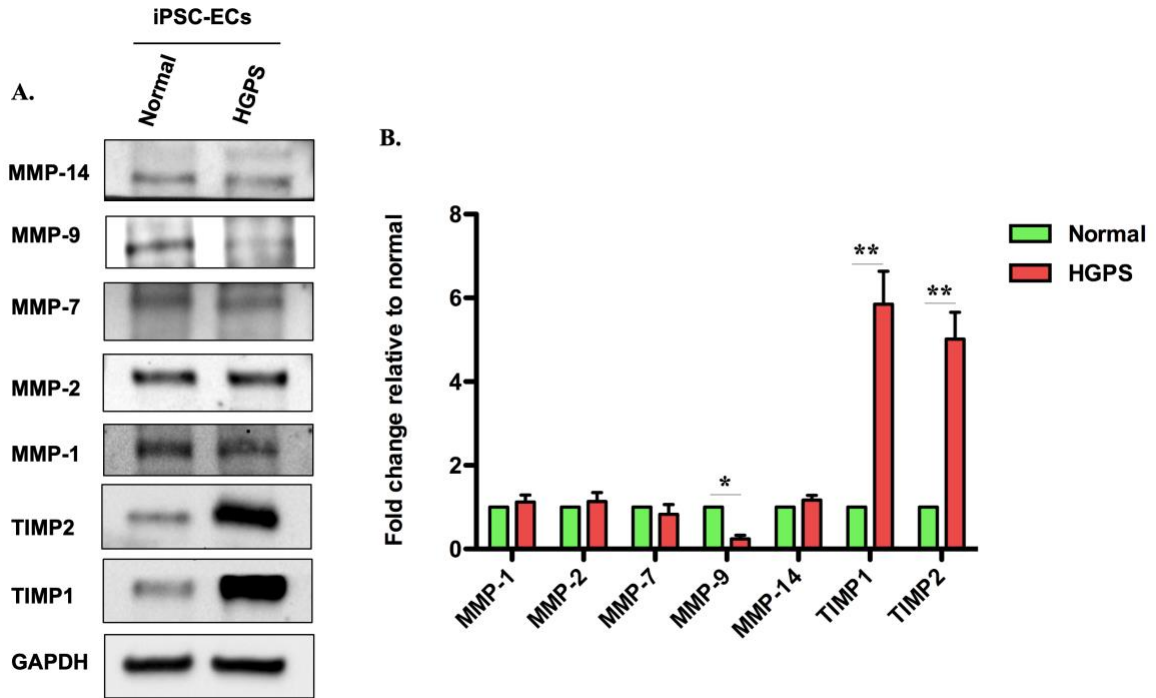


Figure 3-6: Upregulation of TIMP1, TIMP2, and a reduced expression of MMP-9 in HGPS iPSC-ECs. (A) Western blotting analysis with indicated antibodies on the lysates of normal and HGPS iPSC-ECs. (B). Quantification of fold change for western blot band densitometry of HGPS MMPs and TIMPs levels normalized to healthy control. Data are presented as mean \pm SEM, * $p < 0.05$; ** $p < 0.01$; $n = 3$ independent experiments.

3.2.5 Adenine base editors (ABEs) efficiently correct the pathogenic HGPS mutation in HGPS iPSC-ECs

HGPS is caused by a single C>T point mutation in nuclear Lamin A (*LMNA* c.1824 C>T) that can be corrected by an adenine base editor (ABE7.10max-VRQR) programmed to correct the pathogenic c.1824 C>T mutation (N. M. Gaudelli et al., 2017; L. W. Koblan et al., 2021). ABE7.10max-VRQR includes a catalytically impaired Cas9 D10A nickase programmed to recognize to an NGA protospacer adjacent motif (PAM; VRQR Cas9) fused to an evolved single-stranded DNA-specific (ssDNA) deoxyadenosine deaminase that can be targeted to the pathogenic *LMNA* allele by

specific single guide RNA (sgRNA) (Kleinstiver et al., 2016). Upon recognition of the appropriate PAM motif, unwinding of the double-stranded DNA occurs as an RNA•DNA heteroduplex form between the sgRNA spacer and the target DNA strand. Heteroduplex formation liberates a displaced single-stranded segment of genomic DNA where some of this single-stranded DNA, termed an R-loop, is exposed outside of the Cas protein complex and is accessible to the ssDNA-specific deoxyadenosine deaminase (Figure 3-7a)(Anzalone, Koblan, & Liu, 2020). The deoxyadenosine deaminase domain catalyzes the conversion of adenine to inosine, which is read as guanosine (G) by cellular polymerases. Through DNA repair and replication, the original A•T base pair is replaced with a G•C base pair at the target site (N. M. Gaudelli et al., 2017). The ABE-based gene editing method is extensively studied in HGPS patient-derived fibroblast cell lines and in an HGPS mouse model (L. W. Koblan et al., 2021)

To test the efficacy of this approach in iPSC-derived ECs, I cloned lentiviruses expressing ABE7.10max-VRQR as well as either a c.1824 C>T correcting sgRNA or with control non-targeting sgRNA. Following transduction of normal and HGPS iPSC-ECs, I isolated and sequenced genomic DNA. I observed efficient correction of the HGPS mutation (*LMNA* c.1824 C>T) to the wild-type sequence in cells treated with ABE and the c.1824 C>T correcting sgRNA with 96 % correction at 20 days, but not in cells transduced with ABE and the non-targeting sgRNA (Figure 3-7b,c). Indel frequencies were minimal ($\leq 0.1\%$) for both HGPS and ABE-corrected HGPS iPSC-ECs. Together the results establish that ABEs efficiently correct the pathogenic HGPS mutation to wild type in HGPS iPSC-ECs.

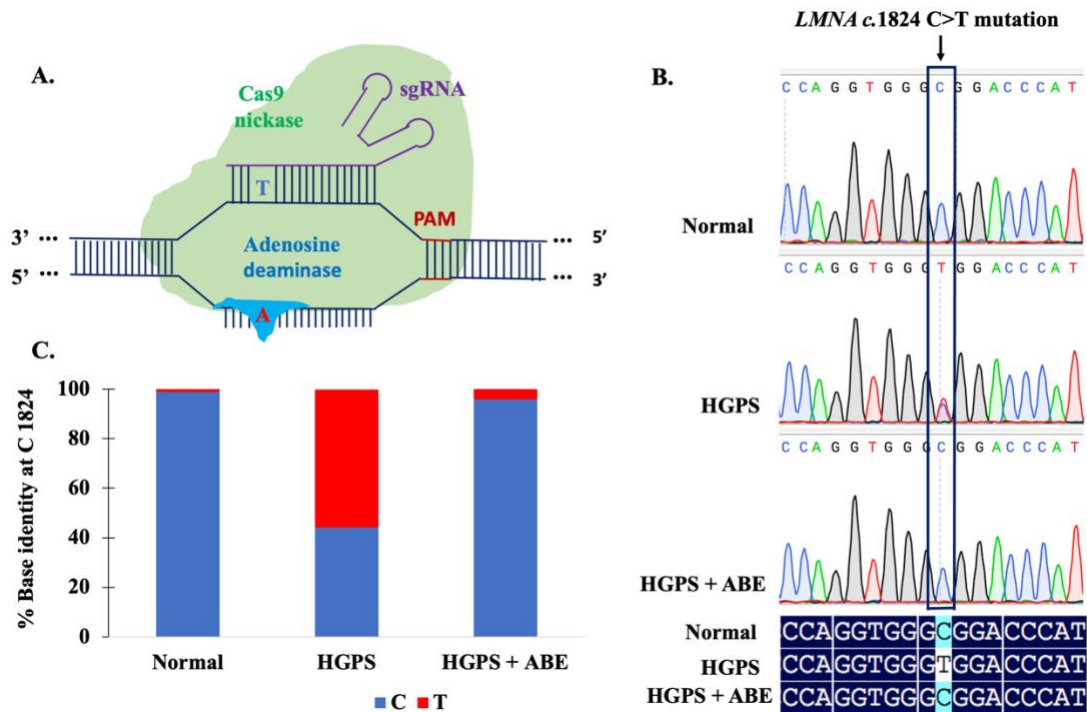


Figure 3-7: Correction of HGPS causing mutation by ABEs in HGPS iPSC-ECs. (A). Scheme of ABE-mediated genome editing strategy. ABE targets the pathogenic adenosine (A) nucleobase in the human *LMNA* (c. 1824C>T) allele. A catalytically impaired Cas9 nickase-deoxyadenosine deaminase complex localizes to the *LMNA* gene locus by an allele-specific sgRNA, generating a single-stranded R-loop of target genomic sequence. Exposed adenosines within the R-loop can be deaminated by the fused evolved ssDNA-specific deoxyadenosine deaminase domain. (B) Sanger sequence traces of normal, HGPS, and ABE-edited HGPS iPSC-ECs (top); sequence alignment of part of *LMNA* exon 11 from normal, HGPS, and ABE-corrected HGPS ECs by DNAMAN software (bottom). (C) DNA sequence at the *LMNA* c.1824 nucleotide in normal, HGPS, and ABE7.10max-VRQR lentivirus treated HGPS iPSC-ECs after 20 days.

3.2.6 ABEs reduce progerin expression and rescue nuclear abnormalities in HGPS iPSC-ECs

I next sought to determine whether the HGPS mutation correction by ABE decreases progerin abundance. Analysis of western blot from whole cell lysates from normal, HGPS and ABE transduced HGPS iPSC-ECs demonstrated that ABE-mediated

correction of the pathogenic allele reduced progerin expression levels by 95% (Figure 3-8a). Similarly, ABE treated HGPS iPSC-ECs exhibit a significant reduction of progerin expression as determined by immunofluorescence analysis of fixed cells (Figure 3-8b). I also examined the potential of ABE gene editing to rescue defects in nuclear morphology of HGPS iPSC-ECs. ABE treatment of the HGPS iPSC-ECs reduced the number of misshapen nuclei by 54% relative to non-targeting sgRNA control treated cells (Figure 3-8b,c). Together, the results establish that ABE-mediated correction of the pathogenic HGPS mutation reduces progerin protein abundance and rescues nuclear abnormalities.

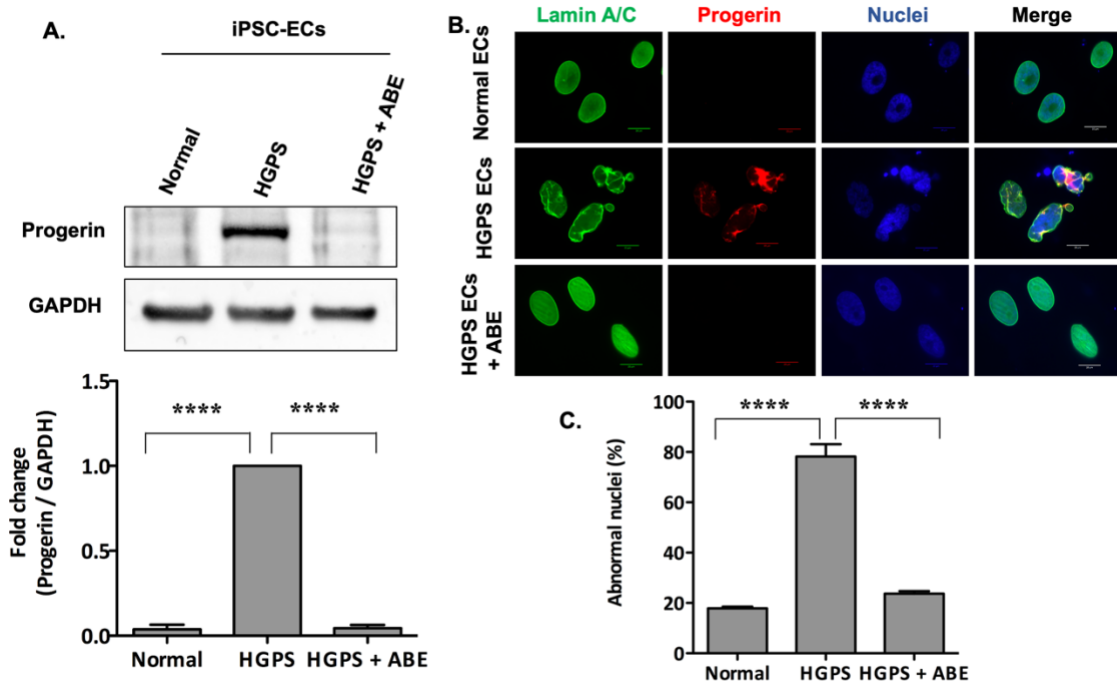


Figure 3-8: Reduction of progerin expression and rescue of the HGPS nuclear blebbing phenotype in ABE-corrected HGPS ECs. (A) Western blotting analysis with indicated antibodies on the lysates of normal and HGPS iPSC-ECs (*top*), and quantifications of the western blot band densitometry (*bottom*). (B) Immunofluorescence staining with anti-lamin A/C, anti-progerin antibody, and DAPI on normal, HGPS, and ABE treated HGPS ECs (scale bars = 20 μ m). (C) Quantification of the abnormal nuclei in normal, HGPS, and ABE treated HGPS ECs. Data are presented as mean \pm SEM, **** p < 0.0001; n = three independent experiments.

3.2.7 ABEs restore intracellular NO level in HGPS iPSC-ECs

Next, I tested whether ABE treatment increases NO in HGPS iPSC-ECs. To do so, I treated normal control, HGPS and ABE treated HGPS iPSC-ECs, and measured intracellular NO abundance. Fluorescence image analysis of NO, measured by DAF-FM staining, was performed for normal, HGPS, and ABE treated HGPS iPSC-ECs.

Intracellular NO is significantly restored with ABE treatment in HGPS iPSC-ECs compared to HGPS iPSC-ECs transfected with scrambled gRNA (Figure 3-9a,c). The result further confirmed by colorimetric assay that showed the total NO significantly increased in ABE treated HGPS iPSC-ECs than the HGPS iPSC-EC controls. These results suggest that intracellular NO levels are restored in HGPS iPSC-ECs with ABE treatment.

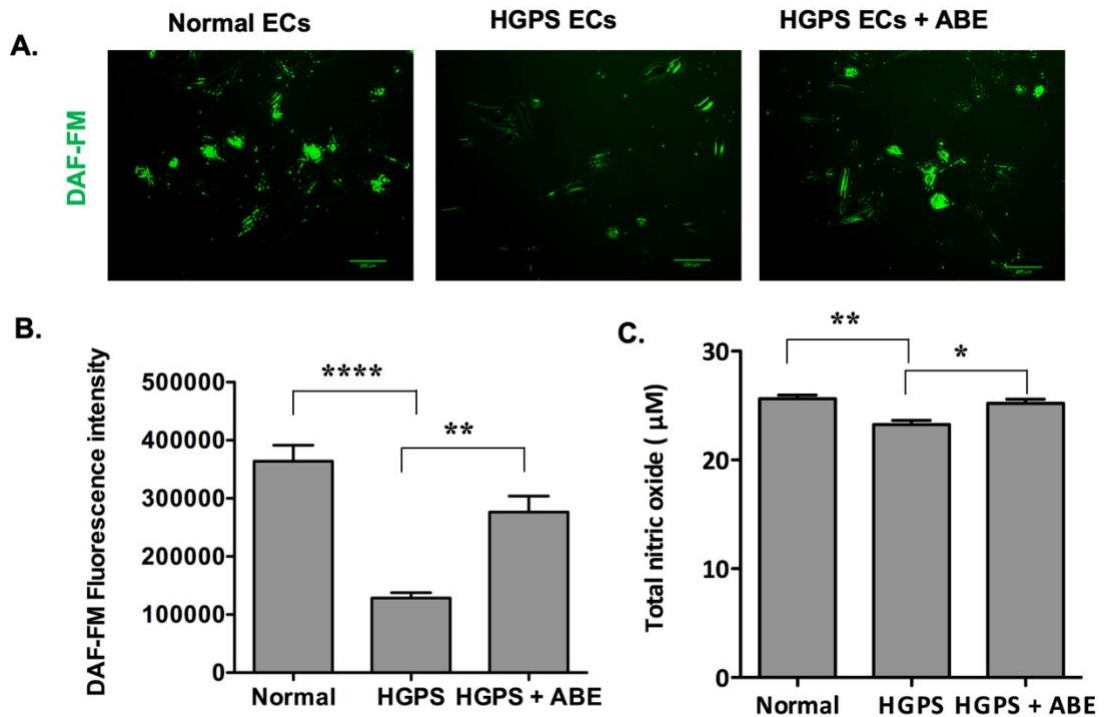


Figure 3-9: Adenine base editors (ABEs) restore intracellular NO level in HGPS iPSC-ECs. (A) Fluorescence images of intracellular NO level, measured by DAF-FM staining, in normal, HGPS, and ABE treated HGPS ECs (scale bars = 200 μm). (B) Quantification of the DAF-FM fluorescence intensity for intracellular NO level in normal, HGPS, and ABE treated HGPS ECs. (C) Total NO bioavailability in normal, HGPS, and ABE-corrected HGPS ECs using a colorimetric assay. Data are presented as mean \pm SEM, * $p < 0.05$, ** $p < 0.01$, **** $p < 0.0001$; n= three independent experiments.

3.2.8 ABEs normalize misregulated TIMPs and increase angiogenic competence in HGPS iPSC-ECs

Next I examined whether ABE-treatment normalizes the misregulated MMP-9, TIMP1, and TIMP2. Western blotting analysis of fold change for western blot band densitometry of MMP-9, TIMP1, and TIMP2 levels normalized to healthy control revealed that ABE-treatment corrected the misregulated TIMPs in HGPS iPSC-EC (Figure 3-10a,b). Remarkably, ABE-treatment also increased iPSC-EC capillary-like tube length from 3510 μm in control sgRNA treated HGPS cells to 5638 μm in ABE-corrected cells per field, which is comparable to normal control tube lengths (Figure 3-10c,d). Together, the results establish that ABE-mediated correction of the HGPS mutation increases intracellular NO level, and restores angiogenic competence of HGPS iPSC-ECs.

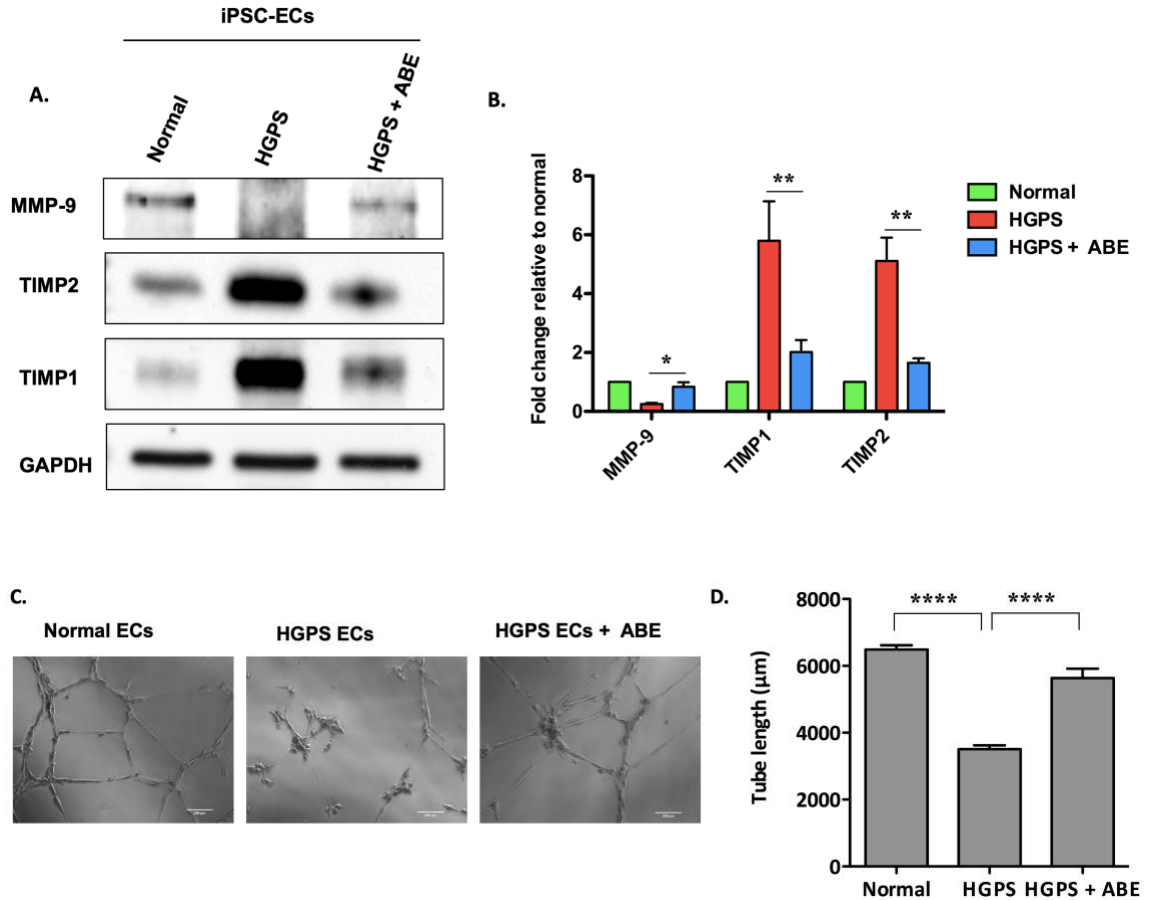


Figure 3-10: Adenine base editors (ABE) normalizes TIMPs and increase angiogenic competence in HGPS iPSC-ECs. (A) Western blotting analysis with indicated antibodies on the lysates of normal , HGPS and ABE-treated HGPS iPSC-ECs. (B) Quantification of fold change for western blot band densitometry of MMP-9,TIMP1, and TIMP2 levels normalized to healthy control. (C) Matrigel-based tube formation assay to assess the angiogenic activity of iPSC-derived normal, HGPS, and ABE treated HGPS ECs (scale bars = 200 μm). (D). Quantification of tube length per field in (C). Data are presented as mean ± SEM, *p < 0.05; **p < 0.01, ***p < 0.0001, n = three independent experiments; for tube length, n = nine fields per group).

3.3 Discussion

The underlying cause of death in most HGPS patients is cardiovascular failure. While it is well appreciated that endothelial dysfunction leads to cardiovascular remodeling and deregulated angiogenesis, very little is known about the mechanisms of

progerin-induced angiogenic incompetence in HGPS. Using iPSC-ECs cultured in both static and fluidic conditions, I characterized the progerin-induced defects on capillary-like microvascular network formation in HGPS iPSC-ECs and elucidated the mechanisms responsible for this phenotype (Figure 3-5). I then use adenine base editing to directly correct the pathogenic allele and measure the consequences of genotypic correction on the vascular phenotypes of our iPSC-EC model cells (Figures 3-7, 3-8, 3-9, 3-10).

I demonstrated that HGPS iPSC-ECs show progerin-dependent deficits in angiogenesis. I identify eNOS as a key regulator of these deficits where HGPS endothelial cells show reduced eNOS expression and activity and determine that progerin-mediated deficiencies in eNOS function also impair responses to shear stress in HGPS iPSC-ECs, likely driven by decreased expression of PECAM-1 (Figure 2-2; Figure 3-3). Furthermore, I show that eNOS deregulation leads to depleted intracellular NO level under both static and fluidic culture conditions in HGPS iPSC-ECs (Figure 3-1) as well as under static conditions in progerin over-expressing HUVEC HGPS model cells (Figure 3-2). These findings helped me identify misregulated TIMP1, TIMP2, and MMP-9 protein expression as a potential driver of progerin-dependent angiogenic deficits in HGPS iPSC-ECs (Figure 3-9). It is tempting to speculate that the angiogenic incompetence of the HGPS ECs is related to the rarity of cancer in HGPS patients despite the high levels of DNA damage (Gonzalo & Kreienkamp, 2015; Kubben & Misteli, 2017; Musich & Zou, 2011). The upregulation of TIMP1 and TIMP2 may also explain the massive depositions of collagen and fibronectin that result in fibrosis and hardening of the vessels in the cardiovascular of children with HGPS.

The rescue of angiogenic competence by small concentration of nitric oxide donor, SNAP, corroborate the therapeutic effect of dietary nitrate supplement for vascular dysfunction in HGPS mouse model (Del Campo et al., 2020; Del Campo et al., 2019), and in human (Rammos et al., 2014; Rossman et al., 2021; Sindler et al., 2011). Finally, I use ABE7.10max-VRQR to efficiently correct the HGPS mutation. ABE-mediated genomic correction of the pathogenic allele reduces progerin protein abundance, rescues nuclear morphology similar in (L. W. Koblan et al., 2021), and increases the angiogenic competence of corrected HGPS iPSC-ECs (Figures 3-8, 3-10).

Collectively, my findings show that HGPS leads to eNOS-mediated angiogenic incompetence driven by reduced intracellular NO level and associated protein expression changes of metalloproteinases, TIMPs, and important cell surface proteins responsible for sensing shear stresses. I further show that ABEs efficiently corrected HGPS mutation by rescuing the nuclear blebbing and increasing the angiogenic competence of treated cells. Given that HGPS is a fatal premature aging disease, the improvement of angiogenic competence by this approach provides a promising path of intervention for clinical application. Moreover, minimal random insertion and deletion (indels) of the method offers feasible translational application. Despite its infancy, ABEs could be a promising therapeutic approach for HGPS and other devastating monogenic diseases.

Chapter 4: Elucidate the molecular mechanisms in 3D *in vitro* vascular tissue model

4.1 Introduction

Cardiovascular tissue engineering has made considerable progress in the past few years (Song et al., 2018; Q. Zhang et al., 2021; Q. Zhang et al., 2020). Given cardiovascular disease is the leading cause of death globally, there is a growing interest in the tissue engineering and medical fields toward using vascular tissue-engineered systems to model normal and disease states *in vitro* and develop treatment and diagnostic alternatives (Truskey, 2016, 2018; Z. Wang, Mithieux, & Weiss, 2019). Despite several challenges, the methods to develop vascular microphysiological systems are constantly growing with scaffold design and cell seeding (Abutaleb & Truskey, 2020; Q. Zhang et al., 2021). To overcome the limitations of animal models, human vascular microphysiological systems have been developed to improve the accuracy of experimental predictions, minimize experimental time and cost, and reduce patient risk (Jones & Zhang, 2016; Q. Zhang et al., 2020).

In addition, the recent advances in generating iPSCs and the potential to differentiate into cells from all three germ layers (ectoderm, mesoderm and endoderm) makes 3D *in vitro* model development more feasible (Bao et al., 2015; Patsch et al., 2015; Takahashi & Yamanaka, 2006). Tissue engineered blood vessels (TEBVs) have been designed to model many vascular diseases, including atherosclerosis, thrombotic

disorders, and HGPS (Atchison et al., 2017; Kumar, Brewster, Caves, & Chaikof, 2011; Robert et al., 2013; Zheng et al., 2012).

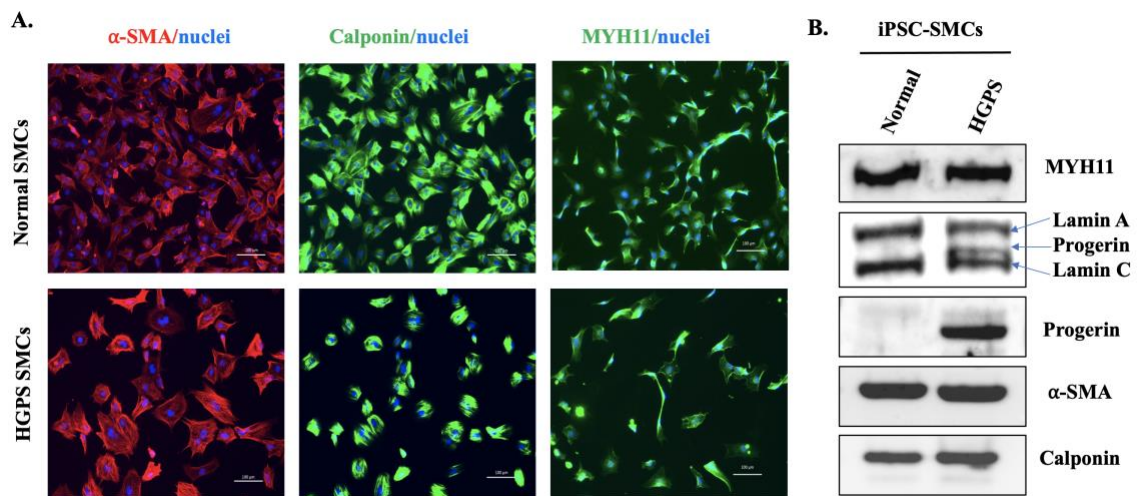
In the last two decades, a number of animal models of HGPS are generated that exhibit progerin expression, premature aging and cardiovascular defects that lead to pathology (Benedicto et al., 2021; H. Zhang et al., 2013). Despite significant progress in understanding the mechanisms of HGPS cardiovascular disease, the current HGPS therapeutics result modest, but significant increase lifespan (Gordon et al., 2018; Harhoury et al., 2018). Due to the inadequacy of 2D culture and animal models in studying the HGPS mechanisms, and limitations in clinical translation, there is a need to develop an improved 3D model to study disease mechanisms and to develop novel therapeutics. Since EC and SMCs are the major cellular components of a vessel, I hypothesize that the TEBV fabricated using iPSC-derived EC and SMCs will recapitulate the *in vivo* state, and the TEBV from HGPS patient donor cells exhibit the disease phenotype.

4.2 Results

4.2.1 Develop and characterize Tissue Engineered Blood Vessel (TEBV) model for normal and HGPS using iPSC-derived SMCs and ECs

Vascular SMCs and ECs are the key structural and functional elements of the vessel wall. Thus to develop TEBVs, in collaboration with Dr. Truskey's lab at Duke, we use iPSC-SMC and ECs. The iPSC-ECs from healthy and HGPS donors extensively characterized in chapter II of this dissertation. The iPSC-SMCs also generated using an established protocol in (Patsch et al., 2015). First, human iPSCs were induced to

mesoderm using GSK3 β inhibitor (CHIR99021) and BMP4. Then, contractile SMCs were induced using platelet-derived growth factor BB (PDGF-BB) and Activin A. The identity of iPSC-SMCs was determined using SMC specific markers, alpha-smooth muscle actin (α -SMA), and calponin, and Myosin Heavy Chain-11 (MYH11) via immunofluorescence staining and western blots (Figure 4-1a,b). The functional property of iPSC-derived SMCs was determined using a commercially available vasoconstrictor synthetic drug (U46619, 1 μ M) that both normal and HGPS iPSC-SMCs exhibit contraction property in response to U46619 (Figure 4-1c,d; supplemental videos 2a,b). The comprehensive characterization of iPSC-derived SMCs with specific expression markers and functional property suggests that the cells could be used to model human disease.



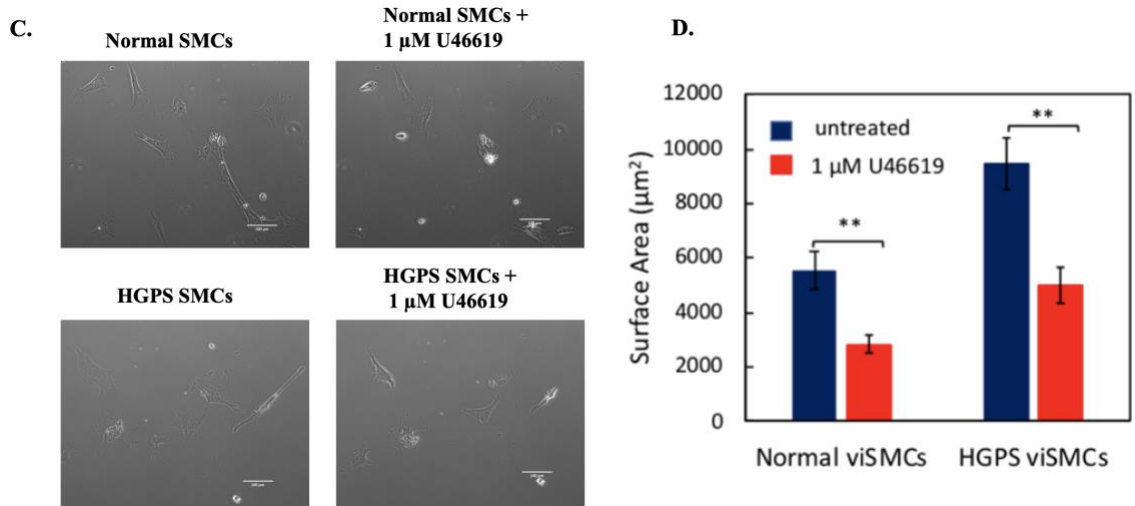


Figure 4-1: Characterization of human iPSC-SMCs. (A) Representative images of immunofluorescent staining with α -smooth muscle actin (α -SMA), calponin, and myosin heavy chain 11 on iPSC-SMCs from healthy and HGPS donors after differentiated and plating in contractile condition. Scale bars 100 μ m. (B) Immunoblot with indicated antibodies from lysates of healthy and HGPS iPSC-SMCs. (C) Representative image of normal and HGPS iPSC-derived SMCs contraction property in response to vasoconstrictor drug (U46619, 1 μ M) treatment after 10 minutes. Scale bars 100 μ m. (D) Quantification of healthy and HGPS iPSC-SMCs contraction property (surface area change) in response to vasoconstrictor drug (U46619, 1 μ M) treatment after 10 minutes (mean standard deviation, Students *t*-test; ***p* < 0.01; n= 3 independent experiments).

Following functional characterization, iPSC-SMCs are then incorporated into a dense collagen gel construct that is seeded with ECs on the luminal surface to create vascular TEBVs, using the process described previously in (Atchison et al., 2017; Fernandez et al., 2016). Vascular TEBVs are then incorporated into a flow loop and perfused with steady laminar flow at a shear stress of 6.8 dynes/cm² for 1 to 4 weeks for further maturation and functional characterization studies (Figure 4-2).

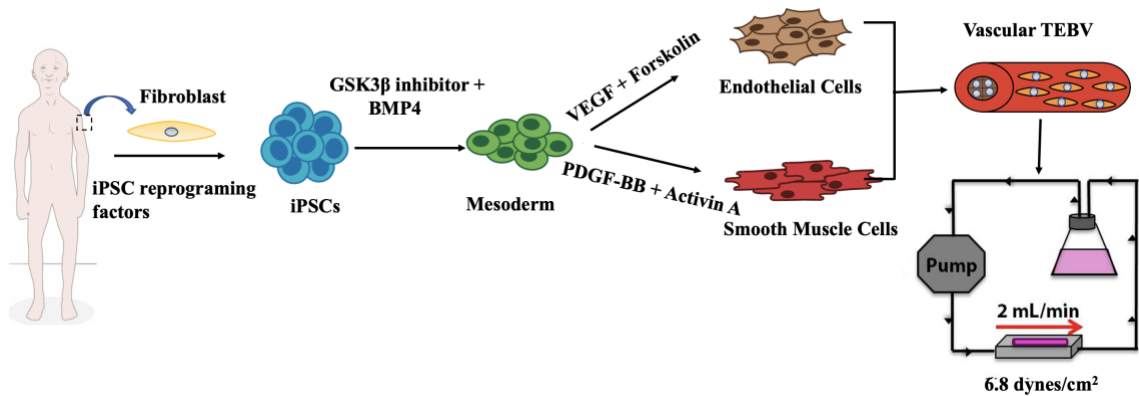


Figure 4-2: Schematic diagram to develop iPSC-derived TEBVs from healthy and HGPS patients. iPSCs are differentiated into smooth muscle cells or endothelial cells using an established protocol as described previously in (Patsch et al., 2015). SMCs are then incorporated into a dense collagen gel construct that is seeded with ECs on the luminal surface to create vascular TEBVs using the process described previously by Fernandez et al. (2016). Vascular TEBVs are then incorporated into a flow loop and perfused with steady laminar flow at a shear stress of 6.8 dynes/cm^2 for 1 to 4 weeks for further maturation and functional characterization studies.

4.2.2 HGPS TEBVs exhibited decreased expressions of contractile proteins, and increased progerin and extracellular matrix proteins

After 4 weeks of perfusion (experiment conducted at Dr. Truskey's lab at Duke university), SMCs in TEBVs expressed the contractile proteins α -SMA and MYH11, which are markers of terminally differentiated SMCs, indicating a more accurate vascular phenotype. Moreover, HGPS TEBVs showed reduced expression of all contractile proteins compared with healthy TEBV controls as well as increased expression of progerin and extracellular matrix proteins, collagen IV and fibronectin, compared with normal TEBVs (Figures 4-3).

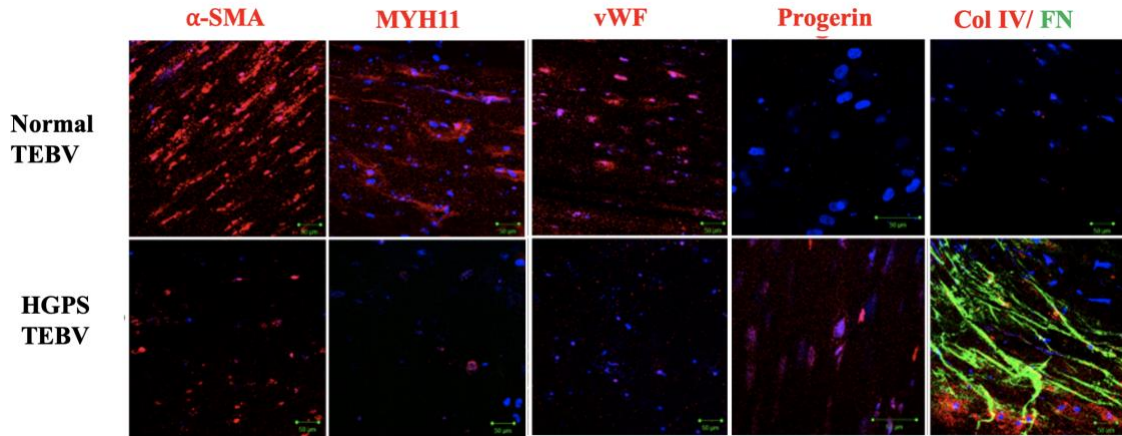


Figure 4-3: Characterization of TEBVs fabricated from SMCs and ECs of normal and HGPS donors. (A) Representative images of immunofluorescence staining with α -SMA, myosin heavy chain 11, collagen IV and fibronectin, progerin, and vWF antibodies at week 4 of perfusion on normal and HGPS TEBVs. Scale bar, 50 μ m.

4.2.3 HGPS ECs affect TEBVs function

To further evaluate if HGPS iPSC-ECs influenced vascular structure and function, In collaboration with Dr. Truskey's lab, we tested the response of TEBVs fabricated from different combinations of healthy and HGPS SMCs and ECs after 1 week of perfusion. In response to 1 mM phenylephrine, we observed a significant difference in contractility between TEBVs fabricated from normal SMCs and HGPS ECs and TEBVs fabricated from HGPS SMCs and HGPS ECs. Most interestingly, TEBVs fabricated from normal ECs showed comparable dilation responses to 1 mM acetylcholine, while TEBVs fabricated from HGPS ECs showed a reduced response to acetylcholine for either SMC donor (normal or HGPS) used. TEBVs fabricated from HGPS- derived SMCs and ECs not only showed a significantly reduced contractile response after exposure to phenylephrine, but a significantly reduced response to acetylcholine compared with

TEBVs fabricated from healthy donor ECs (Figure 4-4a). The results establish that the HGPS iPSC-EC affect the TEBV functions.

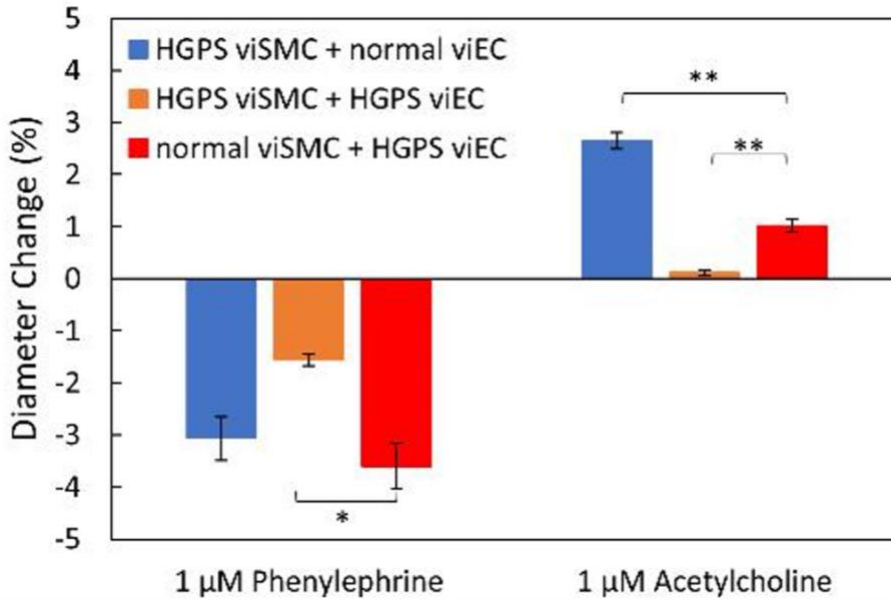


Figure 4-4: Effects of HGPS ECs on TEBV function. Response to 1 μ M phenylephrine and 1 μ M acetylcholine of TEBVs fabricated from combinations of either HGPS or normal SMCs with either normal or HGPS ECs.

4.2.4 HGPS TEBVs exhibit inflammation

To further explore whether the HGPS TEBVs recapitulate disease state, in collaboration with Dr. Truskey’s lab, we evaluated inflammatory adhesion molecule expression in normal and HGPS TEBVs. After 1 and 4 weeks of perfusion, E-selectin and VCAM-1 were strongly expressed in HGPS TEBVs, but not present in healthy donor TEBVs (Figure 4-5). The result suggest that TEBV from HGPS donor mimic the HGPS disease state.

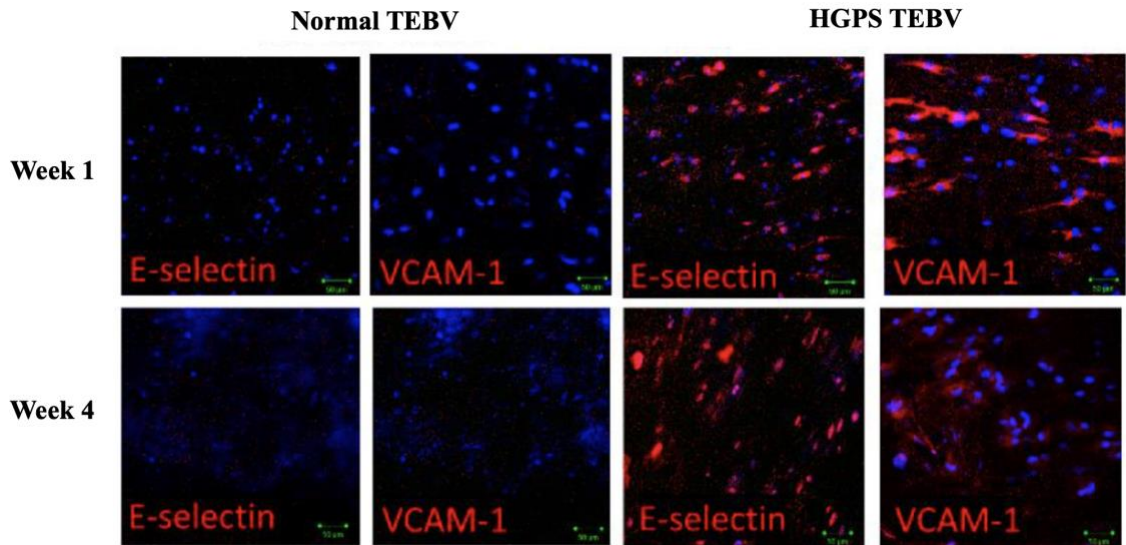


Figure 4-5: HGPS TEBVs exhibit inflammation. Representative images of immunofluorescence staining with VCAM-1 and E-selectin antibodies at week 1 and week 4 of perfusion on normal and HGPS vascular TEBVs. Scale bar, 50 μ m. Data are represented as mean \pm SEM. n = 3–4 TEBVs for each TEBV type. *p < 0.05, **p < 0.01.

4.3 Discussion

Despite the vast knowledge of endothelial dysfunction and its role in cardiovascular pathology, there is still little evidence of how these cells play a role in the development of cardiovascular alteration in HGPS. Since the HGPS patient population is so small, it has been difficult to directly study the vasculature of these patients to parse out the true causes or cell types responsible for cardiovascular pathology. Hence, it is essential that a better cardiovascular model be developed that can directly compare the effects of these cells on vascular structure and function.

Using a differentiation protocol for iPSCs that produced vascular ECs and SMCs, we improved TEBV structure and function over previously developed HGPS TEBVs

(Atchison et al., 2017). Unlike the previous model, these TEBVs exhibit improved contractile function through the expression of the terminal differentiation marker, MYH11. This improved iPSC-derived TEBV provides a more sensitive platform that allows for better evaluation of differences in the HGPS disease state at the 3D tissue level. Moreover, TEBVs exhibit a decrease in vasodilation of when HGPS ECs are incorporated into the constructs, no matter the SMC donor. This indicates a potential role of ECs in HGPS disease development and not just a co-culture effect from the HGPS SMCs.

In addition, 2D cell culture does not fully replicate an *in vivo* microenvironment and therefore is not a true depiction of how certain cells or tissues will react in a specific disease state. These TEBV studies show the importance of a 3D microenvironment to demonstrate differences in cell structure and function. Although HGPS ECs display the basic characteristics of endothelial function in 2D culture, once incorporated into the TEBV constructs, they exhibit many signs of endothelial dysfunction and activation normally present in general atherosclerosis.

EC activation of adhesion molecules, VCAM-1 and E-selectin, is common in various inflammatory conditions and cardiovascular disease development. HGPS TEBVs show an increase in expression of both VCAM-1 and E-selectin after 1 and 4 weeks of perfusion compared with normal TEBVs, indicating a chronic activation of the endothelium in this disease state. This difference shows how various disease states can have different effects on the same pathological processes. Further studies are needed to decipher the exact mechanism behind this activation in HGPS TEBVs.

Chapter 5: Summary and future directions

5.1 Summary

The goal of this study was to investigate the molecular mechanisms of vascular endothelial dysfunction in HGPS through *in vitro* 2D and 3D models. To address the central question of how progerin disrupts endothelial function in HGPS, I proposed three aims that stated in chapter 2, 3, and 4.

In chapter 2, I characterized the human iPSC-derived endothelial cells. Since HGPS is very rare and patients are frail, it is challenging to tissue specific biopsies and cell lines. Hence, I differentiated iPSCs to endothelial lineage. Control and HGPS iPSC-ECs both express human VE-cadherin and PECAM-1 (aka CD31), indicating consistent differentiation in both HGPS and normal controls. Progerin transcripts and protein were both abundant in HGPS iPSC-ECs, leading to significant nuclear abnormalities compared to normal controls ten days post-differentiation. Moreover, the HGPS iPSC-ECs exhibited functional defects in forming microvascular networks on matrigel-based tube formation assay. Progerin overexpressing HUVECs also exhibited a significant reduction in capillary-like microvascular network formation compared to the GFP-lamin A and GFP expressing controls after 18 hours confirming that progerin induces angiogenic defects in ECs.

In chapter 3, I examined the underlying molecular mechanisms of the progerin-induced endothelial dysfunction in HGPS iPSC-ECs. I used human iPSC-ECs models that cultured under both static and fluidic culture conditions. HGPS iPSC-ECs show

reduced eNOS expression and activity compared to normal controls and concomitant decreases in intracellular NO level, which result in deficits in capillary-like microvascular network formation. In addition, expression of MMP-9 was reduced in HGPS iPSC-ECs while expressions of TIMP1 and TIMP2 were upregulated relative to healthy controls. Moreover, I used an adenine base editor (ABE7.10max-VRQR) to correct the pathogenic c.1824C > T allele in HGPS iPSC-ECs. Remarkably, ABE7.10max-VRQR correction of the HGPS mutation significantly reduced progerin expression to a basal level, rescued nuclear blebbing, increased intracellular NO level, normalized TIMPs , and restored angiogenic competence in HGPS iPSC-ECs.

In chapter 4, to elucidate the effects of progerin on endothelial cells and vascular remodeling, in collaboration with Dr. Truskey's group at Duke University, we developed tissue-engineered blood vessels (TEBVs) using iPSC-ECs and iPSC-SMCs from normal and HGPS patients. Due to the inadequacy of 2D culture and animal models in studying the HGPS mechanisms, and limitations in clinical translation, there is a need to develop an improved 3D model to study disease mechanisms and to develop novel therapeutics. Relative to TEBVs with healthy cells, HGPS TEBVs showed reduced function and exhibited markers of cardiovascular disease associated with endothelium. HGPS TEBVs also exhibited a reduction in both vasoconstriction and vasodilation with increased inflammation markers, VCAM-1 and E-selectin protein, suggesting the TEBV model has identified a role of the endothelium in HGPS.

5.2 Future directions

Blood vessel walls are comprised primarily of vascular SMCs and ECs. Interaction between these two major cell types is fundamental to the maintenance of vascular homeostasis and tone (Lilly, 2014). ECs secrete various vasodilators and vasoconstrictors that act on SMCs to induce blood vessel contraction and relaxation (Ignarro et al., 2001; Jacot & Wong, 2008). Emerging evidence also demonstrates that both direct and indirect interplay between ECs and SMCs promoted atherogenesis (Li, Qian, Kyler, & Xu, 2018). Direct EC-SMC crosstalk involves physical contact through cell surface proteins, such as Connexin, Eph/ephrins, and Jagged/Notch3, whereas indirect EC-SMC dialogue is biochemical interactions mediated by cell-released or secreted factors (e.g., EDHF, EVs, miRNA) and matrix (ECM)(Abraham et al., 2009; Cerutti & Ridley, 2017; Dejana, Tournier-Lasserre, & Weinstein, 2009; Giannotta, Trani, & Dejana, 2013; Li et al., 2018).

Studies have shown that co-culturing ECs and SMCs affect their gene expression and function (Heydarkhan-Hagvall et al., 2003). Thus, examining the impacts of progerin in heterocellular interactions environment provides deeper insights into the cardiovascular disease in HGPS. To demonstrate the heterocellular communications between EC and SMCs, I carried out a pilot trial, co-culturing iPSC-ECs (GFP labeled) and SMCs (DsRed labeled) on matrigel-based matrix and observed that the cells spontaneously formed microvascular structures within 24 hours (Figure 5-1). This result suggests that ECs and SMCs actively communicate with each other.

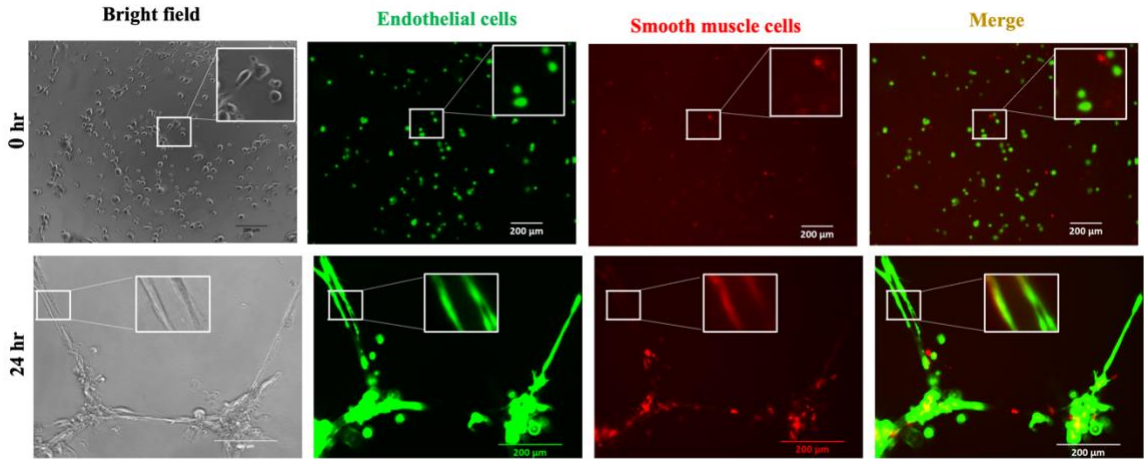


Figure 5-1: Co-culturing of human iPSC-ECs (GFP labeled) and iPSC-SMCs (DsRed labeled) form vessel-like structures on matrigel-based matrix in 24 hours.

Motivated by the 2D co-culturing results, I conducted another pilot study to evaluate the heterocellular communications between ECs and SMCs under shear stress in 3D-printed bioreactor. Structurally, the bioreactor consists of two halves: a lower half containing the scaffold supported by a modular scaffold holder and an upper half for sealing and additional inlets and outlets (Figure 5-2a,b). The lower half is covered with glass, permitting live cell imaging. The two halves are sealed with a rubber gasket and pinned down with eight screws for a watertight fit. Media will enter through the lower chamber, perfuse through the scaffold, and exit through the upper half on the opposite side, thus traversing the entire volume of the bioreactor chamber as shown by the flow trajectories (Figure 5-2a, red arrows). The modular scaffold holder is designed to hold a 10x10x10 mm hydrogel scaffold, which can support both SMC and EC layers, allowing me to recapitulate the complexity of native tissues. Furthermore, the shear stress applied

across the scaffold mimics the *in vivo* vessel environment and promotes vessel maturation.

After 3D-printing and sterilizing the bioreactor, I first cast the scaffold consisting of hydrogel mixed with 1×10^6 DsRed-labeled normal SMCs, then added GFP-labeled normal ECs to the hydrogel-SMCs scaffold at a concentration of 1×10^6 cells/ml. Then the bioreactor was sealed and the vessel wall was put under the shear stress of 0.01 Pa inside a culture incubator at 37 degrees and 5% CO₂ (Figure 5-2b). After three weeks of perfusion, I found that both SMCs and ECs appeared healthy under a fluorescence microscope; no noticeable cell death was identified (Figure 5-2c). This pilot study suggests that the tissue in the bioreactor is stable for at least 3 weeks. This setup has the potential to provide an easy and affordable way to build vessel walls for studying SMC and EC interactions under long-term exposure of shear stress.

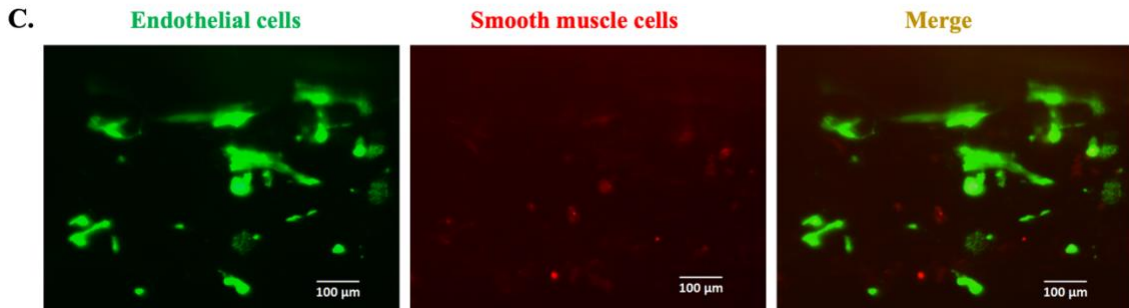
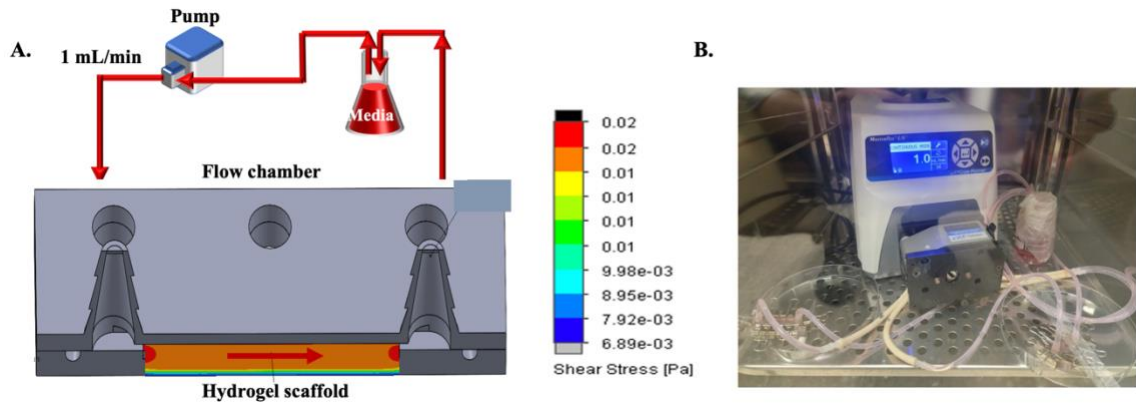


Figure 5-2: Experimental setup of perfusion-based bioreactor. (A) Schematic illustrations of experimental setup of perfusion-based bioreactor (left), and chamber inner surface fluid flow simulation (right). (B) picture of perfusion based-bioreactors with 1 ml/min flow rate. (C) ECs (GFP labeled) and SMCs (DsRed labeled) on hydrogel surface after a week of average shear stress of 0.01 Pa. iPSC-EC, iPSC-derived endothelial cells; iPSC-SMCs, iPSC-derived smooth muscle cells, GFP, green fluorescent protein; DsRed, red fluorescent protein.

Since HGPS-associated vascular dysfunction is due to progerin-induced alterations of multiple pathways in the vessel wall that affect both SMC and ECs, it is crucial to decipher the underlying mechanisms of progerin in heterocellular interactions (i.e., SMC vs. EC). Thus, the method in the pilot study and examining the role of progerin in co-culturing environment may provide deeper insights into the distinct role of vascular cells in HGPS-associated cardiovascular dysfunction.

Chapter 6: Materials and methods

6.1 Endothelial and smooth muscle cells differentiation

For human iPSCs differentiation, iPSC-lines were derived from the normal father skin fibroblasts (HGADFN168) and HGPS patient (son) skin fibroblasts (HGADFN167) with the classic G608G HGPS mutation from Progeria Research Foundation Cell and Tissue Bank. EC differentiation was carried out using an *in vitro* monolayer endothelial differentiation of iPSC based on a previously established protocol with minor modifications in (Atchison et al., 2020; Patsch et al., 2015). In brief, feeder-free iPSCs were cultured in differentiation medium (DMEM/F12; Life Technologies, 11320-033), supplemented with Wnt agonist, glycogen synthase kinase 3 beta (GSK3 β) inhibitor, CHIR-99021, 5 μ M (Cayman, 13122), bone morphogenetic protein-4 (BMP4, 25 ng/ml) (Peprotech, 120-05), B27 supplement (Life technologies, 12587010), and N2 supplement (Life technologies, 17502048) for three days. Then, to induce commitment to the endothelial lineage, cells were cultured in StemPro media (Life technologies, 10639-011) supplemented with forskolin, 5 μ M (Abcam, ab120058) and vascular endothelial growth factor (VEGF165) 100 ng/mL (Peprotech, 100-20) for two days. iPSC-ECs were then isolated by sorting on a FACS (BD) flow cytometer as described in (Atchison et al., 2020) using a PE-CD144 conjugated antibody (mouse anti-human, BD Pharmingen, 560411). Finally, cells were cultured in StemPro media supplemented with VEGF165 (50 ng/ml) and maintained at 37°C, and 5% CO₂ in a humidified incubator. Cells were passaged once they reached 80–90% confluency.

For SMC differentiation, on day 4 the medium in mesodermal cells was changed to SMC induction medium consisting of N2B27 medium supplemented with 10 ng/mL PDGF-BB (PeproTech) and 2 ng/mL Activin A (PeproTech). The SMC induction medium was changed daily. On day 6, cells were dissociated with accutase and replated on collagen-coated plates in SMC medium containing 2 ng/mL Activin A and 2 mg/mL heparin (Stem Cell) to induce a contractile SMC phenotype. The medium was changed every other day and SMCs were routinely passaged at 80%–90% confluency using accutase onto collagen-coated plates and continuously cultured in SMC medium.

6.2 Adenine base editor lentiviral vector cloning

The ABE lentivirus construct was generated as described in (L. W. Koblan et al., 2021). The ABEmax-VRQR gene was inserted into the lentiCRISPRv2 backbone (Addgene 52961) via restriction cloning. Backbone plasmid was digested using AgeI and BamHI according to the manufacturer's protocol. ABEmax-VRQR was amplified from (Addgene 119811) using the primers LWK901 and LWK902. Gibson assembly was performed using a 3:1 molar ratio of insert to vector backbone according to the manufacturer's protocol. The *LMNA* c.1824 C>T targeted sgRNA was installed by digesting the cloned backbone with BsmBI and gel-extracting the resulting cleaved backbone. DNA oligonucleotides encoding the sgRNA were ordered to match the corresponding overhangs generated by BsmBI digestion (5'-CACCGGTCCACCCACCTGGGCTCC-3' and 5'-AAACGGAGCCCAGGTGGGTGGACC-3'). Oligonucleotides were annealed and phosphorylated using T4-PNK according to the manufacturer's instructions and ligated

into the digested backbone as previously described. LWK901: 5'-TTTGCCGCCAG AACACAGGACCGGT GCCACCATGAAACGGACAGCCGACG-3'; LWK902: 5'-GGGAAAAGTT GGTGGCCCCGGATCCGACTTTCCTCTT CTTCTTGGGCTCG-3'.

The human non-targeting control sgRNA sequences are from (Doench et al., 2016). Oligos containing these non-targeting sgRNAs with 5' overhang BsmBI digestion sites were synthesized by Integrated DNA Technologies, Inc. The oligos were first annealed and inserted into the lentiCRISPR v2 plasmids (a gift from Feng Zhang, Addgene plasmid #52961) as described previously in (Sanjana, Shalem, & Zhang, 2014). The fragments containing these non-targeting sgRNAs were digested from the recombinant lentiCRISPR v2 plasmids by restriction enzymes KpnI and NheI. These fragments were then ligated into the ABEmax7.10 backbone, which was extracted from the digests of KpnI and NheI. The sequences of the recombinant plasmids were confirmed by Sanger sequencing. Control sgRNA oligonucleotide sequences:

ctrl sgRNA F 5'-CACCGGCCTGCCCTAAACCCCGGAA-3';

ctrl sgRNA R 5'-AACTTCCGGGGTTTAGGGCAGGCC-3'.

6.3 Lentiviral production

The lentivirus production was carried out as described in (L. W. Koblan et al., 2021). HEK239T/17 (ATCC CRL-11268) cells were maintained in antibiotic-free DMEM (Thermo Fisher Scientific 10569044) supplemented with 10% (v/v) fetal bovine serum (Thermo Fisher Scientific), at 37 °C with 5% CO₂. On day 1, cells were split 1:3

from rapidly dividing HEK293T/17 flasks that had been split 1:10 three days prior. The following day, the medium was changed on cells and cells were transfected using FuGENE HD according to the manufacturer's protocol. Transfection mix included 9 µg of transfer vector (the packaging genome of interest), 9 µg of psPAX2 (encoding the viral packaging proteins) and 6 µg of pVSV-G (encoding the VSV-G envelope protein). Transfection mix was then supplemented with 70 µl of room temperature equilibrated FuGENE and brought to a final volume of 1,500 µl per flask with Opti-MEM. Two days after transfection, medium was collected and spun at 3,000g for 15 min to remove remaining cells. Centrifuged supernatant was passed through a 0.45-µm PVDF filter to eliminate all non-viral debris. Supernatant was transferred directly to target cells.

6.4 Fabrication of fluidic chambers

Fluidic culture chambers were designed in SOLIDWORKS (Dassault Systems), as described in (Lembong et al., 2018) with minor modifications. The inner culture chamber was 56 x 12 x 5 mm in length, breadth, and height with no internal geometries that could hinder fluid flow. The chambers were 3D printed using the EnvisionTEC Perfactory IV 3D printer and EShell®300 as the resin material. Following printing, chambers were washed in isopropanol to eliminate residual, uncross-linked material, and then flash cured. For sterilization, chambers were filled with ethanol and then exposed to ultraviolet light for an hour. Chambers were then rehydrated by serial washes in the following sterile solutions: (1) 75% ethanol/25% phosphate-buffered saline (PBS), (2) 50% ethanol/50% PBS, (3) 25% ethanol/75% PBS, and (4) 100% PBS, then stored in PBS. Before cell seeding, flow chambers were coated with 3 µg/cm² fibronectin

(Corning, 356008) in PBS for 1h at 37°C to facilitate cell attachment. Chambers were connected to a peristaltic pump set to 5 ml/min with media circulation.

6.5 Immunocytochemistry

For immunocytochemistry, cells were washed once with PBS and fixed in 4% paraformaldehyde (PFA) for 15 min. Cells were then blocked with 10% normal donkey serum in PBS (Blocking buffer) for 1 hour. When probing for an intracellular antigen, 0.3% Triton-X was included in the blocking buffer. Cells were then incubated with the primary antibodies lamin A/C (MAB3211, Millipore, 1:250), progerin (Cao, Graziotto, et al., 2011) with a dilution of 1: 250, goat anti-VE-cadherin (AF938; R &D systems, 1:100), and sheep anti-PECAM1 (AF806, R &D systems, 1:100), in 5% normal donkey serum in PBS overnight at 4°C. After three washes with PBS, cells were incubated in 1% BSA in PBS containing secondary antibodies and DAPI (Vector Laboratories). Secondary antibodies used for immunocytochemistry were Alexa Fluor[®]594 donkey anti-rabbit IgG (Invitrogen, 1:1000), and Alexa Fluor[®] 488 donkey anti-mouse IgG (Invitrogen, 1:1000 dilution). Cells were washed three times with PBS, and images were acquired with Zeiss AX10 microscope equipped with a SPOT PURSUIT camera. For the analysis of nuclear morphology, greater than 120 nuclei were analyzed per condition where the nuclei were assigned by visual inspection into normal or abnormal nuclear phenotype.

6.6 Western blotting

Whole cell lysates for immunoblotting were prepared by dissolving cells in Laemmli Sample Buffer containing 5% of 2-mercaptoethanol (Bio-Rad). Primary antibodies used for immunoblotting include: anti-lamin A/C (MAB3211, Millipore, 1:500 dilution), progerin (Cao, Graziotto, et al., 2011) with a dilution of 1:500, anti-eNOS (D9A5L, Cell signaling, 1:1000), anti-pThr eNOS (Cell signaling, 1:1000), mouse anti-GAPDH (sc-47724, Santa Cruz, 1:3000), goat anti-VE-cadherin (AF938; R &D systems, 1:500), and anti-PECAM1 (AF806, R &D systems, 1:500), anti-MMP-1, 2, 7, 9,14, TIMP1, and TIMP2 (Kit # 73959, Cell signaling, 1:1000 dilution), anti-smooth muscle Myosin heavy chain 11 (ab53219, Abcam, 1:1000 dilution). Secondary antibodies include : anti-mouse (sc-516102, Santa Cruz, 1:5000), anti-rabbit (211-035-109, Jackson Immuno-Research, 1:5000), anti-goat (HAF017, R&D systems, 1:1000), and anti-goat (HAF019, R&D systems, 1:1000 dilution).

6.7 RNA extraction, cDNA synthesis, and RT-qPCR

Total RNA from human cell lines was extracted with Trizol reagent (Life Technologies, 15596026) and purified using the RNeasy mini kit (Qiagen) per the manufacturer's instructions. RNA yield was determined using the NanoDrop 2000 spectrophotometer (Thermo Scientific). Total RNA (1 μ g) was converted to cDNA using the iScript select cDNA synthesis kit (Bio-Rad) according to manufacturer's instructions. Quantitative RT-PCR was carried out in triplicate using SYBR Green supermix (BioRad) and detection was achieved using CFX96 real time system (C1000 Thermal Cycler, Bio-Rad). Gene expression was calculated as a relative fold change using the Δ Ct method of analysis and normalized to GAPDH. The specific primers sequences are in Table 1.

6.8 Nitric Oxide assays

After 48 hours of incubation, 1 ml media was taken and flash frozen in liquid nitrogen and frozen at -80°C. For the cell in the fluidic bioreactors, after 24 hours of perfusion, 1 ml media was removed from the flow circuit and flash frozen in liquid nitrogen and frozen at -80°C. Prior to testing, samples were spun at 9,500 RCF for 7 minutes with a 10,000 MWCO spin column (Corning). Total nitrate and nitrite were measured using a colorimetric Assay (Arbor Assays) per kit instructions. Absorbance was measured at 540 nm using a 96 well microplate reader. For the second method of intracellular NO levels measurement, we used DAF-FM (Thermo Scientific). iPSC-ECs were treated with 0, 0.25, 0.5, and 1 mM nitric oxide donor S-Nitroso-N-acetyl-DL-penicillamine (SNAP, N3398, Sigma-Aldrich), and with an eNOS inhibitor (0.2 mM N-omega-Nitro-L-arginine methyl ester hydrochloride; L-NAME, N5751, Sigma-Aldrich), then incubated with DAF-FM 10 μ M at 37°C, and 5% CO₂ for 30 min per manufacturer recommendation. Excess probe was removed by washing with PBS and the cells were switched to fresh media prior to imaging. Images were acquired with Zeiss AX10 microscope equipped with a SPOT PURSUIT camera. The intensity of the DAF-FM fluorescent signal (intracellular NO level) was measured using imageJ and plotted as mean of the fluorescent signal (integrated density) in each cell.

6.9 Tube formation assay

150 μ L of Matrigel (Corning Matrigel Basement Membrane Matrix Growth Factor Reduced, Phenol Red Free, 356231) was aliquoted to 48-well plates and incubated for 30 minutes at 37°C to allow the gel to solidify. 20,000 iPSC-ECs were seeded onto

the Matrigel matrix and cultured for 18 hours at 37°C and images were acquired using Zeiss AX10 microscope equipped with a SPOT PURSUIT camera. The tube length was measured using ImageJ software. For the cell density and time course experiment in supplemental figure-3, the specified cells were seeded on 96-well plate using 75 μ L of Matrigel. To test the angiogenic potentials of the live normal and HGPS iPSC-ECs, 10,000 cells were seeded on 96 well plate with iPSC-ECs media. Then, Spinning disk confocal images were acquired for 18 hours using an UltraVIEW VoX system (PerkinElmer, Waltham, MA) attached to an inverted microscope (Eclipse Ti; Nikon Instruments, Melville, NY) with a 10 \times NA 1.3 objective (Nikon) and a CCD camera (C9100-50; Hamamatsu Photonics, Bridgewater, NJ) with maintaining the culture condition of 37°C, and 5% CO₂.

6.10 TEBV fabrication and functional testing

TEBVs were fabricated as described previously in (Fernandez et al., 2016). In brief, 1.5×10^6 normal or HGPS SMCs were dissociated with accutase and resuspended in 300 μ L of SMC medium and incorporated in a 2.05 mg/mL rat tail collagen type 1 solution (Corning, Corning, NY) in 0.6% acetic acid. Serum-free 10 \times DMEM (Sigma Aldrich, Raleigh, NC) was added at a 1:10 ratio to the collagen solution. The pH of the solution was raised to 8.5 by adding 5 M NaOH, causing gelation. Before complete gelation, the solution was placed in a 3-mL syringe mold (BD Biosciences, San Jose, CA) with the stopper completely removed and a two-way luer lock stopcock attached to the luer lock end of the syringe. An 800- μ m diameter steel mandrel was inserted in the middle of the solution in the syringe and held in the center with parafilm wrapped over

the syringe opening. The solution gelled for 30 min at room temperature before compression. After gelation, the vessel construct was transferred onto 0.2- μm nylon filter paper (Whatman, Maidstone, UK) on 10 KimWipes. Plastic compression was applied to the construct by suspension in the filter paper for 7 min to remove over 90% of the water content. Once compressed, the TEBVs were placed in custom perfusion chambers and sutured onto grips at both ends.

After gelation and mounting, TEBVs were endothelialized by dissociating adherent normal ECs, or HGPS ECs with 0.05% Trypsin/EDTA (Lonza) or Accutase, respectively. The ECs were resuspended at 0.5×10^6 cells in 0.5 mL with EC media. ECs were perfused through the lumen using 1 mL luer lock syringes (BD) connected to the grips of the custom chambers. The TEBVs were evenly endothelialized by rotating the chambers at 10 revolutions per hour for 30 min at 37°C on a rotator. Chambers were attached to a flow circuit containing a 25-mL media reservoir connected by tubing. Continuous, steady, laminar flow at 2 mL/min was applied to the TEBVs by attaching the perfusion circuit to a peristaltic pump that applied a physiological shear stress of 6.8 dynes/cm² (Masterflex, Gelsenkirchen, Germany). The TEBVs were matured for up to 6 weeks and the medium was changed three times per week. All TEBVs were perfused in SMC medium.

6.11 Vessel vasoactivity assay

Vessel vasoactivity was calculated as the change in diameter of the TEBVs after exposure to 1 μM phenylephrine (Sigma) and 1 μM acetylcholine (Sigma). Vasoactivity was measured in the same perfusion circuit that TEBVs were cultured in at room

temperature and imaged using a stereoscope (AmScope) while being recorded with ISCapture software. After 30 s of normal perfusion, 1 μ M phenylephrine was added to a syringe port (Ibidi) integrated in the flow circuit, and after 5 min 1 μ M acetylcholine was added. This process was performed weekly for all studies. Screen shots were taken at 30 s (before phenylephrine addition) to establish baseline, at 5 min (after phenylephrine addition), and at 10 min (after acetylcholine addition). The diameter at each time point was determined by averaging four random widths along the length of the vessel using ImageJ. Vessel diameter measurements were defined at the 30-s time point. Vasoconstriction in response to phenylephrine was calculated as the percent change in diameter from the initial diameter at 30 s before addition of phenylephrine to the diameter at 5 min after addition of phenylephrine. The vasodilation in response to acetylcholine was calculated as the percent change in diameter from the constricted state at 5 min to the diameter at 10 min.

6.12 Statistical analysis

Statistical analyses were performed using GraphPad Prism 7 software. Data were evaluated using Students' unpaired *t-test* for two groups, and one-way analysis of variance (ANOVA), and a post hoc Tukey test to compare means of three or more groups. Results are presented as the mean \pm S.E.M. p value < 0.05 was considered significant.

Table 1: Primer sequences used for RT-PCR experiment

Target gene	Primer sequence
GAPDH	Forward: 5'-GTCTCCTCTGACTTCAACAGCG-3'
	Reverse: 5'-ACCACCCTGTTGCTGTAGCCAA-3'
CDH5	Forward:5'-GAAGCCTCTGATTGGCACAGTG-3'
	Reverse: 5'-TTTTGTGACTCGGAAGAACTGGC-3'
PECAM-1	Forward: 5'-AAGTGGAGTCCAGCCGCATATC-3'
	Reverse: 5'-ATGGAGCAGGACAGGTTTCAGTC-3'
LMNA	Forward: 5'-GCAACAAGTCCAATGAGGACCA-3'
	Reverse: 5'-CATGATGCTGCAGTTCTGGGGGCTCTGGAT-3'
progerin	Forward: 5'-GCAACAAGTCCAATGAGGACCA-3'
	Reverse: 5'-CATGATGCTGCAGTTCTGGGGGCTCTGGAC-3'

Appendices

Besides the above study, I am also involved in the following two projects that were published in *Nucleus* and *Nature* (L. W. Koblan et al., 2021; Tariq et al., 2017).

- (1). Tariq Z, Zhang H, Chia-Liu A, Shen Y, **Gete Y**, Xiong ZM, Tocheny C, Campanello L, Wu D, Losert W, Cao K. Lamin A and microtubules collaborate to maintain nuclear morphology. *Nucleus*. 2017 Jul 4;8(4):433-446.

In this study, we elucidated the role of the cytoskeleton in regulation and misregulation of nuclear morphology through perturbations of both the lamina and the microtubule network. We found that lamin A knockout cells exhibit a crescent shape morphology associated with the microtubule-organizing center. Furthermore, this crescent shape ameliorates upon treatment with microtubule drugs, Nocodazole or Taxol. Expression of progerin, in lamin A knockout cells also rescues the crescent shape, although the response to Nocodazole or Taxol treatment is altered in comparison to cells expressing lamin A. Together these results describe a collaborative effort between lamin A and the microtubule network to maintain nuclear morphology.

- (2). Koblan LW, Erdos MR, Wilson C, Cabral WA, Levy JM, Xiong ZM, Tavares UL, Davison LM, **Gete YG**, Mao X, Newby GA, Doherty SP, Narisu N, Sheng Q, Krilow C, Lin CY, Gordon LB, Cao K, Collins FS, Brown JD, Liu DR. *In vivo* base editing rescues Hutchinson-Gilford progeria syndrome in mice. *Nature*. 2021 Jan; 589(7843):608-614.

In this study, we describe the use of adenine base editors (ABEs) to directly correct the pathogenic HGPS mutation in cultured fibroblasts derived from children with

progeria and in a mouse model of HGPS. Lentiviral delivery of the ABE to fibroblasts from children with HGPS resulted in 87-91% correction of the pathogenic allele, mitigation of RNA mis-splicing, reduced levels of progerin and correction of nuclear abnormalities. Unbiased off-target DNA and RNA editing analysis did not detect off-target editing in treated patient-derived fibroblasts. In transgenic mice that are homozygous for the human LMNA c.1824 C>T allele, a single retro-orbital injection of adeno-associated virus 9 (AAV9) encoding the ABE resulted in substantial, durable correction of the pathogenic mutation (around 20-60% across various organs six months after injection), restoration of normal RNA splicing and reduction of progerin protein levels. *In vivo* base editing rescued the vascular pathology of the mice, preserving vascular smooth muscle cell counts and preventing adventitial fibrosis. A single injection of ABE-expressing AAV9 at postnatal day 14 improved vitality and greatly extended the median lifespan of the mice from 215 to 510 days. These findings demonstrate the potential of *in vivo* base editing as a possible treatment for HGPS and other genetic diseases by directly correcting their root cause.

Bibliography

- Abraham, S., Yeo, M., Montero-Balaguer, M., Paterson, H., Dejana, E., Marshall, C. J., & Mavria, G. (2009). VE-Cadherin-mediated cell-cell interaction suppresses sprouting via signaling to MLC2 phosphorylation. *Curr Biol*, *19*(8), 668-674. doi:10.1016/j.cub.2009.02.057
- Abutaleb, N. O., & Truskey, G. A. (2020). Human iPSCs Stretch to Improve Tissue-Engineered Vascular Grafts. *Cell Stem Cell*, *26*(2), 136-137. doi:10.1016/j.stem.2020.01.011
- Amoasii, L., Long, C., Li, H., Mireault, A. A., Shelton, J. M., Sanchez-Ortiz, E., . . . Olson, E. N. (2017). Single-cut genome editing restores dystrophin expression in a new mouse model of muscular dystrophy. *Sci Transl Med*, *9*(418). doi:10.1126/scitranslmed.aan8081
- Andrique, L., Recher, G., Alessandri, K., Pujol, N., Feyeux, M., Bon, P., . . . Bikfalvi, A. (2019). A model of guided cell self-organization for rapid and spontaneous formation of functional vessels. *Sci Adv*, *5*(6), eaau6562. doi:10.1126/sciadv.aau6562
- Anzalone, A. V., Koblan, L. W., & Liu, D. R. (2020). Genome editing with CRISPR-Cas nucleases, base editors, transposases and prime editors. *Nat Biotechnol*, *38*(7), 824-844. doi:10.1038/s41587-020-0561-9
- Atchison, L., Abutaleb, N. O., Snyder-Mounts, E., Gete, Y., Ladha, A., Ribar, T., . . . Truskey, G. A. (2020). iPSC-Derived Endothelial Cells Affect Vascular Function in a Tissue-Engineered Blood Vessel Model of Hutchinson-Gilford Progeria Syndrome. *Stem Cell Reports*, *14*(2), 325-337. doi:10.1016/j.stemcr.2020.01.005

- Atchison, L., Zhang, H., Cao, K., & Truskey, G. A. (2017). A Tissue Engineered Blood Vessel Model of Hutchinson-Gilford Progeria Syndrome Using Human iPSC-derived Smooth Muscle Cells. *Sci Rep*, 7(1), 8168. doi:10.1038/s41598-017-08632-4
- Baker, A. H., Edwards, D. R., & Murphy, G. (2002). Metalloproteinase inhibitors: biological actions and therapeutic opportunities. *J Cell Sci*, 115(Pt 19), 3719-3727. doi:10.1242/jcs.00063
- Baker, P. B., Baba, N., & Boesel, C. P. (1981). Cardiovascular abnormalities in progeria. Case report and review of the literature. *Arch Pathol Lab Med*, 105(7), 384-386.
- Bao, X., Lian, X., Dunn, K. K., Shi, M., Han, T., Qian, T., . . . Palecek, S. P. (2015). Chemically-defined albumin-free differentiation of human pluripotent stem cells to endothelial progenitor cells. *Stem Cell Res*, 15(1), 122-129. doi:10.1016/j.scr.2015.05.004
- Benedicto, I., Dorado, B., & Andres, V. (2021). Molecular and Cellular Mechanisms Driving Cardiovascular Disease in Hutchinson-Gilford Progeria Syndrome: Lessons Learned from Animal Models. *Cells*, 10(5). doi:10.3390/cells10051157
- Beyret, E., Liao, H. K., Yamamoto, M., Hernandez-Benitez, R., Fu, Y., Erikson, G., . . . Izpisua Belmonte, J. C. (2019). Single-dose CRISPR-Cas9 therapy extends lifespan of mice with Hutchinson-Gilford progeria syndrome. *Nat Med*, 25(3), 419-422. doi:10.1038/s41591-019-0343-4
- Boo, Y. C., Hwang, J., Sykes, M., Michell, B. J., Kemp, B. E., Lum, H., & Jo, H. (2002). Shear stress stimulates phosphorylation of eNOS at Ser(635) by a protein kinase

- A-dependent mechanism. *Am J Physiol Heart Circ Physiol*, 283(5), H1819-1828.
doi:10.1152/ajpheart.00214.2002
- Booth-Gauthier, E. A., Du, V., Ghibaudo, M., Rape, A. D., Dahl, K. N., & Ladoux, B. (2013). Hutchinson-Gilford progeria syndrome alters nuclear shape and reduces cell motility in three dimensional model substrates. *Integr Biol (Camb)*, 5(3), 569-577. doi:10.1039/c3ib20231c
- Brew, K., Dinakarpanian, D., & Nagase, H. (2000). Tissue inhibitors of metalloproteinases: evolution, structure and function. *Biochim Biophys Acta*, 1477(1-2), 267-283. doi:10.1016/s0167-4838(99)00279-4
- Burke, B., & Stewart, C. L. (2006). The laminopathies: the functional architecture of the nucleus and its contribution to disease. *Annu Rev Genomics Hum Genet*, 7, 369-405. doi:10.1146/annurev.genom.7.080505.115732
- Burke, B., & Stewart, C. L. (2013). The nuclear lamins: flexibility in function. *Nat Rev Mol Cell Biol*, 14(1), 13-24. doi:10.1038/nrm3488
- Burtner, C. R., & Kennedy, B. K. (2010). Progeria syndromes and ageing: what is the connection? *Nat Rev Mol Cell Biol*, 11(8), 567-578. doi:10.1038/nrm2944
- Cabral, W. A., Tavares, U. L., Beeram, I., Yeritsyan, D., Boku, Y. D., Eckhaus, M. A., . . . Collins, F. S. (2021). Genetic reduction of mTOR extends lifespan in a mouse model of Hutchinson-Gilford Progeria syndrome. *Aging Cell*, 20(9), e13457. doi:10.1111/acel.13457
- Cao, K., Blair, C. D., Faddah, D. A., Kieckhafer, J. E., Olive, M., Erdos, M. R., . . . Collins, F. S. (2011). Progerin and telomere dysfunction collaborate to trigger

- cellular senescence in normal human fibroblasts. *J Clin Invest*, 121(7), 2833-2844. doi:10.1172/JCI43578
- Cao, K., Capell, B. C., Erdos, M. R., Djabali, K., & Collins, F. S. (2007). A lamin A protein isoform overexpressed in Hutchinson-Gilford progeria syndrome interferes with mitosis in progeria and normal cells. *Proc Natl Acad Sci U S A*, 104(12), 4949-4954. doi:10.1073/pnas.0611640104
- Cao, K., Graziotto, J. J., Blair, C. D., Mazzulli, J. R., Erdos, M. R., Krainc, D., & Collins, F. S. (2011). Rapamycin reverses cellular phenotypes and enhances mutant protein clearance in Hutchinson-Gilford progeria syndrome cells. *Sci Transl Med*, 3(89), 89ra58. doi:10.1126/scitranslmed.3002346
- Capell, B. C., & Collins, F. S. (2006). Human laminopathies: nuclei gone genetically awry. *Nat Rev Genet*, 7(12), 940-952. doi:10.1038/nrg1906
- Capell, B. C., Olive, M., Erdos, M. R., Cao, K., Faddah, D. A., Tavaréz, U. L., . . . Collins, F. S. (2008). A farnesyltransferase inhibitor prevents both the onset and late progression of cardiovascular disease in a progeria mouse model. *Proc Natl Acad Sci U S A*, 105(41), 15902-15907. doi:10.1073/pnas.0807840105
- Cerutti, C., & Ridley, A. J. (2017). Endothelial cell-cell adhesion and signaling. *Exp Cell Res*, 358(1), 31-38. doi:10.1016/j.yexcr.2017.06.003
- Cheng, C., van Haperen, R., de Waard, M., van Damme, L. C., Tempel, D., Hanemaaijer, L., . . . Krams, R. (2005). Shear stress affects the intracellular distribution of eNOS: direct demonstration by a novel in vivo technique. *Blood*, 106(12), 3691-3698. doi:10.1182/blood-2005-06-2326

- Choi, J. Y., Lai, J. K., Xiong, Z. M., Ren, M., Moorer, M. C., Stains, J. P., & Cao, K. (2018). Diminished Canonical beta-Catenin Signaling During Osteoblast Differentiation Contributes to Osteopenia in Progeria. *J Bone Miner Res*, *33*(11), 2059-2070. doi:10.1002/jbmr.3549
- Coenen, A. M. J., Bernaerts, K. V., Harings, J. A. W., Jockenhoevel, S., & Ghazanfari, S. (2018). Elastic materials for tissue engineering applications: Natural, synthetic, and hybrid polymers. *Acta Biomater*, *79*, 60-82. doi:10.1016/j.actbio.2018.08.027
- Cong, L., Ran, F. A., Cox, D., Lin, S., Barretto, R., Habib, N., . . . Zhang, F. (2013). Multiplex genome engineering using CRISPR/Cas systems. *Science*, *339*(6121), 819-823. doi:10.1126/science.1231143
- Cox, D. B., Platt, R. J., & Zhang, F. (2015). Therapeutic genome editing: prospects and challenges. *Nat Med*, *21*(2), 121-131. doi:10.1038/nm.3793
- Csoka, A. B., English, S. B., Simkevich, C. P., Ginzinger, D. G., Butte, A. J., Schatten, G. P., . . . Sedivy, J. M. (2004). Genome-scale expression profiling of Hutchinson-Gilford progeria syndrome reveals widespread transcriptional misregulation leading to mesodermal/mesenchymal defects and accelerated atherosclerosis. *Aging Cell*, *3*(4), 235-243. doi:10.1111/j.1474-9728.2004.00105.x
- Davis, G. E., & Senger, D. R. (2005). Endothelial extracellular matrix: biosynthesis, remodeling, and functions during vascular morphogenesis and neovessel stabilization. *Circ Res*, *97*(11), 1093-1107. doi:10.1161/01.RES.0000191547.64391.e3

- de Leeuw, R., Gruenbaum, Y., & Medalia, O. (2018). Nuclear Lamins: Thin Filaments with Major Functions. *Trends Cell Biol*, 28(1), 34-45.
doi:10.1016/j.tcb.2017.08.004
- De Sandre-Giovannoli, A., Bernard, R., Cau, P., Navarro, C., Amiel, J., Boccaccio, I., . . . Levy, N. (2003). Lamin a truncation in Hutchinson-Gilford progeria. *Science*, 300(5628), 2055. doi:10.1126/science.1084125
- DeBusk, F. L. (1972). The Hutchinson-Gilford progeria syndrome. Report of 4 cases and review of the literature. *J Pediatr*, 80(4), 697-724. doi:10.1016/s0022-3476(72)80229-4
- Dechat, T., Adam, S. A., & Goldman, R. D. (2009). Nuclear lamins and chromatin: when structure meets function. *Adv Enzyme Regul*, 49(1), 157-166.
doi:10.1016/j.advenzreg.2008.12.003
- Dechat, T., Adam, S. A., Taimen, P., Shimi, T., & Goldman, R. D. (2010). Nuclear lamins. *Cold Spring Harb Perspect Biol*, 2(11), a000547.
doi:10.1101/cshperspect.a000547
- Dechat, T., Pflieger, K., Sengupta, K., Shimi, T., Shumaker, D. K., Solimando, L., & Goldman, R. D. (2008). Nuclear lamins: major factors in the structural organization and function of the nucleus and chromatin. *Genes Dev*, 22(7), 832-853. doi:10.1101/gad.1652708
- Dejana, E., Tournier-Lasserre, E., & Weinstein, B. M. (2009). The control of vascular integrity by endothelial cell junctions: molecular basis and pathological implications. *Dev Cell*, 16(2), 209-221. doi:10.1016/j.devcel.2009.01.004

- Del Campo, L., Sanchez-Lopez, A., Gonzalez-Gomez, C., Andres-Manzano, M. J., Dorado, B., & Andres, V. (2020). Vascular Smooth Muscle Cell-Specific Progerin Expression Provokes Contractile Impairment in a Mouse Model of Hutchinson-Gilford Progeria Syndrome that Is Ameliorated by Nitrite Treatment. *Cells*, 9(3). doi:10.3390/cells9030656
- Del Campo, L., Sanchez-Lopez, A., Salaires, M., von Kleeck, R. A., Exposito, E., Gonzalez-Gomez, C., . . . Andres, V. (2019). Vascular smooth muscle cell-specific progerin expression in a mouse model of Hutchinson-Gilford progeria syndrome promotes arterial stiffness: Therapeutic effect of dietary nitrite. *Aging Cell*, 18(3), e12936. doi:10.1111/accel.12936
- Dittmer, T. A., & Misteli, T. (2011). The lamin protein family. *Genome Biol*, 12(5), 222. doi:10.1186/gb-2011-12-5-222
- Doench, J. G., Fusi, N., Sullender, M., Hegde, M., Vaimberg, E. W., Donovan, K. F., . . . Root, D. E. (2016). Optimized sgRNA design to maximize activity and minimize off-target effects of CRISPR-Cas9. *Nat Biotechnol*, 34(2), 184-191. doi:10.1038/nbt.3437
- Dorado, B., Ploen, G. G., Baretino, A., Macias, A., Gonzalo, P., Andres-Manzano, M. J., . . . Andres, V. (2019). Generation and characterization of a novel knockin minipig model of Hutchinson-Gilford progeria syndrome. *Cell Discov*, 5, 16. doi:10.1038/s41421-019-0084-z
- Ebrahem, Q., Qi, J. H., Sugimoto, M., Ali, M., Sears, J. E., Cutler, A., . . . Anand-Apte, B. (2011). Increased neovascularization in mice lacking tissue inhibitor of

metalloproteinases-3. *Invest Ophthalmol Vis Sci*, 52(9), 6117-6123.

doi:10.1167/iovs.10-5899

Erdos, M. R., Cabral, W. A., Tavares, U. L., Cao, K., Gvozdenovic-Jeremic, J., Narisu, N., . . . Collins, F. S. (2021). A targeted antisense therapeutic approach for Hutchinson-Gilford progeria syndrome. *Nat Med*, 27(3), 536-545.

doi:10.1038/s41591-021-01274-0

Eriksson, M., Brown, W. T., Gordon, L. B., Glynn, M. W., Singer, J., Scott, L., . . . Collins, F. S. (2003). Recurrent de novo point mutations in lamin A cause Hutchinson-Gilford progeria syndrome. *Nature*, 423(6937), 293-298.

doi:10.1038/nature01629

nature01629 [pii]

Fernandez, C. E., Yen, R. W., Perez, S. M., Bedell, H. W., Povsic, T. J., Reichert, W. M., & Truskey, G. A. (2016). Human Vascular Microphysiological System for in vitro Drug Screening. *Sci Rep*, 6, 21579. doi:10.1038/srep21579

Fleming, I. (2010). Molecular mechanisms underlying the activation of eNOS. *Pflugers Arch*, 459(6), 793-806. doi:10.1007/s00424-009-0767-7

Fong, L. G., Ng, J. K., Lammerding, J., Vickers, T. A., Meta, M., Cote, N., . . . Young, S. G. (2006). Prelamin A and lamin A appear to be dispensable in the nuclear lamina. *J Clin Invest*, 116(3), 743-752. doi:10.1172/JCI27125

Fukumura, D., Gohongi, T., Kadambi, A., Izumi, Y., Ang, J., Yun, C. O., . . . Jain, R. K. (2001). Predominant role of endothelial nitric oxide synthase in vascular endothelial growth factor-induced angiogenesis and vascular permeability. *Proc Natl Acad Sci U S A*, 98(5), 2604-2609. doi:10.1073/pnas.041359198

- Galiova, G., Bartova, E., Raska, I., Krejci, J., & Kozubek, S. (2008). Chromatin changes induced by lamin A/C deficiency and the histone deacetylase inhibitor trichostatin A. *Eur J Cell Biol*, 87(5), 291-303. doi:10.1016/j.ejcb.2008.01.013
- Gao, X., Tao, Y., Lamas, V., Huang, M., Yeh, W. H., Pan, B., . . . Liu, D. R. (2018). Treatment of autosomal dominant hearing loss by in vivo delivery of genome editing agents. *Nature*, 553(7687), 217-221. doi:10.1038/nature25164
- Gaudelli, N. M., Komor, A. C., Rees, H. A., Packer, M. S., Badran, A. H., Bryson, D. I., & Liu, D. R. (2017). Programmable base editing of A•T to G•C in genomic DNA without DNA cleavage. *Nature*, 551(7681), 464-471. doi:10.1038/nature24644
- Gaudelli, N. M., Komor, A. C., Rees, H. A., Packer, M. S., Badran, A. H., Bryson, D. I., & Liu, D. R. (2017). Programmable base editing of A•T to G•C in genomic DNA without DNA cleavage. *Nature*, 551(7681), 464-471. doi:10.1038/nature24644
- Gerhard-Herman, M., Smoot, L. B., Wake, N., Kieran, M. W., Kleinman, M. E., Miller, D. T., . . . Gordon, L. B. (2012). Mechanisms of premature vascular aging in children with Hutchinson-Gilford progeria syndrome. *Hypertension*, 59(1), 92-97. doi:10.1161/HYPERTENSIONAHA.111.180919
- Gete, Y. G., Koblan, L. W., Mao, X., Trappio, M., Mahadik, B., Fisher, J. P., . . . Cao, K. (2021). Mechanisms of angiogenic incompetence in Hutchinson-Gilford progeria via downregulation of endothelial NOS. *Aging Cell*, 20(7), e13388. doi:10.1111/acel.13388
- Giannotta, M., Trani, M., & Dejana, E. (2013). VE-cadherin and endothelial adherens junctions: active guardians of vascular integrity. *Dev Cell*, 26(5), 441-454. doi:10.1016/j.devcel.2013.08.020

- Gilford, H. (1897). On a Condition of Mixed Premature and Immature Development. *Med Chir Trans*, 80, 17-46 25. doi:10.1177/095952879708000105
- Gimbrone, M. A., Jr., & Garcia-Cardena, G. (2016). Endothelial Cell Dysfunction and the Pathobiology of Atherosclerosis. *Circ Res*, 118(4), 620-636. doi:10.1161/CIRCRESAHA.115.306301
- Goldman, R. D., Gruenbaum, Y., Moir, R. D., Shumaker, D. K., & Spann, T. P. (2002). Nuclear lamins: building blocks of nuclear architecture. *Genes Dev*, 16(5), 533-547. doi:10.1101/gad.960502
- Goldman, R. D., Shumaker, D. K., Erdos, M. R., Eriksson, M., Goldman, A. E., Gordon, L. B., . . . Collins, F. S. (2004). Accumulation of mutant lamin A causes progressive changes in nuclear architecture in Hutchinson-Gilford progeria syndrome. *Proc Natl Acad Sci U S A*, 101(24), 8963-8968. doi:10.1073/pnas.0402943101
- Gonzalez, J. M., Navarro-Puche, A., Casar, B., Crespo, P., & Andres, V. (2008). Fast regulation of AP-1 activity through interaction of lamin A/C, ERK1/2, and c-Fos at the nuclear envelope. *J Cell Biol*, 183(4), 653-666. doi:10.1083/jcb.200805049
- Gonzalo, S., & Kreienkamp, R. (2015). DNA repair defects and genome instability in Hutchinson-Gilford Progeria Syndrome. *Curr Opin Cell Biol*, 34, 75-83. doi:10.1016/j.ceb.2015.05.007
- Gordon, L. B., Kleinman, M. E., Massaro, J., D'Agostino, R. B., Sr., Shappell, H., Gerhard-Herman, M., . . . Kieran, M. W. (2016). Clinical Trial of the Protein Farnesylation Inhibitors Lonafarnib, Pravastatin, and Zoledronic Acid in Children

With Hutchinson-Gilford Progeria Syndrome. *Circulation*, *134*(2), 114-125.
doi:10.1161/CIRCULATIONAHA.116.022188

Gordon, L. B., Kleinman, M. E., Miller, D. T., Neuberg, D. S., Giobbie-Hurder, A.,
Gerhard-Herman, M., . . . Kieran, M. W. (2012). Clinical trial of a
farnesyltransferase inhibitor in children with Hutchinson-Gilford progeria
syndrome. *Proc Natl Acad Sci U S A*, *109*(41), 16666-16671.
doi:10.1073/pnas.1202529109

Gordon, L. B., Rothman, F. G., Lopez-Otin, C., & Misteli, T. (2014). Progeria: a
paradigm for translational medicine. *Cell*, *156*(3), 400-407.
doi:10.1016/j.cell.2013.12.028

Gordon, L. B., Shappell, H., Massaro, J., D'Agostino, R. B., Sr., Brazier, J., Campbell, S.
E., . . . Kieran, M. W. (2018). Association of Lonafarnib Treatment vs No
Treatment With Mortality Rate in Patients With Hutchinson-Gilford Progeria
Syndrome. *JAMA*, *319*(16), 1687-1695. doi:10.1001/jama.2018.3264

Graziotto, J. J., Cao, K., Collins, F. S., & Krainc, D. (2012). Rapamycin activates
autophagy in Hutchinson-Gilford progeria syndrome: implications for normal
aging and age-dependent neurodegenerative disorders. *Autophagy*, *8*(1), 147-151.
doi:10.4161/auto.8.1.18331

Gruenbaum, Y., & Foisner, R. (2015). Lamins: nuclear intermediate filament proteins
with fundamental functions in nuclear mechanics and genome regulation. *Annu
Rev Biochem*, *84*, 131-164. doi:10.1146/annurev-biochem-060614-034115

- Hagting, A., Jackman, M., Simpson, K., & Pines, J. (1999). Translocation of cyclin B1 to the nucleus at prophase requires a phosphorylation-dependent nuclear import signal. *Curr Biol*, 9(13), 680-689. doi:10.1016/s0960-9822(99)80308-x
- Hakelien, A. M., Delbarre, E., Gaustad, K. G., Buendia, B., & Collas, P. (2008). Expression of the myodystrophic R453W mutation of lamin A in C2C12 myoblasts causes promoter-specific and global epigenetic defects. *Exp Cell Res*, 314(8), 1869-1880. doi:10.1016/j.yexcr.2008.02.018
- Hamczyk, M. R., & Andres, V. (2018). Accelerated atherosclerosis in HGPS. *Aging (Albany NY)*, 10(10), 2555-2556. doi:10.18632/aging.101608
- Hamczyk, M. R., del Campo, L., & Andres, V. (2018). Aging in the Cardiovascular System: Lessons from Hutchinson-Gilford Progeria Syndrome. *Annu Rev Physiol*, 80, 27-48. doi:10.1146/annurev-physiol-021317-121454
- Hamczyk, M. R., Villa-Bellosta, R., Quesada, V., Gonzalo, P., Vidak, S., Nevado, R. M., . . . Andrés, V. (2019). Progerin accelerates atherosclerosis by inducing endoplasmic reticulum stress in vascular smooth muscle cells. *EMBO Molecular Medicine*, 11(4), e9736. doi:10.15252/emmm.201809736
- Harborth, J., Elbashir, S. M., Bechert, K., Tuschl, T., & Weber, K. (2001). Identification of essential genes in cultured mammalian cells using small interfering RNAs. *J Cell Sci*, 114(Pt 24), 4557-4565.
- Harhour, K., Frankel, D., Bartoli, C., Roll, P., De Sandre-Giovannoli, A., & Levy, N. (2018). An overview of treatment strategies for Hutchinson-Gilford Progeria syndrome. *Nucleus*, 9(1), 246-257. doi:10.1080/19491034.2018.1460045

- Harhour, K., Navarro, C., Depetris, D., Mattei, M. G., Nissan, X., Cau, P., . . . Levy, N. (2017). MG132-induced progerin clearance is mediated by autophagy activation and splicing regulation. *EMBO Mol Med*, 9(9), 1294-1313. doi:10.15252/emmm.201607315
- Hegele, R. A., Cao, H., Liu, D. M., Costain, G. A., Charlton-Menys, V., Rodger, N. W., & Durrington, P. N. (2006). Sequencing of the reannotated LMNB2 gene reveals novel mutations in patients with acquired partial lipodystrophy. *Am J Hum Genet*, 79(2), 383-389. doi:10.1086/505885
- Hennekam, R. C. (2006). Hutchinson-Gilford progeria syndrome: review of the phenotype. *Am J Med Genet A*, 140(23), 2603-2624. doi:10.1002/ajmg.a.31346
- Heydarkhan-Hagvall, S., Helenius, G., Johansson, B. R., Li, J. Y., Mattsson, E., & Risberg, B. (2003). Co-culture of endothelial cells and smooth muscle cells affects gene expression of angiogenic factors. *J Cell Biochem*, 89(6), 1250-1259. doi:10.1002/jcb.10583
- Houben, F., Ramaekers, F. C., Snoeckx, L. H., & Broers, J. L. (2007). Role of nuclear lamina-cytoskeleton interactions in the maintenance of cellular strength. *Biochim Biophys Acta*, 1773(5), 675-686. doi:10.1016/j.bbamcr.2006.09.018
- Hutchinson, J. (1886). Congenital Absence of Hair and Mammary Glands with Atrophic Condition of the Skin and its Appendages, in a Boy whose Mother had been almost wholly Bald from Alopecia Areata from the age of Six. *Med Chir Trans*, 69, 473-477. doi:10.1177/095952878606900127
- Ignarro, L. J., Buga, G. M., Wei, L. H., Bauer, P. M., Wu, G., & del Soldato, P. (2001). Role of the arginine-nitric oxide pathway in the regulation of vascular smooth

muscle cell proliferation. *Proc Natl Acad Sci U S A*, 98(7), 4202-4208.

doi:10.1073/pnas.071054698

Jacot, J. G., & Wong, J. Y. (2008). Endothelial injury induces vascular smooth muscle cell proliferation in highly localized regions of a direct contact co-culture system.

Cell Biochem Biophys, 52(1), 37-46. doi:10.1007/s12013-008-9023-6

Jones, J. R., & Zhang, S. C. (2016). Engineering human cells and tissues through pluripotent stem cells. *Curr Opin Biotechnol*, 40, 133-138.

doi:10.1016/j.copbio.2016.03.010

Kang, H. T., Park, J. T., Choi, K., Choi, H. J. C., Jung, C. W., Kim, G. R., . . . Park, S. C. (2017). Chemical screening identifies ROCK as a target for recovering

mitochondrial function in Hutchinson-Gilford progeria syndrome. *Aging Cell*, 16(3), 541-550. doi:10.1111/acel.12584

Kang, S. M., Yoon, M. H., Ahn, J., Kim, J. E., Kim, S. Y., Kang, S. Y., . . . Park, B. J.

(2021). Author Correction: Progerinin, an optimized progerin-lamin A binding inhibitor, ameliorates premature senescence phenotypes of Hutchinson-Gilford progeria syndrome. *Commun Biol*, 4(1), 297. doi:10.1038/s42003-021-01843-6

Kleinstiver, B. P., Pattanayak, V., Prew, M. S., Tsai, S. Q., Nguyen, N. T., Zheng, Z., &

Joung, J. K. (2016). High-fidelity CRISPR-Cas9 nucleases with no detectable genome-wide off-target effects. *Nature*, 529(7587), 490-495.

doi:10.1038/nature16526

Koblan, L. W., Doman, J. L., Wilson, C., Levy, J. M., Tay, T., Newby, G. A., . . . Liu, D.

R. (2018). Improving cytidine and adenine base editors by expression

- optimization and ancestral reconstruction. *Nature Biotechnology*, 36(9), 843-846.
doi:10.1038/nbt.4172
- Koblan, L. W., Erdos, M. R., Wilson, C., Cabral, W. A., Levy, J. M., Xiong, Z. M., . . .
Liu, D. R. (2021). In vivo base editing rescues Hutchinson-Gilford progeria
syndrome in mice. *Nature*, 589(7843), 608-614. doi:10.1038/s41586-020-03086-7
- Kolluru, G. K., Siamwala, J. H., & Chatterjee, S. (2010). eNOS phosphorylation in health
and disease. *Biochimie*, 92(9), 1186-1198. doi:10.1016/j.biochi.2010.03.020
- Kolluru, G. K., Sinha, S., Majumder, S., Muley, A., Siamwala, J. H., Gupta, R., &
Chatterjee, S. (2010). Shear stress promotes nitric oxide production in endothelial
cells by sub-cellular delocalization of eNOS: A basis for shear stress mediated
angiogenesis. *Nitric Oxide*, 22(4), 304-315. doi:10.1016/j.niox.2010.02.004
- Komor, A. C., Badran, A. H., & Liu, D. R. (2017). CRISPR-Based Technologies for the
Manipulation of Eukaryotic Genomes. *Cell*, 169(3), 559.
doi:10.1016/j.cell.2017.04.005
- Komor, A. C., Kim, Y. B., Packer, M. S., Zuris, J. A., & Liu, D. R. (2016).
Programmable editing of a target base in genomic DNA without double-stranded
DNA cleavage. *Nature*, 533(7603), 420-424. doi:10.1038/nature17946
- Kubben, N., & Misteli, T. (2017). Shared molecular and cellular mechanisms of
premature ageing and ageing-associated diseases. *Nat Rev Mol Cell Biol*, 18(10),
595-609. doi:10.1038/nrm.2017.68
- Kubben, N., Zhang, W., Wang, L., Voss, Ty C., Yang, J., Qu, J., . . . Misteli, T. (2016).
Repression of the Antioxidant NRF2 Pathway in Premature Aging. *Cell*, 165(6),
1361-1374. doi:10.1016/j.cell.2016.05.017

- Kukreja, R. C., & Xi, L. (2007). eNOS phosphorylation: a pivotal molecular switch in vasodilation and cardioprotection? *J Mol Cell Cardiol*, *42*(2), 280-282.
doi:10.1016/j.yjmcc.2006.10.011
- Kumar, V. A., Brewster, L. P., Caves, J. M., & Chaikof, E. L. (2011). Tissue Engineering of Blood Vessels: Functional Requirements, Progress, and Future Challenges. *Cardiovasc Eng Technol*, *2*(3), 137-148. doi:10.1007/s13239-011-0049-3
- Kumaran, R. I., Muralikrishna, B., & Parnaik, V. K. (2002). Lamin A/C speckles mediate spatial organization of splicing factor compartments and RNA polymerase II transcription. *J Cell Biol*, *159*(5), 783-793. doi:10.1083/jcb.200204149
- L'Heureux, N., Dusserre, N., Konig, G., Victor, B., Keire, P., Wight, T. N., . . . McAllister, T. N. (2006). Human tissue-engineered blood vessels for adult arterial revascularization. *Nat Med*, *12*(3), 361-365. doi:10.1038/nm1364
- L'Heureux, N., Paquet, S., Labbe, R., Germain, L., & Auger, F. A. (1998). A completely biological tissue-engineered human blood vessel. *FASEB J*, *12*(1), 47-56.
doi:10.1096/fasebj.12.1.47
- Lahtenvuo, J., & Rosenzweig, A. (2012). Effects of aging on angiogenesis. *Circ Res*, *110*(9), 1252-1264. doi:10.1161/CIRCRESAHA.111.246116
- Larsson, O., Morita, M., Topisirovic, I., Alain, T., Blouin, M. J., Pollak, M., & Sonenberg, N. (2012). Distinct perturbation of the translome by the antidiabetic drug metformin. *Proc Natl Acad Sci U S A*, *109*(23), 8977-8982.
doi:10.1073/pnas.1201689109
- Lee, S. J., Jung, Y. S., Yoon, M. H., Kang, S. M., Oh, A. Y., Lee, J. H., . . . Park, B. J. (2016). Interruption of progerin-lamin A/C binding ameliorates Hutchinson-

- Gilford progeria syndrome phenotype. *J Clin Invest*, 126(10), 3879-3893.
doi:10.1172/JCI84164
- Lee, S. J., Tsang, P. S., Diaz, T. M., Wei, B. Y., & Stetler-Stevenson, W. G. (2010). TIMP-2 modulates VEGFR-2 phosphorylation and enhances phosphodiesterase activity in endothelial cells. *Lab Invest*, 90(3), 374-382.
doi:10.1038/labinvest.2009.136
- Lembong, J., Lerman, M. J., Kingsbury, T. J., Civin, C. I., & Fisher, J. P. (2018). A Fluidic Culture Platform for Spatially Patterned Cell Growth, Differentiation, and Cocultures. *Tissue Eng Part A*, 24(23-24), 1715-1732.
doi:10.1089/ten.TEA.2018.0020
- Li, M. N., Qian, M., Kyler, K., & Xu, J. (2018). Endothelial-Vascular Smooth Muscle Cells Interactions in Atherosclerosis. *Frontiers in Cardiovascular Medicine*, 5.
doi:ARTN 15110.3389/fcvm.2018.00151
- Libby, P., & Hansson, G. K. (2015). Inflammation and immunity in diseases of the arterial tree: players and layers. *Circ Res*, 116(2), 307-311.
doi:10.1161/CIRCRESAHA.116.301313
- Lilly, B. (2014). We have contact: endothelial cell-smooth muscle cell interactions. *Physiology (Bethesda)*, 29(4), 234-241. doi:10.1152/physiol.00047.2013
- Liu, B., Ghosh, S., Yang, X., Zheng, H., Liu, X., Wang, Z., . . . Zhou, Z. (2012). Resveratrol Rescues SIRT1-Dependent Adult Stem Cell Decline and Alleviates Progeroid Features in Laminopathy-Based Progeria. *Cell Metabolism*, 16(6), 738-750. doi:<http://dx.doi.org/10.1016/j.cmet.2012.11.007>

- Liu, B., Wang, J., Chan, K. M., Tjia, W. M., Deng, W., Guan, X., . . . Zhou, Z. (2005). Genomic instability in laminopathy-based premature aging. *Nat Med*, *11*(7), 780-785. doi:10.1038/nm1266
- Liu, Y., Wang, Y., Rusinol, A. E., Sinensky, M. S., Liu, J., Shell, S. M., & Zou, Y. (2008). Involvement of xeroderma pigmentosum group A (XPA) in progeria arising from defective maturation of prelamin A. *FASEB J*, *22*(2), 603-611. doi:10.1096/fj.07-8598com
- Lopez-Otin, C., Blasco, M. A., Partridge, L., Serrano, M., & Kroemer, G. (2013). The hallmarks of aging. *Cell*, *153*(6), 1194-1217. doi:10.1016/j.cell.2013.05.039
- Lu, A., Wang, L., & Qian, L. (2015). The role of eNOS in the migration and proliferation of bone-marrow derived endothelial progenitor cells and in vitro angiogenesis. *Cell Biol Int*, *39*(4), 484-490. doi:10.1002/cbin.10405
- Manju, K., Muralikrishna, B., & Parnaik, V. K. (2006). Expression of disease-causing lamin A mutants impairs the formation of DNA repair foci. *J Cell Sci*, *119*(Pt 13), 2704-2714. doi:10.1242/jcs.03009
- Matrone, G., Thandavarayan, R. A., Walther, B. K., Meng, S., Mojiri, A., & Cooke, J. P. (2019). Dysfunction of iPSC-derived endothelial cells in human Hutchinson-Gilford progeria syndrome. *Cell Cycle*, *18*(19), 2495-2508. doi:10.1080/15384101.2019.1651587
- McClintock, D., Ratner, D., Lokuge, M., Owens, D. M., Gordon, L. B., Collins, F. S., & Djabali, K. (2007). The mutant form of lamin A that causes Hutchinson-Gilford progeria is a biomarker of cellular aging in human skin. *PLoS One*, *2*(12), e1269. doi:10.1371/journal.pone.0001269

- McCord, R. P., Nazario-Toole, A., Zhang, H., Chines, P. S., Zhan, Y., Erdos, M. R., . . .
Cao, K. (2013). Correlated alterations in genome organization, histone methylation, and DNA-lamin A/C interactions in Hutchinson-Gilford progeria syndrome. *Genome Res*, 23(2), 260-269. doi:10.1101/gr.138032.112
- Meier, J., Campbell, K. H., Ford, C. C., Stick, R., & Hutchison, C. J. (1991). The role of lamin LIII in nuclear assembly and DNA replication, in cell-free extracts of *Xenopus* eggs. *J Cell Sci*, 98 (Pt 3), 271-279.
- Merideth, M. A., Gordon, L. B., Clauss, S., Sachdev, V., Smith, A. C., Perry, M. B., . . .
Introne, W. J. (2008). Phenotype and course of Hutchinson-Gilford progeria syndrome. *N Engl J Med*, 358(6), 592-604. doi:10.1056/NEJMoa0706898
- Mount, P. F., Kemp, B. E., & Power, D. A. (2007). Regulation of endothelial and myocardial NO synthesis by multi-site eNOS phosphorylation. *J Mol Cell Cardiol*, 42(2), 271-279. doi:10.1016/j.yjmcc.2006.05.023
- Musich, P. R., & Zou, Y. (2009). Genomic instability and DNA damage responses in progeria arising from defective maturation of prelamin A. *Aging (Albany NY)*, 1(1), 28-37. doi:10.18632/aging.100012
- Musich, P. R., & Zou, Y. (2011). DNA-damage accumulation and replicative arrest in Hutchinson-Gilford progeria syndrome. *Biochem Soc Trans*, 39(6), 1764-1769. doi:10.1042/BST20110687
- Nagase, H., Visse, R., & Murphy, G. (2006). Structure and function of matrix metalloproteinases and TIMPs. *Cardiovasc Res*, 69(3), 562-573. doi:10.1016/j.cardiores.2005.12.002

- Nikolova, V., Leimena, C., McMahon, A. C., Tan, J. C., Chandar, S., Jogia, D., . . . Fatkin, D. (2004). Defects in nuclear structure and function promote dilated cardiomyopathy in lamin A/C-deficient mice. *J Clin Invest*, *113*(3), 357-369. doi:10.1172/JCI19448
- Olive, M., Harten, I., Mitchell, R., Beers, J. K., Djabali, K., Cao, K., . . . Gordon, L. B. (2010). Cardiovascular pathology in Hutchinson-Gilford progeria: correlation with the vascular pathology of aging. *Arterioscler Thromb Vasc Biol*, *30*(11), 2301-2309. doi:10.1161/ATVBAHA.110.209460
- Osmanagic-Myers, S., Kiss, A., Manakanatas, C., Hamza, O., Sedlmayer, F., Szabo, P. L., . . . Foisner, R. (2019). Endothelial progerin expression causes cardiovascular pathology through an impaired mechanoresponse. *J Clin Invest*, *129*(2), 531-545. doi:10.1172/JCI121297
- Osorio, F. G., Navarro, C. L., Cadinanos, J., Lopez-Mejia, I. C., Quiros, P. M., Bartoli, C., . . . Lopez-Otin, C. (2011). Splicing-directed therapy in a new mouse model of human accelerated aging. *Sci Transl Med*, *3*(106), 106ra107. doi:10.1126/scitranslmed.3002847
- Padiath, Q. S., Saigoh, K., Schiffmann, R., Asahara, H., Yamada, T., Koeppen, A., . . . Fu, Y. H. (2006). Lamin B1 duplications cause autosomal dominant leukodystrophy. *Nat Genet*, *38*(10), 1114-1123. doi:10.1038/ng1872
- Pagano, G., Talamanca, A. A., Castello, G., Cordero, M. D., d'Ischia, M., Gadaleta, M. N., . . . Zatterale, A. (2014). Oxidative stress and mitochondrial dysfunction across broad-ranging pathologies: toward mitochondria-targeted clinical strategies. *Oxid Med Cell Longev*, *2014*, 541230. doi:10.1155/2014/541230

- Patsch, C., Challet-Meylan, L., Thoma, E. C., Ulrich, E., Heckel, T., O'Sullivan, J. F., . . . Cowan, C. A. (2015). Generation of vascular endothelial and smooth muscle cells from human pluripotent stem cells. *Nat Cell Biol*, *17*(8), 994-1003. doi:10.1038/ncb3205
- Poh, M., Boyer, M., Solan, A., Dahl, S. L., Pedrotty, D., Banik, S. S., . . . Niklason, L. E. (2005). Blood vessels engineered from human cells. *Lancet*, *365*(9477), 2122-2124. doi:10.1016/S0140-6736(05)66735-9
- Potente, M., & Carmeliet, P. (2017). The Link Between Angiogenesis and Endothelial Metabolism. *Annu Rev Physiol*, *79*, 43-66. doi:10.1146/annurev-physiol-021115-105134
- Prakash, A., Gordon, L. B., Kleinman, M. E., Gurary, E. B., Massaro, J., D'Agostino, R., Sr., . . . Smoot, L. (2018). Cardiac Abnormalities in Patients With Hutchinson-Gilford Progeria Syndrome. *JAMA Cardiol*, *3*(4), 326-334. doi:10.1001/jamacardio.2017.5235
- Puttaraju, M., Jackson, M., Klein, S., Shilo, A., Bennett, C. F., Gordon, L., . . . Misteli, T. (2021). Systematic screening identifies therapeutic antisense oligonucleotides for Hutchinson-Gilford progeria syndrome. *Nat Med*, *27*(3), 526-535. doi:10.1038/s41591-021-01262-4
- Ramos, C., Hendgen-Cotta, U. B., Sobierajski, J., Bernard, A., Kelm, M., & Rassaf, T. (2014). Dietary nitrate reverses vascular dysfunction in older adults with moderately increased cardiovascular risk. *J Am Coll Cardiol*, *63*(15), 1584-1585. doi:10.1016/j.jacc.2013.08.691

- Ran, F. A., Hsu, P. D., Wright, J., Agarwala, V., Scott, D. A., & Zhang, F. (2013). Genome engineering using the CRISPR-Cas9 system. *Nat Protoc*, 8(11), 2281-2308. doi:10.1038/nprot.2013.143
- Rees, H. A., & Liu, D. R. (2018). Base editing: precision chemistry on the genome and transcriptome of living cells. *Nat. Rev. Genet.* , 19, 770-788.
- Richards, S. A., Muter, J., Ritchie, P., Lattanzi, G., & Hutchison, C. J. (2011). The accumulation of un-repairable DNA damage in laminopathy progeria fibroblasts is caused by ROS generation and is prevented by treatment with N-acetyl cysteine. *Human Molecular Genetics*, 20(20), 3997-4004. doi:10.1093/hmg/ddr327
- Richards, S. A., Muter, J., Ritchie, P., Lattanzi, G., & Hutchison, C. J. (2011). The accumulation of un-repairable DNA damage in laminopathy progeria fibroblasts is caused by ROS generation and is prevented by treatment with N-acetyl cysteine. *Hum Mol Genet*, 20(20), 3997-4004. doi:10.1093/hmg/ddr327
- Rivera-Torres, J., Acin-Perez, R., Cabezas-Sanchez, P., Osorio, F. G., Gonzalez-Gomez, C., Megias, D., . . . Andres, V. (2013). Identification of mitochondrial dysfunction in Hutchinson-Gilford progeria syndrome through use of stable isotope labeling with amino acids in cell culture. *J Proteomics*, 91, 466-477. doi:10.1016/j.jprot.2013.08.008
- Robert, J., Weber, B., Frese, L., Emmert, M. Y., Schmidt, D., von Eckardstein, A., . . . Hoerstrup, S. P. (2013). A three-dimensional engineered artery model for in vitro atherosclerosis research. *PLoS One*, 8(11), e79821. doi:10.1371/journal.pone.0079821

- Rodriguez, S., Coppede, F., Sagelius, H., & Eriksson, M. (2009). Increased expression of the Hutchinson-Gilford progeria syndrome truncated lamin A transcript during cell aging. *Eur J Hum Genet*, *17*(7), 928-937. doi:10.1038/ejhg.2008.270
- Rossmann, M. J., Gioscia-Ryan, R. A., Santos-Parker, J. R., Ziemba, B. P., Lubieniecki, K. L., Johnson, L. C., . . . Seals, D. R. (2021). Inorganic Nitrite Supplementation Improves Endothelial Function With Aging: Translational Evidence for Suppression of Mitochondria-Derived Oxidative Stress. *Hypertension*, *77*(4), 1212-1222. doi:10.1161/HYPERTENSIONAHA.120.16175
- Saito, S., Trovato, M. J., You, R., Lal, B. K., Fasehun, F., Padberg, F. T., Jr., . . . Pappas, P. J. (2001). Role of matrix metalloproteinases 1, 2, and 9 and tissue inhibitor of matrix metalloproteinase-1 in chronic venous insufficiency. *J Vasc Surg*, *34*(5), 930-938. doi:10.1067/mva.2001.119503
- Sander, J. D., & Joung, J. K. (2014). CRISPR-Cas systems for editing, regulating and targeting genomes. *Nat Biotechnol*, *32*(4), 347-355. doi:10.1038/nbt.2842
- Sanjana, N. E., Shalem, O., & Zhang, F. (2014). Improved vectors and genome-wide libraries for CRISPR screening. *Nat Methods*, *11*(8), 783-784. doi:10.1038/nmeth.3047
- Santiago-Fernandez, O., Osorio, F. G., Quesada, V., Rodriguez, F., Basso, S., Maeso, D., . . . Lopez-Otin, C. (2019). Development of a CRISPR/Cas9-based therapy for Hutchinson-Gilford progeria syndrome. *Nat Med*, *25*(3), 423-426. doi:10.1038/s41591-018-0338-6
- Scaffidi, P., & Misteli, T. (2006). Lamin A-dependent nuclear defects in human aging. *Science*, *312*(5776), 1059-1063. doi:10.1126/science.1127168

- Senger, D. R., & Davis, G. E. (2011). Angiogenesis. *Cold Spring Harb Perspect Biol*, 3(8), a005090. doi:10.1101/cshperspect.a005090
- Seo, D. W., Li, H., Guedez, L., Wingfield, P. T., Diaz, T., Salloum, R., . . . Stetler-Stevenson, W. G. (2003). TIMP-2 mediated inhibition of angiogenesis: an MMP-independent mechanism. *Cell*, 114(2), 171-180. doi:10.1016/s0092-8674(03)00551-8
- Shi, Y., Inoue, H., Wu, J. C., & Yamanaka, S. (2017). Induced pluripotent stem cell technology: a decade of progress. *Nat Rev Drug Discov*, 16(2), 115-130. doi:10.1038/nrd.2016.245
- Shumaker, D. K., Dechat, T., Kohlmaier, A., Adam, S. A., Bozovsky, M. R., Erdos, M. R., . . . Goldman, R. D. (2006). Mutant nuclear lamin A leads to progressive alterations of epigenetic control in premature aging. *Proc Natl Acad Sci U S A*, 103(23), 8703-8708. doi:10.1073/pnas.0602569103
- Sindler, A. L., Fleenor, B. S., Calvert, J. W., Marshall, K. D., Zigler, M. L., Lefer, D. J., & Seals, D. R. (2011). Nitrite supplementation reverses vascular endothelial dysfunction and large elastic artery stiffness with aging. *Aging Cell*, 10(3), 429-437. doi:10.1111/j.1474-9726.2011.00679.x
- Song, H. G., Rumma, R. T., Ozaki, C. K., Edelman, E. R., & Chen, C. S. (2018). Vascular Tissue Engineering: Progress, Challenges, and Clinical Promise. *Cell Stem Cell*, 22(3), 340-354. doi:10.1016/j.stem.2018.02.009
- Spann, T. P., Goldman, A. E., Wang, C., Huang, S., & Goldman, R. D. (2002). Alteration of nuclear lamin organization inhibits RNA polymerase II-dependent transcription. *J Cell Biol*, 156(4), 603-608. doi:10.1083/jcb.200112047

- Spann, T. P., Moir, R. D., Goldman, A. E., Stick, R., & Goldman, R. D. (1997). Disruption of nuclear lamin organization alters the distribution of replication factors and inhibits DNA synthesis. *J Cell Biol*, *136*(6), 1201-1212. doi:10.1083/jcb.136.6.1201
- Stuurman, N., Heins, S., & Aebi, U. (1998). Nuclear lamins: their structure, assembly, and interactions. *J Struct Biol*, *122*(1-2), 42-66. doi:10.1006/jsbi.1998.3987
- Sun, S., Qin, W., Tang, X., Meng, Y., Hu, W., Zhang, S., . . . Liu, B. (2020). Vascular endothelium-targeted Sirt7 gene therapy rejuvenates blood vessels and extends life span in a Hutchinson-Gilford progeria model. *Sci Adv*, *6*(8), eaay5556. doi:10.1126/sciadv.aay5556
- Takahashi, K., & Yamanaka, S. (2006). Induction of pluripotent stem cells from mouse embryonic and adult fibroblast cultures by defined factors. *Cell*, *126*(4), 663-676. doi:10.1016/j.cell.2006.07.024
- Tariq, Z., Zhang, H., Chia-Liu, A., Shen, Y., Gete, Y., Xiong, Z. M., . . . Cao, K. (2017). Lamin A and microtubules collaborate to maintain nuclear morphology. *Nucleus*, *8*(4), 433-446. doi:10.1080/19491034.2017.1320460
- Truskey, G. A. (2016). Advancing cardiovascular tissue engineering. *F1000Res*, *5*. doi:10.12688/f1000research.8237.1
- Truskey, G. A. (2018). Human Microphysiological Systems and Organoids as in Vitro Models for Toxicological Studies. *Front Public Health*, *6*, 185. doi:10.3389/fpubh.2018.00185

- Truskey, G. A., & Fernandez, C. E. (2015). Tissue-engineered blood vessels as promising tools for testing drug toxicity. *Expert Opin Drug Metab Toxicol*, *11*(7), 1021-1024. doi:10.1517/17425255.2015.1047342
- Tzima, E., Irani-Tehrani, M., Kiosses, W. B., Dejana, E., Schultz, D. A., Engelhardt, B., . . . Schwartz, M. A. (2005). A mechanosensory complex that mediates the endothelial cell response to fluid shear stress. *Nature*, *437*(7057), 426-431. doi:10.1038/nature03952
- Ullrich, N. J., & Gordon, L. B. (2015). Hutchinson-Gilford progeria syndrome. *Handb Clin Neurol*, *132*, 249-264. doi:10.1016/B978-0-444-62702-5.00018-4
- Vanhoutte, P. M. (2009). Endothelial dysfunction: the first step toward coronary arteriosclerosis. *Circ J*, *73*(4), 595-601. doi:10.1253/circj.cj-08-1169
- Vanhoutte, P. M., Shimokawa, H., Feletou, M., & Tang, E. H. (2017). Endothelial dysfunction and vascular disease - a 30th anniversary update. *Acta Physiol (Oxf)*, *219*(1), 22-96. doi:10.1111/apha.12646
- Wang, W., Ha, C. H., Jhun, B. S., Wong, C., Jain, M. K., & Jin, Z. G. (2010). Fluid shear stress stimulates phosphorylation-dependent nuclear export of HDAC5 and mediates expression of KLF2 and eNOS. *Blood*, *115*(14), 2971-2979. doi:10.1182/blood-2009-05-224824
- Wang, Z., Mithieux, S. M., & Weiss, A. S. (2019). Fabrication Techniques for Vascular and Vascularized Tissue Engineering. *Adv Healthc Mater*, *8*(19), e1900742. doi:10.1002/adhm.201900742
- Widmer, R. J., & Lerman, A. (2014). Endothelial dysfunction and cardiovascular disease. *Glob Cardiol Sci Pract*, *2014*(3), 291-308. doi:10.5339/gcsp.2014.43

- Worman, H. J., & Bonne, G. (2007). "Laminopathies": a wide spectrum of human diseases. *Exp Cell Res*, 313(10), 2121-2133. doi:10.1016/j.yexcr.2007.03.028
- Xiong, Z. M., Choi, J. Y., Wang, K., Zhang, H., Tariq, Z., Wu, D., . . . Cao, K. (2016). Methylene blue alleviates nuclear and mitochondrial abnormalities in progeria. *Aging Cell*, 15(2), 279-290. doi:10.1111/accel.12434
- Xiong, Z. M., LaDana, C., Wu, D., & Cao, K. (2013). An inhibitory role of progerin in the gene induction network of adipocyte differentiation from iPS cells. *Aging (Albany NY)*, 5(4), 288-303. doi:10.18632/aging.100550
- Xiong, Z. M., O'Donovan, M., Sun, L., Choi, J. Y., Ren, M., & Cao, K. (2017). Anti-Aging Potentials of Methylene Blue for Human Skin Longevity. *Sci Rep*, 7(1), 2475. doi:10.1038/s41598-017-02419-3
- Yang, Y., Wang, L., Bell, P., McMenamin, D., He, Z., White, J., . . . Wilson, J. M. (2016). A dual AAV system enables the Cas9-mediated correction of a metabolic liver disease in newborn mice. *Nat Biotechnol*, 34(3), 334-338. doi:10.1038/nbt.3469
- Yang, Y. M., Huang, A., Kaley, G., & Sun, D. (2009). eNOS uncoupling and endothelial dysfunction in aged vessels. *Am J Physiol Heart Circ Physiol*, 297(5), H1829-1836. doi:10.1152/ajpheart.00230.2009
- Young, S. G., Yang, S. H., Davies, B. S., Jung, H. J., & Fong, L. G. (2013). Targeting protein prenylation in progeria. *Sci Transl Med*, 5(171), 171ps173. doi:10.1126/scitranslmed.3005229
- Zastrow, M. S., Vlcek, S., & Wilson, K. L. (2004). Proteins that bind A-type lamins: integrating isolated clues. *J Cell Sci*, 117(Pt 7), 979-987. doi:10.1242/jcs.01102

- Zhang, H., Kieckhafer, J. E., & Cao, K. (2013). Mouse models of laminopathies. *Aging Cell*, 12(1), 2-10. doi:10.1111/ace1.12021
- Zhang, H., Sun, L., Wang, K., Wu, D., Trappio, M., Witting, C., & Cao, K. (2016). Loss of H3K9me3 Correlates with ATM Activation and Histone H2AX Phosphorylation Deficiencies in Hutchinson-Gilford Progeria Syndrome. *PLOS ONE*, 11(12), e0167454. doi:10.1371/journal.pone.0167454
- Zhang, H., Xiong, Z. M., & Cao, K. (2014). Mechanisms controlling the smooth muscle cell death in progeria via down-regulation of poly(ADP-ribose) polymerase 1. *Proc Natl Acad Sci U S A*, 111(22), E2261-2270. doi:10.1073/pnas.1320843111
- Zhang, J., Lian, Q., Zhu, G., Zhou, F., Sui, L., Tan, C., . . . Colman, A. (2011). A human iPSC model of Hutchinson Gilford Progeria reveals vascular smooth muscle and mesenchymal stem cell defects. *Cell Stem Cell*, 8(1), 31-45. doi:10.1016/j.stem.2010.12.002
- Zhang, Q., Bosch-Rue, E., Perez, R. A., & Truskey, G. A. (2021). Biofabrication of tissue engineering vascular systems. *APL Bioeng*, 5(2), 021507. doi:10.1063/5.0039628
- Zhang, Q., Zhang, X., & Truskey, G. A. (2020). Vascular Microphysiological Systems to Model Diseases. *Cell Gene Ther Insights*, 6(1), 93-102. doi:10.18609/cgti.2020.012
- Zhang, Y., Liao, B., Li, M., Cheng, M., Fu, Y., Liu, Q., . . . Yu, F. (2016). Shear stress regulates endothelial cell function through SRB1-eNOS signaling pathway. *Cardiovasc Ther*, 34(5), 308-313. doi:10.1111/1755-5922.12199
- Zhao, Y., Vanhoutte, P. M., & Leung, S. W. (2015). Vascular nitric oxide: Beyond eNOS. *J Pharmacol Sci*, 129(2), 83-94. doi:10.1016/j.jphs.2015.09.002

Zheng, Y., Chen, J., Craven, M., Choi, N. W., Totorica, S., Diaz-Santana, A., . . .

Stroock, A. D. (2012). In vitro microvessels for the study of angiogenesis and thrombosis. *Proc Natl Acad Sci U S A*, *109*(24), 9342-9347.

doi:10.1073/pnas.1201240109